

DEPARTMENT OF BIOCHEMISTRY
UNIVERSITY OF OXFORD



Mechanism of SigR inhibition by the anti-sigma factor RsrA from *Streptomyces coelicolor*

Marie-Louise Rosina Francis

Masters of Science by Research degree (MRes) in Biochemistry

Hertford College

OSS ID; 682670

Supervisor; Professor Colin Kleanthous

Department of Biochemistry, University of Oxford

South Parks Road, Oxfordshire, OX1 3QU

Abstract

The extracytoplasmic function (ECF) sigma factor SigR (σ^R) is a bacterial transcription factor involved in the regulation of cytosolic redox homeostasis in *Streptomyces coelicolor*. SigR activity is regulated by its cognate anti-sigma factor RsrA. RsrA is a member of the zinc-anti-sigma (ZAS) family, which in its reduced state binds a single Zn^{2+} ion coordinated by 3 cysteine residues and a histidine. RsrA senses oxidative stress within the cytosol and responds by the formation of intramolecular disulphide bonds between its Zn-ligating cysteine residues. This results in the loss of the metal ion, a conformational rearrangement, and dissociation of SigR by an unknown mechanism. This releases SigR to bind RNA polymerase and direct the expression of a large regulon including that of the thioredoxin pathway, thereby re-establishing redox homeostasis. No structural information is available for the SigR-RsrA complex in *Streptomyces coelicolor*. Moreover, little is known of the mechanism by which RsrA associates with SigR and regulates gene transcription, or the role of zinc in SigR binding. In this work, a stopped-flow fluorescence-based assay was developed for investigating the kinetics of SigR-RsrA complex formation to aid our understanding of the role of the metal ion. Ultimately, trying to understand how oxidative stress causes dissociation of the *Streptomyces coelicolor* complex. Through tryptophan fluorescence emission quenching experiments, the SigR region 2 tryptophan (W88) and region 4 tryptophan (W159) were found to be sensitive to RsrA binding, likely denoting the binding sites for the anti-sigma factor. Pre-steady state experiments demonstrated that the metal ion has little effect on the rate of association (k_{on} 8.9 and 17.3×10^6 $M^{-1}s^{-1}$ at 35°C in the presence and absence of zinc, respectively) but a large effect on the dissociation rate constant (>500-fold faster in the absence of zinc at 35°C). Moreover, the kinetically derived K_ds (0.27 nM and 62.4 nM with and without zinc respectively) agreed with the equilibrium constant for the complex derived through isothermal titration calorimetry (0.78 nM and 101.7 nM), validating the kinetic model for binding experiments. Zinc therefore has an important role in the structure of RsrA, affecting SigR-RsrA complex affinity, the off-rate for the complex and inhibition of SigR activity. Future work will exploit these assays to determine the role of zinc in redox sensing by RsrA.

Table of Contents

Abstract 2

Acknowledgements 12

Abbreviations 13

1- Introduction 14

1.1. σ; A transcriptional subunit of RNA polymerase holoenzyme 14

1.2. The role of σ in the gene transcription cycle 15

1.3. Regulation of gene transcription 16

1.4. Sigma factor families are based on function of transcribed genes 17

1.5. σ^{70} family structure and function 18

1.6. σ regions and subregions 19

1.7. σ factor subgroups 20

1.8. Extracytoplasmic function (ECF) σ subfamily 21

1.9. σ factor regulation mechanisms 23

1.10. Anti-sigma factors 24

1.11. Reducing environment of the cytoplasm 27

1.12. Cysteine oxidation 28

1.13. Thioredoxin antioxidant system 29

1.14. Glutaredoxin antioxidant system 30

1.15. Low molecular weight (LMW) thiols 31

1.16. Sigma anti-sigma complexes in other bacterial species 34

1.16.1. *Rhodobacter sphaeroides* ChrR-SigE 35

1.16.2. *Mycobacterium tuberculosis* σ anti-σ factors 36

1.16.3. *Mycobacterium tuberculosis* RshA-SigH 36

1.16.4. *Mycobacterium tuberculosis* RslA-SigL 38

1.16.5. *Cupriavidus metallidurans* CnrY-CnrH 39

1.16.6. Escherichia coli RseA-SigE 40

1.17. Actinobacteria 42

1.17.1. *Streptomyces coelicolor* SigR-RsrA complex 43

1.17.2. The SigR regulon 44

1.17.3. Effect of a SigR null mutant 47

1.17.4. SigR-RsrA system 48

1.17.5. RsrA anti-sigma factor 49

1.17.6. Residues important for redox-sensitivity of ZAS proteins 50
1.17.7. Zinc coordination ligands in RsrA 51
1.17.8. Residues involved in disulphide bond formation 53
1.17.9. Residues important for SigR-RsrA binding and RsrA activity *in vivo* 54
1.17.10. Importance and role of zinc in RsrA 55
1.17.11. Structural rearrangement of RsrA on oxidation 55
Aim of this work 57
Objectives 57
2- Materials and Methods 58
2.1. Microbiology 58
2.1.1. Bacterial strains and growth conditions 58
2.1.2. Plasmids and strains 58
2.2. Molecular Biology 59
2.2.1. Purification of plasmid DNA 59
2.2.2. Polymerase chain reaction (PCR) 60
2.2.3. Preparation of competent cells 62
2.2.4. Transformation of competent cells (DH5α, BL21 (DE3), (DE3) pLysS, Rosetta 2 pLysS) 62
2.3. Biochemical methods 63
2.3.1. Polyacrylamide gel electrophoresis (PAGE) 63
2.3.2. Native PAGE gels 63
2.3.3. Oxidative and reducing Native PAGE 64
2.3.4. Measurement of protein concentrations 64
2.3.5. Test expressions 65
2.3.6. RsrA expression and purification 66
2.3.7. SigR expression and purification 68
2.3.8. HiTrap desalting column; buffer exchange of SigR and RsrA proteins 69
2.4. Biophysical methods 70
2.4.1. Electrospray-Ionisation Mass spectrometry 70
2.4.2. Isothermal Titration Calorimetry (ITC) 70
2.4.3. Steady-state Tryptophan Fluorescence emission quenching 71
2.4.4. Association kinetics of SigR-RsrA complex formation 72
2.4.5. Dissociation kinetics by competition fluorescence Stopped-flow 74
2.4.6. Circular Dichroism (CD) Spectroscopy 74
3- Establishing a fluorescence-based assay to monitor SigR-RsrA complex formation 76

3.1. SigR Tryptophan mutagenesis and purification 76
3.1.1. SigR mutant test expressions 78
3.1.2. Large-scale SigR protein expression 79
3.1.3. Ammonium sulphate precipitation 79
3.1.4. SigR size exclusion purification 81
3.1.5. Final Size exclusion purifications of all SigR proteins 83
3.2. RsrA purification 83
3.2.1. RsrA test expression 83
3.2.2. Large-scale RsrA protein expression and Nickel affinity purification 84
3.2.3. RsrA nickel affinity column re-bind 85
3.2.4. RsrA size exclusion purification 87
3.3. Complex formation between SigR-RsrA by Native PAGE 88
3.4. Development of a tryptophan fluorescence-based assay for monitoring SigR-RsrA complex formation 89
3.5. Introducing tryptophans into SigR region 4 95
4- Results 99
Determining the thermodynamics and kinetics of SigR-RsrA complex formation 99
4.1. Characterisation of interaction by Isothermal Titration Calorimetry (ITC) 99
4.1.1. Thermodynamic analysis of SigR binding RsrA 100
4.1.2. Thermodynamic analysis of RsrA binding to SigR wild-type and tryptophan-to-isoleucine mutants 101
4.2. Kinetics of the association and dissociation of SigR and RsrA in the presence and absence of zinc 106
4.2.1. Association kinetics 109
4.2.2. Dissociation kinetics 114
4.2.3. Binding affinity of SigR-RsrA through Pre-steady-state stopped-flow 119
4.3. Developing an oxidation assay for the dissociation of SigR-RsrA complex 120
4.3.1. Oxidation of complex by Native PAGE 121
5- Discussion 123
5.1. Where does RsrA bind on SigR during complex formation and how does it suppress transcriptional activity of SigR? 123
5.2. What is the importance and role of zinc in RsrA? 125
5.3. The kinetics of SigR-RsrA complex formation 128
5.4. Major conclusions from this study 130
5.5. Implications of study for future research 131

Appendix 132
1.1. Developing expression systems for other sigma factors and anti-sigma proteins 132
1.2. New ZAS-ECF complexes 136
References 141

List of Tables

Table number and description **Page**

Table 1- Core genes within the conserved regulon across actinomycete species that respond to oxidative stress……46

Table 2- Plasmids and strains used in this study……58

Table 3- Antibiotics and chemicals used and their concentrations……59

Table 4- Composition of a PCR reaction for whole plasmid site-directed mutagenesis……60

Table 5- PCR programme for whole plasmid site-directed mutagenesis……61

Table 6- List of primers used in this study……61

Table 7- Sequencing primers used in this study……62

Table 8- Theoretical extinction coefficients for proteins used in this study……65

Table 9- Final SigR protein concentrations, predicted and observed molecular weights used in this study……82

Table 10- Thermodynamic parameters for wild-type and mutant SigR-RsrA complexes in the presence and absence of zinc……103

Table 11- Rates of association of SigR-RsrA in the presence and absence of zinc at 25°C and 35°C……114

Table 12- Rates of association and dissociation of SigR-RsrA in the presence and absence of zinc at 25°C and 35°C……118

Table 13- Summary of rate constants and binding constants for the association (k_{on}) and dissociation (k_{off}) of SigR-RsrA in the presence and absence of zinc at 25 and 35°C……120

Appendix table 1- Molecular weight and genome location of the ZAS and ECF proteins used in this study……136

List of Figures

Figure number and description **Page**

Figure 1- Prokaryotic RNA polymerase holoenzyme $\alpha_2\beta\beta'\sigma$ bound to DNA……..15

Figure 2- Prokaryotic transcription cycle……16

Figure 3- Four distinct regions of highly conserved amino acid sequences within the σ^{70} family; σ^1, σ^2, σ^3 and σ^4.....19

Figure 4- The four phylogenetically distinct σ subfamilies within the σ^{70} family……21

Figure 5 – Anti-σ factor regulation mechanisms……25

Figure 6- Anti-σ factor regulation by secretion from the cell……25/26

Figure 7- Signals for proteolysis of anti-σ……26

Figure 8- Cysteine oxidation products……..29

Figure 9 – Maintaining the reducing environment of the cytoplasm……..30

Figure 10- Structure of mycothiol……31

Figure 11- Formation of disulphide bonds within the periplasm by members of the protein disulphide isomerases (PDI) family; DsbA, B, C and D……..33

Figure 12- Structure of ChrR-SigE complex……35

Figure 13- Complexity of sigma factors in *Mycobacterium tuberculosis*……..37

Figure 14- Structure of SigL-RslA complex……..38

Figure 15- Mechanism of oxidative stress sensing by SigL-RslA……39

Figure 16- Mechanism of CnrY-CnrH complex……....39/40

Figure 17- CnrH sigma factor in complex with CnrY anti-sigma cytosolic domain……..40

Figure 18- Structure of RseA-SigE complex……41

Figure 19- Mechanism of SigE-RseA activation……42

Figure 20- *sigR* and *rsrA* genes are present on the same operon and are translationally coupled……44

Figure 21- X-ray crystal structure of SigR region 2……47

Figure 22- SigR-RsrA system in *Streptomyces coelicolor* and its response to oxidative stress……48

Figure 23- Alignment of several members of the ZAS family by their N-terminus……49

Figure 24- Sequence alignment of redox-sensitive and insensitive members of the ZAS family……...51

Figure 25- Proposed coordination ligands for zinc, and the residues that form disulphide bonds on oxidation of RsrA……52

Figure 26- Proposed coordination ligands for zinc……52/53

Figure 27- Proposed model of RsrA and its coordination ligands……53

Figure 28- SigR structure……76/77

Figure 29- SigR mutants generated in this study……77

Figure 30- Homology model of SigR……78

Figure 31- SDS-PAGE gel test expressions of SigR tryptophan mutants using BL21 (DE3) and BL21 (DE3) pLysS cells……78

Figure 32- SigR* ammonium sulphate precipitation purification……79

Figure 33- SigR* Q Sepharose Anion Exchange chromatography purification……80

Figure 34- 16% SDS-PAGE of samples from SigR* Q-Sepharose Anion exchange chromatography…80/81

Figure 35- SigR* Size exclusion chromatography purification……81

Figure 36- 16% SDS-PAGE of samples from SigR*size exclusion chromatography……82

Figure 37- Final SigR Size exclusion chromatography purifications……83

Figure 38- 16% SDS-PAGE test expression of RsrA in Rosetta 2 pLysS cells……84

Figure 39- RsrA IMAC nickel affinity purification using a 2-50% imidazole gradient (20-500 mM)……85

Figure 40- RsrA Immobilised metal affinity chromatography (IMAC) nickel column purification……85

Figure 41- Second RsrA IMAC nickel affinity purification……86

Figure 42- RsrA IMAC nickel column re-bind purification……86

Figure 43- Size exclusion chromatography purification elution profile of RsrA……87

Figure 44- RsrA Size exclusion chromatography purification……88

Figure 45- Complex formation between RsrA+Zn and SigR mutants at 50 µM……88/89

Figure 46- Fluorescence emission spectra of SigR, SigR W88I, SigR W119I, SigR* and SigR* F159W……91

Figure 47- Quenching of SigR tryptophan fluorescence on titration with RsrA……92

Figure 48- Quenching of SigR Wild-type tryptophan fluorescence upon addition of RsrA……92/93

Figure 49- Tryptophan fluorescence of SigR W88I when titrated with RsrA……93

Figure 50- Representative change in fluorescence intensity of SigR W88I at 350 nm……93

Figure 51- Quenching of SigR W119I tryptophan fluorescence on titration with RsrA……94

Figure 52- Quenching of SigR W119I tryptophan fluorescence upon addition of RsrA……94

Figure 53- Circular dichroism spectroscopy far UV spectra for SigR wild-type, SigR* F171W and SigR* F159W mutant at 20°C, 25°C and 35°C in 10 mM Tris pH 7.5……95/96

Figure 54- Fluorescence intensity change on complex formation between SigR* F159W-RsrA……97

Figure 55- Representative change in fluorescence intensity of SigR* F159W at 337 nm……97

Figure 56- Representative ITC data of SigR-RsrA binding……..101

Figure 57- Representative ITC data of SigR-RsrA binding using SigR W88I and SigR W119I……101/102

Figure 58- Representative ITC data of SigR-RsrA binding using SigR* and SigR* F171W……102

Figure 59- Representative ITC data of SigR-RsrA binding using SigR* F159W……103

Figure 60 – Formation of complex between SigR and RsrA……106

Figure 61- Fluorescence controls for the association of SigR-RsrA……107

Figure 62- Fluorescence controls for the dissociation of SigR-RsrA……108

Figure 63- Representative association kinetic trace of SigR-RsrA complex using pre-steady state tryptophan fluorescence stopped-flow……109

Figure 64- Linear concentration dependence of the observed rates, k_{obs}, between SigR and RsrA under pseudo-first order conditions, at 25°C in the presence of zinc……110

Figure 65- Representative association kinetic trace of SigR-RsrA complex in the absence of zinc at 25°C……111

Figure 66- Linear concentration dependence of the observed rates, k_{obs}, between SigR and RsrA under pseudo-first order conditions, at 25°C in the absence of zinc……112

Figure 67- Representative association kinetic traces of SigR-RsrA complex in the presence (a) and absence (c) of zinc at 35°C……113

Figure 68- Representative dissociation kinetic trace of SigR-RsrA complex using pre-steady state tryptophan fluorescence stopped-flow at 25°C……115

Figure 69- Representative dissociation kinetic trace of SigR-RsrA complex in the absence of zinc at 25°C……116

Figure 70- Representative dissociation kinetic traces of SigR-RsrA complex in the presence and absence of zinc at 35°C……117

Figure 71- 12% Native PAGE of complex in the presence and absence of zinc under oxidising conditions……122

Figure 72- RshA pET-21a test expression in Rosetta 2 pLysS, BL21 (DE3) and BL21 (DE3) pLysS at 20°C……132/133

Figure 73- SigH pET-21a test expression in BL21 (DE3) at 37°C and 20°C……133

Figure 74- SigH pCDFDuet-1 test expression in Rosetta 2 pLysS, BL21 (DE3) and BL21 (DE3) pLysS at 20°C……134

Figure 75- SigH pCDFDuet-1 and RshA pET-21a large scale expression in BL21 (DE3) cells at 20°C overnight……134

Figure 76- SigH pCDFDuet-1 and RshA pET-21a DE3 expression after lysis of cells……135

Figure 77- SigH pCDFDuet-1 and RshA pET-21a test expression in BL21 (DE3) cells at 20°C in the presence and absence of 10 µM zinc……136

Figure 78- ZAS1-ECF1 pCDFDuet-1 test expression in BL21 Rosetta 2, DE3 and pLysS at 20°C in the presence of zinc……137

Figure 79- ZAS2A-ECF2 pCDFDuet-1 test expression in BL21 Rosetta 2, DE3 and pLysS at 20°C in the presence of zinc……138

Figure 80- ZAS2B-ECF2 pCDFDuet-1 test expression in BL21 Rosetta 2, DE3 and pLysS at 20°C in the presence of zinc……138

Figure 81- ZAS3-ECF3 pCDFDuet-1 test expression in BL21 Rosetta 2, DE3 and pLysS at 20°C in the absence of zinc……139

Figure 82- ZAS2B-ECF2 IMAC Nickel affinity purification……139

Figure 83- ZAS2B-ECF2 Immobilised metal affinity chromatography (IMAC) Nickel column purification……140

Acknowledgements

I would like to take this opportunity to express my deepest appreciation to Professor Colin Kleanthous for the opportunity to work on the SigR-RsrA project within his Laboratory. Professor Kleanthous provided constant support and advice throughout my project as well as aiding my skills in research and scientific writing, for which I am extremely grateful. I would like to thank Dr Karthik Rajasekar for his assistance and training in the techniques used and for his support throughout the project. His encouragement in my independence and guidance in how to undertake research will prove invaluable in my future projects. I would also like to thank Dr Nicholas Housden and Dr Grigorious Papadakos for their time and expertise in discussions regarding my experimental design, results and problem-solving.

My final acknowledgement is to my parents, Gordon and Elaine, who without their endless support, enduring love, constant guidance, motivation and encouragement, I could not have made it this far. Thank you for supporting me and helping me follow my dreams.

I would like to dedicate this thesis to Professor Cécile Wandersman, who started my passion and excitement for research and helped drive my career in research during my time in her lab, at the Pasteur Institute in Paris.

Abbreviations

Amp	Ampicillin
β-ME	β-Mercaptoethanol
Cam	Chloramphenicol
CD	Circular Dichroism
cDNA	Complementary DNA
CPS	Counts per second, counts/s
dNTPs	deoxynucleotide triphosphates
DTT	Dithiothreitol
ECF	Extracytoplasmic function
FRET	Fluorescence resonance energy transfer
IM	Inner membrane
IMAC	Immobilised metal affinity chromatography
IPTG	Isopropyl β-D-1-thiogalactopyranoside
ITC	Isothermal Titration Calorimetry
LB	Lysogeny Broth
OM	Outer membrane
OMP	Outer membrane protein
PCR	Polymerase chain reaction
PIK	Protease Inhibitor Cocktail tablet
PMSF	phenylmethylsulfonyl fluoride
SDS-PAGE	Sodium dodecyl sulphate Polyacrylamide gel electrophoresis
SigR WI	SigR mutant with a tryptophan (W) mutation into an isoleucine (I) (SigR W88I, SigR W119I, SigR W88I W119I)
SigR*	SigR W88I W119I
SigR* FW	SigR mutant with a phenylalanine (F) mutation into a tryptophan (W) (SigR* F171W, SigR* F159W)
Str	Streptomycin
ZAS	Zinc-anti-sigma

1- Introduction

Gram-positive and Gram-negative bacteria contain sigma factors many of which are regulated by anti-sigma factors. Sigma factors (σ) are a subunit of RNA polymerase and control expression of genes within their regulon. Anti-sigma factors respond to environmental changes in the intracellular or extracellular medium. These proteins act as regulatory sensors maintaining cellular homeostasis and survival. The structure and mechanism for how these proteins can sense and respond to different environmental stresses and what genes are involved in maintaining homeostasis is poorly understood. A thorough biophysical characterisation of many of these sigma-anti-sigmas is lacking.

This study set out to understand the regulation of sigma factors and their interactions with anti-sigma factors, focusing on the model system SigR-RsrA from *Streptomyces coelicolor*. The following sections will provide general introductions to sigma factors and anti-sigma factors, the effect of environmental stresses within the bacterial cell and the response of these proteins to redox imbalance, initiating survival mechanisms to protect the cell from damage.

1.1. σ; A transcriptional subunit of RNA polymerase holoenzyme

All bacteria contain a single ~400kDa RNA polymerase, which catalyses gene expression by the synthesis of RNA transcripts from DNA (Procopio et al. 2012). Core RNA polymerase is a multisubunit protein consisting of $\alpha_2\beta\beta'\omega$ (Figure 1). There is an additional subunit called sigma (σ) that completes RNA polymerase forming the holoenzyme. The α subunits contain an amino-terminal domain responsible for dimersation of the two α subunits and interaction with the β and β' subunits, initiating subunit assembly. The α carboxy-terminal domain is responsible for DNA binding and interaction with the σ subunit (Ross et al. 2001). The β' subunit aids in the binding of RNA polymerase to DNA and contains structures crucial for transcription. The β subunit is involved in antibiotic resistance, and the ω subunit is thought to have a role in maintaining the conformation of the β' subunit in a non-aggregated form so it can form the core enzyme (Murakami 2013).

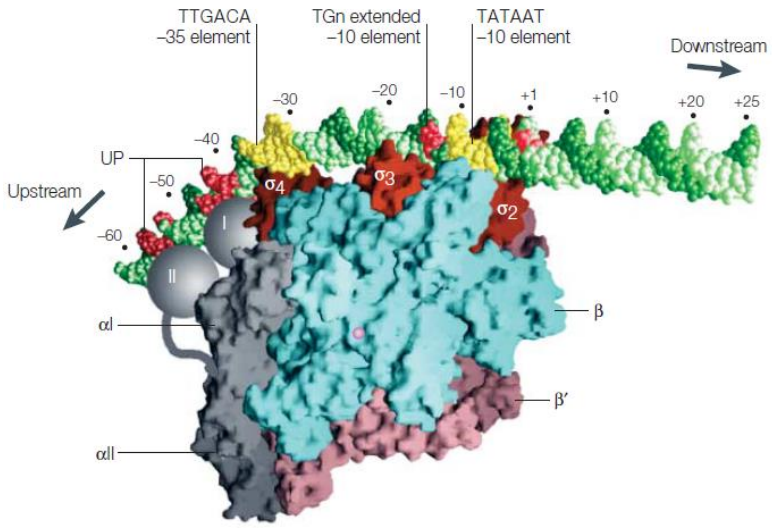


Figure 1- Prokaryotic RNA polymerase holoenzyme $\alpha_2\beta\beta'\sigma$ bound to DNA. RNA polymerase binds DNA via the sigma subunit at promoter regions, -10 and -35, in a closed-complex. Double stranded DNA is shown in green, highlighting the -10 and -35 promoter regions in yellow, and the extended -10 and UP elements in red. α subunits are shown in grey; αI and αII are the amino-terminal domains and I & II spheres represent the carboxy-terminal domains bound to the DNA. β and β' subunits are shown in light blue and pink respectively. σ regions 2-4 are shown in red bound to various regions of the DNA, notable regions 2 and 4 bound to the -10 and -35 DNA promoter regions respectively. ω subunit is not shown but present on the rear side of this structure located near the σ subunits (Murakami et al. 2002).

1.2. The role of σ in the gene transcription cycle

Core RNA polymerase associates with a σ factor forming the holoenzyme, which is then directed by the σ factor to the -10 and -35 DNA promoter regions upstream of the transcription initiation site (+1) on the gene for transcription, forming a closed complex. The DNA in the promoter site is unwound to about ~15 bases, forming an open-promoter complex of ssDNA, which is used as a template for transcription (Borukhov and Severinov 2002). RNA polymerase catalyses the polymerisation of ribonucleoside 5'-triphosphates (NTP's) using the template in a 5'-3' direction. RNA polymerase moves along the template unwinding the double strand and elongating the RNA chain, rewinding the DNA template behind it. Once the RNA transcript reaches ~10 nucleotides, the σ subunit is released from RNA polymerase and synthesis of the RNA transcript continues until a termination signal is encountered and RNA polymerase dissociates (Darst 2001) (Figure 2).

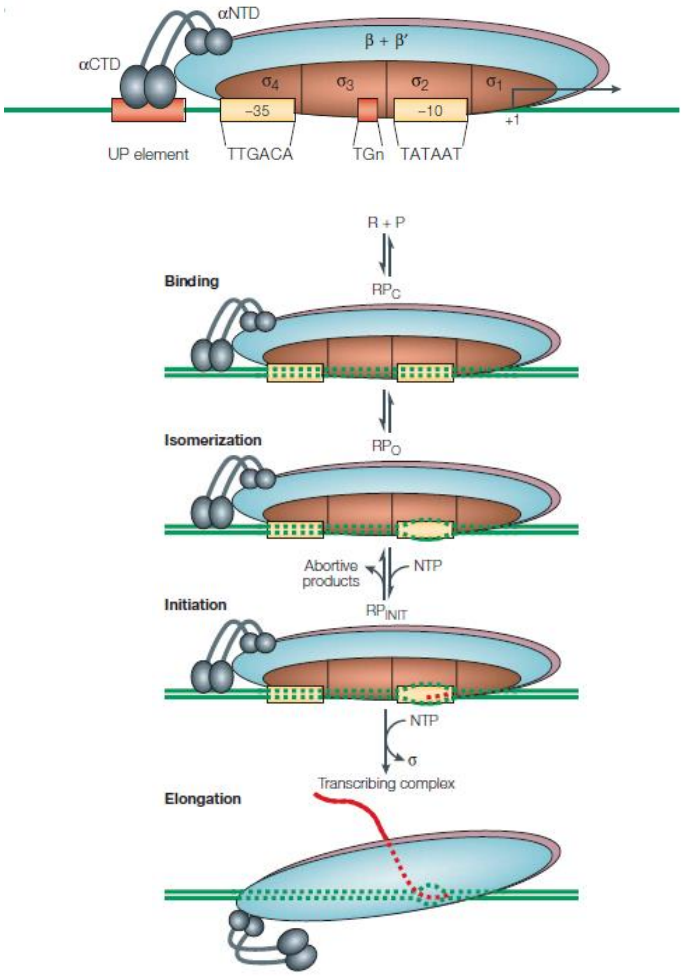


Figure 2- Prokaryotic transcription cycle. RNA polymerase holoenzyme is composed of $\alpha_2\beta\beta'\omega$. The α subunit is composed of a transcriptional activator (NTD and CTD) that binds to an upstream UP element. σ binds RNA polymerase forming the holoenzyme, and directs the enzyme to the specific DNA promoter regions, -10 and -35. DNA is unwound breaking the hydrogen bonds to provide a single-stranded transcription template and an open-promoter complex. RNA polymerase catalyses the polymerisation of NTP's into the elongating RNA transcript as it moves along the DNA. RNA polymerase dissociates when a termination signal is reached (Browning and Busby 2004).

1.3. Regulation of gene transcription

In prokaryotes, the majority of genes are constitutive and are transcribed continuously for the maintenance of housekeeping functions and metabolic homeostasis. Examples of these are genes encoding proteins for DNA and RNA metabolism, protein processing, folding and secretion, cellular division and energy metabolism (Gil et al. 2004). However, certain genes and their products are only transcribed when signalled to do so or repressed when the level is in excess, to reduce the waste of energy and resources to the cell. An example of this regulation is the synthesis of tryptophan (Trp) for use in protein translation. The genes on the Trp operon that are transcribed encode enzymes involved in the biosynthetic pathway of tryptophan. When high levels of tryptophan accumulate, expression of the enzymes involved must be inhibited (Mayer 2010). It is tryptophan that binds as a co-repressor,

allowing an activated repressor to bind the operator site and terminate transcription. The Trp operon is an example of a repressible promoter (Shaw 2008).

Regulation of gene expression at the transcriptional level is a major mechanism in prokaryotes. However, regulation of gene expression is also controlled at other stages of the transcriptional and translational level (Winkler and Breaker 2005).

Some mRNA molecules act as riboswitches. They have a receptor which binds to a range of small molecules in response to environmental signals, such as changes to the pH, temperature, nutrient concentration or presence and absence of a ligand. They undergo a specific conformational change in response, controlling the termination of gene transcription and initiation of protein translation (Winkler and Breaker 2005). siRNA (Short interference RNA) or antisense RNA is a single-stranded non-coding RNA molecule with a sequence complementary to an mRNA transcript (Nishizawa et al. 2012). It interacts with its target RNA by hybridisation forming dsRNA and altering the secondary structure. dsRNA is unable to be translated and is degraded by the cell (Georg and Hess 2011).

Another important mechanism of gene expression regulation at the transcriptional level is by σ factors. σ factors are present in prokaryotes and eukaryotes, and in the latter do not only control gene regulation, but also cell signaling, chromatin modifications and RNA splicing (Phillips 2008). Some sigma factors associate with RNA polymerase under certain environmental conditions, when certain genes are required and when a signal activates them to do so. The binding of the σ factor is therefore regulated by several different mechanisms.

1.4. Sigma factor families are based on function of transcribed genes

All bacteria contain at least 1 σ factor necessary for the transcription of housekeeping genes. Many contain several alternative σ factors with different DNA promoter specificities, to regulate the

transcription of different target genes within their regulon. σ factors are activated by and respond to different signals (Campbell et al. 2008); such as nutrient deprivation, temperature, cell density, environmental stresses (Campbell et al. 2003), protein misfolding, oxidative stress and pH (Paget and Helmann 2003).

σ factors can belong to one of several different families, based on the function of the genes they transcribe within their regulons. One σ family is the σ^{70}, the most abundant family containing σ factors that transcribe housekeeping genes. σ^{32} sigma factors transcribe genes involved in stabilising or refolding of proteins in response to heatshock (Cho et al. 2014). σ^{28} or *fliA,* transcribes genes involved in flagella biosynthesis (Campbell et al. 2008). σ^{38} or *rpoS*, regulates gene expression in the stationary phase (Cho et al. 2014). The σ^{54} family (also known as σ^{N}) transcribe genes for the assembly of nitrogen compounds and metabolism (Mooney et al. 2005).

The σ^{70} and σ^{54} are two major structural families in which σs have been characterised; they are structurally and functionally distinct from each other. They have different DNA promoter specificities with σ^{54} binding -12 and -24 DNA bases, and σ^{70} binding the -10 and -35 bases of DNA (Janaszak et al. 2007). The σ^{54} family also require a source of energy in the form of ATP hydrolysis and additional proteins to aid formation of promoter complexes (Borukhov and Severinov 2002).

1.5. σ^{70} family structure and function

The σ^{70} sigma factors are subdivided into four phylogenetically distinct subfamilies on the basis of their structure and function. There are four distinct regions of highly conserved amino acid sequences within this family; σ^{1}, σ^{2}, σ^{3} and σ^{4}. Proteins of the σ^{70} family contain up to three α-helical domains, each connected by a flexible linker region, allowing a large degree of flexibility in the conformation of the structures (Borukhov and Severinov 2002). Combinations of these different regions and their functions are what group the σ factors.

1.6. σ regions and subregions

σ region 1 (σ^1) corresponds to N-terminal 1.1 subregion (Figure 3). This region is not common in the σ^{70} family and is found to be mobile in the free σ and when bound to RNA polymerase (Borukhov and Severinov 2002). It has a role in aiding efficiency of the holoenzyme binding the DNA promoters. Region 1 inhibits free σ recognising DNA promoter regions through its highly negative charge. In the holoenzyme, subregion 1.1 occludes the DNA binding channel, using the highly negatively charged nature to mimic DNA (Borukhov and Severinov 2002).



Figure 3- Four distinct regions of highly conserved amino acid sequences within the σ^{70} family; σ^1, σ^2, σ^3 and σ^4. The σ^{70} family is composed of regions 1-4, and subregions 1.1-4.2. These four regions and subregions have different functions in associating with RNA polymerase to form the holoenzyme, and with the DNA in initiating gene transcription. Combinations of these different regions and their functions are what group the σ factors.

σ region 2 (σ^2) corresponds to subregions 1.2-2.4 (Figure 3). σ subregion 1.2 and 2.2 mediate the primary interaction with a coiled-coil element of the β' subunit of RNA polymerase (Borukhov and Severinov 2002). Subregion 2.3 has conserved aromatic residues which are thought to aid in the melting of dsDNA during the initiation of gene transcription (Borukhov and Severinov 2002). Conserved basic residues in subregions 2.2 and 2.3 are critical in binding the DNA (Campbell et al. 2002). It is subregion 2.4 that interacts with the -10 DNA promoter sequence, but only on the non-template strand and when bound to RNA polymerase (Borukhov and Severinov 2002). The structure of this region has been solved in several σ factors, and has a bundle of three α-helices. It is the second α-helix which makes contact with the β'-subunit of RNA polymerase (Paget and Helmann 2003).

σ region 3 (σ^3) is a three α-helix domain, with residues of the first α-helix interacting with an extended -10 promoter motif located upstream of the -10 DNA promoter region bound by σ^2 (Campbell et al. 2002). This is thought to provide additional contacts between RNA polymerase and the

DNA (Sterberg et al. 2011). This region is less conserved amongst members of the σ^{70} family (Paget and Helmann 2003) (Figure 3). Subregion 3.2 has been proposed to aid in the formation of a transcription initiation site (Borukhov and Severinov 2002).

σ region 4 (σ^4) corresponds to C-terminal subregions 4.1 and 4.2 (Figure 3). Subregion 4.1 is proposed to bind transcriptional activators when bound to RNA polymerase, to aid initiation of gene transcription (Wösten 1998). It is the side-chains of residues in subregion 4.2 that interacts with the -35 DNA promoter sequence (Campbell et al. 2002). Region 4 also binds the β-subunit flap of RNA polymerase when forming the holoenzyme (Campbell et al. 2008).

These individual regions of free σ are only capable of very weak interactions with the DNA. The distance between regions 2.4 and 4.2 in the conformation of free σ is 40Å. This is shorter than the distance of -10 and -35 promoter DNA regions, meaning it is not possible to bind the DNA promoter regions as free σ. It is only when σ binds to RNA polymerase that it is capable of binding promoter DNA, due to a conformational change caused by the β subunit moving regions 2 and 4 to a distance capable of binding -10 and -35 DNA promoters. This ensures that σ^{70} σ factors cannot bind to the DNA, and occlude the promoter sites when transcription is not necessary (Borukhov and Severinov 2002).

1.7. σ factor subgroups

Group 1 σ factors of the σ^{70} family possess all four σ regions (Figure 4). This group is composed of essential housekeeping σs that direct general transcription for cell survival. There is usually only one group 1 σ in each bacterial species. Group 2 are closely related in sequence to group 1 σ factors, they possess all four σ regions but are not essential for cell growth (Figure 4). These sigma factors aid bacteria when they enter a stationary-phase of growth as a survival mechanism. Genes expressed range from thermotolerance, DNA damage repair and osmoprotection. Group 3 possess σ regions 2, 3 and 4 (Figure 4). They usually play a role in controlling gene expression in response to checkpoints in

development and heat shock. The group 3 σs can be subdivided into groups of functionally related factors. Functions range from preventing and repairing damage by heat shock, sporulation and flagella biosynthesis (Paget and Helmann 2003). Groups 2, 3 and 4 σ factors are all activated by a signal, and respond by initiating transcription of genes within their regulons. They are present in Gram-positive and negative bacterial species (Paget and Helmann 2003).

Group 4 possess σ regions 2 and 4, connected by a flexible linker region (Campbell et al. 2008) (Figure 4). This group is known as the extracytoplasmic function (ECF) subfamily, because it contains the largest and most divergent set of σ factors, which are environmentally responsive to a wide range of extracytoplasmic signals.

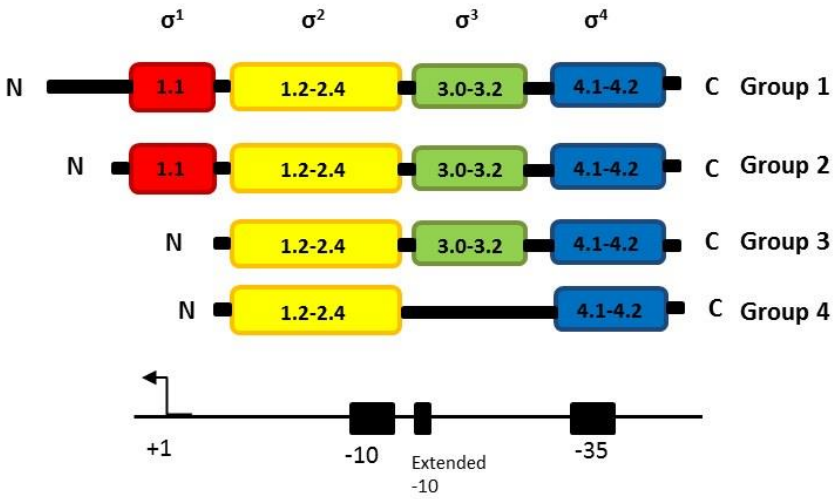


Figure 4- The four phylogenetically distinct σ subfamilies within the σ^{70} family. The four distinct regions of highly conserved amino acid sequences; σ^1 (red), σ^2 (yellow), σ^3 (green) and σ^4 (blue) that make up the four subfamilies within the σ^{70} family. Each region is connected by flexible linker regions. Combinations of these different regions and their functions are what group the σ factors. N and C represent the amino- and carboxy-terminus respectively, -10 and -35 represent the DNA promoter binding sites in which region 2 and region 4 bind, +1 is the transcription start site.

1.8. Extracytoplasmic function (ECF) σ subfamily

σ factors within this subfamily respond to changes within the periplasm, membrane and extracellular environment that have disrupted physiological processes in the cytoplasm (Kazmierczak et al. 2005).

These changes are usually harmful and result in damage or cell death. In bacterial pathogens, ECF σ factors regulate the expression of genes associated with virulence and transmission in response to the host environment. This survival requires sensing of the stress by the appropriate ECF σ factor, and a rapid response in altering gene transcription (Brooks and Buchanan 2008). Bacteria have multiple sets of regulons, encoding specific sets of response genes. These regulons are transcribed by their respective ECF σ factor-RNA polymerase holoenzyme, in response to an environmental activating signal (Brooks and Buchanan 2008).

ECF σ factors contain only region 2 and region 4, connected by a flexible linker region, involved in binding the -10 and -35 DNA promoter regions respectively. This provides them with a unique identification from other σ factors of group 1-3. The ECF σs recognise different sequence promoters for the -10 and -35 regions, and regulate the expression of different regulons of genes to other groups (Raivio and Silhavy 2001).

ECF σ factors are generally 20-30 kDa in size and present in both Gram-positive and Gram-negative bacteria. They are the most abundant type of σ factors, with the number of ECF σs in a bacterial species often outnumbering groups 1-3 of σ factors combined (Campbell et al. 2003). *Streptomyces coelicolor* has a total of 65 σ factors, 51 of these are group 4 ECF σ factors. *Bacillus subtilis* has 7 ECF σ factors (Paget et al. 2002), 13 in *Caulobacter crescentus*, 19 in *Pseudomonas aeruginosa* (Helmann 2002) and 10 in *Mycobacterium tuberculosis* (Cole et al. 1998). This demonstrates the wide range of environmental signals each bacterium can sense. Not all of the environmental signals that activate sigmas have been identified. Mechanisms of activation, structures of ECF σs, mechanisms of gene transcription regulation and the regulons which they transcribe are also poorly understood (Brooks et al. 2008).

For the change in the environment to be communicated inside the cell to initiate gene expression by a specific σ factor, the signal must pass through bacterial membranes to reach the cytosol. The signal molecules may be small enough to diffuse through the membrane, use membrane-

bound anti-σs or require membrane proteins to communicate the signal. Some bacteria contain two-component signalling pathways for the communication across their membranes (Brooks and Buchanan 2008).

1.9. σ factor regulation mechanisms

All identified Gram-negative ECF sigma factors interact and form a complex with an anti-sigma factor (anti-σ), which is the negative-regulator of the complex (Brooks and Buchanan 2008). The role of this anti-σ factor is to reversibly bind the ECF σ factor and control its activity by inhibiting its ability to associate with RNA polymerase and direct the holoenzyme to the DNA promoter regions of its regulon, regulating gene transcription (Brooks and Buchanan 2008).

σ factors are responsible for transcribing their own structural genes, establishing a positive feedback loop for their own synthesis. To prevent continuous transcription and accumulation of the σ factors, genes for the cognate anti-σ factor are present on the same operon downstream of the σ gene. Ensuring both σ and anti-σ are co-transcribed forming a complex and turning off further gene transcription (Kallifidas et al. 2010). Some σ factors are also transcribed as inactive precursors that are activated by a signal causing proteolysis (Helmann 2002).

σ factor activity can also be regulated when bound to RNA polymerase holoenzyme by appropriators. The efficiency with which σ factor region 4.2 binds to the -35 DNA promoter region on its regulon can be either increased or decreased by activators and repressors respectively (Campbell et al. 2008). Some regulatory factors affect DNA promoter recognition by the σ factor by disrupting the interaction of σ region 4 and the β subunit of RNA polymerase holoenzyme, altering the separation between σ region 2 and 4, affecting its ability to bind the DNA promoter regions (Borukhov and Severinov 2002).

1.10. Anti-sigma factors

Anti-σs are either cytoplasmic or membrane-bound. The membrane-bound anti-σ usually have a C-terminal periplasmic domain to anchor them to the membrane where the stress is sensed, and an N-terminal cytoplasmic domain which is bound to the σ factor, controlling its activity (Raivio and Silhavy 2001).

Anti-σ factors can also be regulated. Anti-anti-σ factors relieve the transcriptional repression by binding and inhibiting the anti-σ and allow σ factor activity (Campbell et al. 2008) (Figure 5). The serine and threonine kinase anti-σs can phosphorylate the anti-anti-σ at conserved serine or threonine residues, causing the dissociation of anti-anti-σ, and allowing the anti-σ to bind σ and turn off further gene transcription. This is an example of modulation via partner-switching models, used to determine the concentration of the active σ factor (Greenstein et al. 2007). An example is σ^B and σ^W from *Bacillus subtilis*, the activity of which is regulated by RsbW anti-σ. Anti-anti-σ RsbV binds RsbW to relieve inhibition of σ^B or σ^W, before RsbW phosphorylates bound RsbV causing its dissociation and re-instatement of RsbW anti-σ activity (Greenstein et al. 2007). Some anti-σs can stimulate transcription of a phosphatase, which removes the phosphate from the anti-anti-σ, re-activating it. An example is the *Bacillus subtilis* anti-σ RsbT, which stimulates the expression of RsbU phosphatase (Greenstein et al. 2007).

Co-anti-σ factors work cooperatively with their partner anti-σ to either inhibit or re-direct the activity of σ (Figure 5). An example is *Escherichia coli*, where σ^E is bound to RseA anti-σ, which is anchored within the inner membrane. The periplasmic co-anti-σ RseB functions to stabilise this interaction between σ^E-RseA (Campbell et al. 2008).

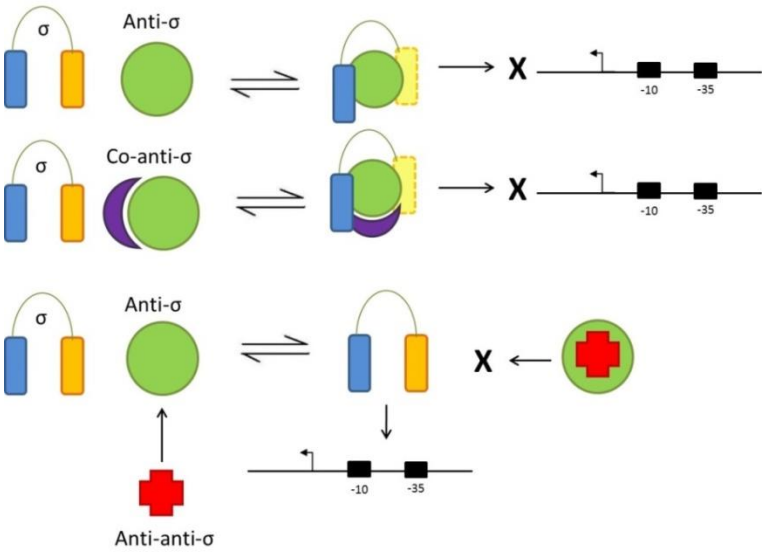


Figure 5 – Anti-σ factor regulation mechanisms. Anti-σ factors bind and regulate the activity of σ factors, inhibiting gene transcription. Anti-σ activity is regulated in several ways, co-anti-σ (purple) works in partner with the anti-σ (green) to inhibit the activity of the σ (blue and yellow corresponding to region 2 and 4). Anti-anti-σ (red) bind anti-σ, preventing it from binding σ, allowing gene transcription to occur. The DNA promoters -10 and -35 regions are shown at the beginning of the gene regulon.

Anti-σ factors can also have their activity regulated by secretion from the cell, relieving inhibition of the σ factor (Helmann 1999) (Figure 6). An example is during flagellar synthesis, and the regulation of transcription of early, middle and late genes. FlgM inhibits σ^{28} from transcribing late genes until middle genes and assembly of the hook-basal-body of the flagellar is completed. FlgM then dissociates from σ^{28} to initiate late gene transcription and FlgM is secreted from the cell (Aldridge et al. 2006).

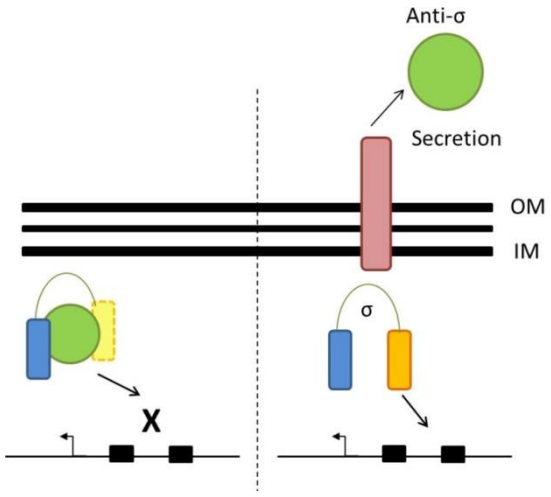


Figure 6- Anti-σ factor regulation by secretion from the cell. Anti-σ factors bind σ factors and control their activity. Another method in which anti-σ factors are themselves regulated, is by the secretion of the anti-σ from the cell, which is controlled by various other proteins. This leaves the σ factor free to initiate gene transcription.

Certain signals generated within the cell can alter activity of anti-σ factors, for example proteolysis of the anti-σ after its translation, relieving the inhibition of the σ factor (Brooks and Buchanan 2008) (Figure 7). An example is σ^E-RseA from *Escherichia coli*, RseB acts to inhibit proteolysis of RseA anti-σ. When the transcription of genes by σ^E is required, a signal leads to the activation of DegS serine protease which proteolytically cleaves the RseA periplasmic domain causing the release of σ^E-RseA into the cytoplasm. RseP intra-membrane protease then further cleaves RseA at a second site. This sequential proteolysis ends with the complete degradation of the anti-σ RseA by ClpXP, relieving the inhibition of σ^E (Brooks and Buchanan 2008).

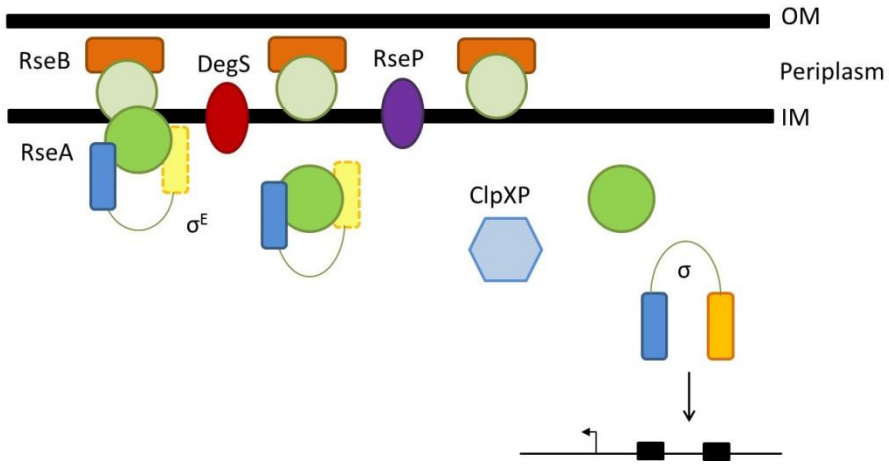


Figure 7- Signals for proteolysis of anti-σ. Some anti-σ factors have their activity regulated by proteolysis. Some anti-σs are membrane-bound, forming a complex with a σ factor. When transcription is needed a signal activating DegS serine protease is sensed. This causes the cleavage of the anti-σ RseA periplasmic domain, releasing the σ-anti-σ into the cytosol. Further cleavage is caused by RseP, causing the release of the σ factor, and complete degradation of the anti-σ by ClpXP.

Anti-σ factors regulate a range of processes within bacterial cells by their interaction with σ factors; sporulation, pigment production, virulence, bacteriophage growth, transcription regulation,

morphological differentiation, antibiotic production and response to cellular stress (Hughes and Mathee 1998).

The structure, function and mechanism of σ factors is well understood and highly conserved. The wide diversity in structure, function and mechanism of anti-σ factors and their regulation of σ factors and anti-σ factor regulation mechanisms, demonstrates the wide range of environmental stresses that bacterial species sense and respond to for their survival (Campbell et al. 2008).

1.11. Reducing environment of the cytoplasm

The bacterial cytoplasm is a reducing environment. Bacteria use oxygen in aerobic metabolism for respiration and the generation of ATP. Reactive oxygen species (ROS), such as hydrogen peroxide (H_2O_2), hydroxyl radicals (·OH) and superoxide anion radicals (O_2^-), are a by-product of aerobic respiration through the incomplete univalent reduction of molecular oxygen during the electron transport chain. Both H_2O_2 and O_2^- have preferred biological targets, whereas ·OH is indiscriminate (Green and Paget 2004). Hydroxyl radicals are also generated from the reaction of H_2O_2 with Fe^{2+} via the Fenton reaction. Iron is present in the cell for growth, transport, storage and electron transport. Iron is rarely found free within the cytoplasm, because it is highly toxic and promotes the activation and partial reduction of oxygen (Green and Paget 2004).

ROS can be produced through ionising and near-UV radiation within the environment. There are also externally applied oxidative stresses, for example when bacteria invade the host immune cells which produce an oxidative burst (Antelmann and Zuber 2010). There is usually a balance between oxidants and antioxidants within the cytoplasm. Low levels of ROS do not cause a change to the cytoplasmic environment, it is only when they accumulate above a certain level that the cell's cytoplasm is unable to balance do they become harmful. This causes oxidative stress affecting proteins, lipids, DNA and RNA (Cabiscol et al. 2000).

These oxygen free radicals target polyunsaturated fatty acids within the membrane, they remove electrons from the lipids causing peroxidation, affecting the fluidity of the membrane and altering the membrane properties. These radicals also attack the sugars and nucleotide bases of DNA, introducing breaks within the dsDNA molecules. Proteins are damaged by oxidation of cysteine sulfhydryl groups (-SH), formation of disulphide bonds (-S-S-), protein cross-linking and peptide fragmentation, affecting their structure or function (Cabiscol et al. 2000).

Bacteria have evolved several highly conserved mechanisms to sense and respond rapidly to protect themselves against oxidative stress, maintain the reducing environment, and to repair damage by oxidative stress (Linke and Jakob 2003). They are termed redox 'switches' as they will either be activated or inactivated by oxidative stress, converting the chemical redox signal into a biological output to alter the redox state. This includes isomerases, reductases, oxidases (Antelmann and Zuber 2010), the oxidoreductase thioredoxin and glutaredoxin proteins, enzymes like catalase, hydroperoxidase and superoxide dismutases. There are also antioxidants like NADPH, NADH, β-carotene, ascorbic acid, α-tocopherol and glutathione (GSH) molecules (Cabiscol et al. 2000). Oxidative stress also induces endonucleases, which act to repair damage caused to DNA and redox-sensitive transcription factors (Cabiscol et al. 2000).

1.12. Cysteine oxidation

Some redox-sensitive proteins contain cysteine thiol side-chains that are able to sense changes in the oxidative status of the cytoplasm. They do so via reversible formation of a variety of oxidation products, altering protein activity. Cysteine residues are not all equal in their sensitivity to oxidative stress. The majority of cysteine residues have 8-9 pKa, so under physiological conditions of ~ pH 7.4, the cysteine sulfhydryl (-SH) groups are protonated, and their reactivity without a catalyst is slow (Antelmann and Zuber 2010). Some cysteine residues have lower pKa values and act as nucleophiles reacting with the electron deficit region of the oxidised electrophile (Antelmann and Zuber 2010),

which becomes deprotonated forming a thiolate anion (-S^-). The thiolate anion group is much more sensitive and susceptible to oxidation and forms the intermediate sulfenic acid (-S-OH), which rapidly reacts with other cysteine thiol groups, forming intra- or intermolecular disulphide bonds. Formation of these oxidation intermediates are reversible until further oxidised into the irreversible products sulfinamide, sulfinic (-SOOH) and sulfonic acid (-SO_3H) (Figure 8) (Groitl and Jakob 2014).

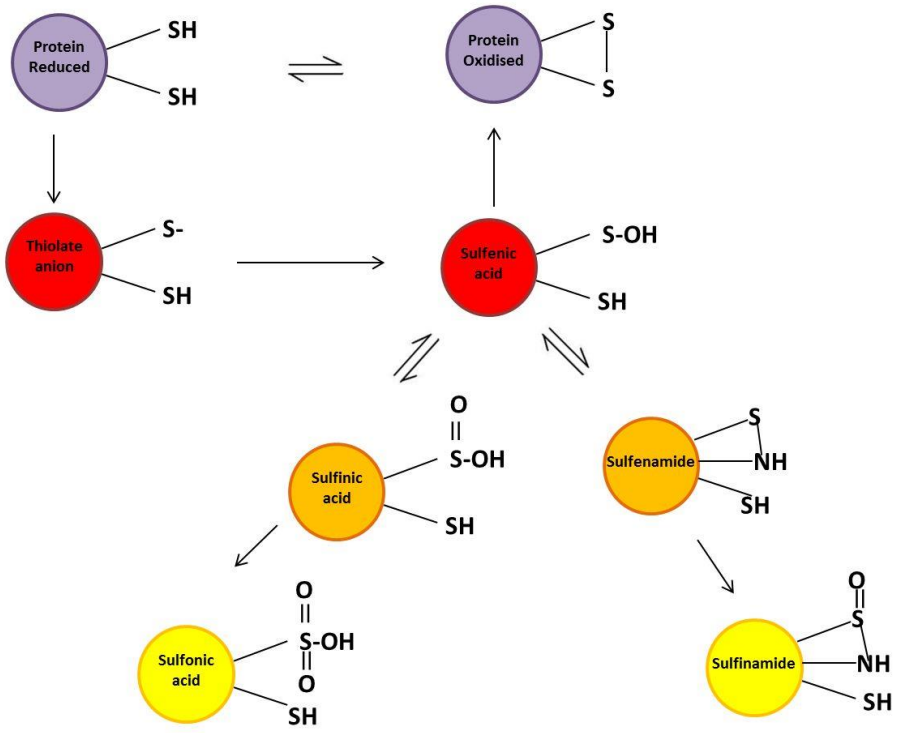


Figure 8- Cysteine oxidation products. Cysteine residues are sensitive to oxidation in redox sensitive proteins. Various states of oxidation of cysteine residues can occur under oxidative stress from the protonated sulfhydryl (-SH) group. The oxidation intermediates are more sensitive to oxidation and formation of intra- or inter-molecular disulphide bonds with other thiol groups. Most oxidation intermediates are reversible, however further oxidation can lead to irreversible cysteine residue products, like sulfinamide, sulfinic and sulfonic acid.

1.13. Thioredoxin antioxidant system

The role of thioredoxin is to maintain the reducing environment of the cytoplasm at a redox potential of -260 to -280 mV (Linke and Jakob 2003). It catalyses the reversible oxidation and reduction of protein disulphide bonds through thiol-disulphide exchange. The thioredoxin system uses thioredoxin reductase and the reducing potential of NADPH to reduce oxidation products via thiol-disulphide

exchange. Thioredoxin contains the conserved Cys-X-X-Cys motif which becomes oxidised during the disulphide exchange (Groitl and Jakob 2014).

One cysteine in the motif undergoes nucleophilic attack with the oxidised thiol group, forming a mixed intermolecular disulphide bond. The other cysteine in the motif further undergoes nucleophilic attack of this intermolecular disulphide bond, forming an intramolecular disulphide bond between both cysteine residues of thioredoxin (Figure 9). Oxidised thioredoxin can then be reduced by thioredoxin reductase and the reducing power of NADPH and recycled for further use in reducing the cytoplasm and protein-thiol groups (Groitl and Jakob 2014).

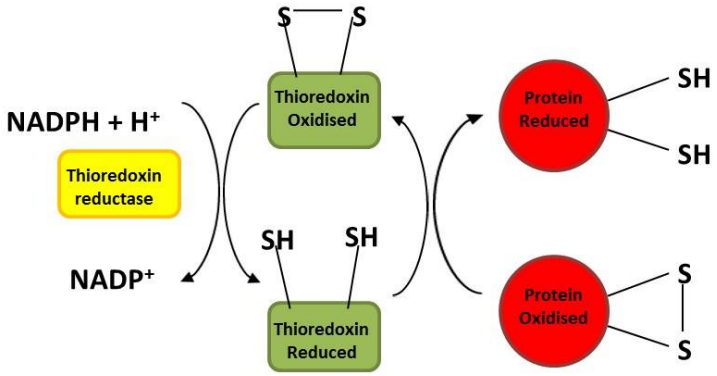


Figure 9 – Maintaining the reducing environment of the cytoplasm. The bacterial cytoplasm is a reducing environment, bacteria have developed several mechanisms to maintain this reducing environment and reverse the effect of oxidation. In red is an example of a protein with thiol (-SH) groups under reducing conditions, and the oxidised thiol groups (-S-S-). Thioredoxin (green) is an example of one mechanism in the cytoplasm that can reduce oxidised protein thiol groups via thiol-disulphide exchange. Thioredoxin then becomes oxidised itself, but can become re-reduced using thioredoxin reductase (yellow) and the reducing potential of NADPH and its redox active disulphide next to the flavin ring.

1.14. Glutaredoxin antioxidant system

Prokaryotes and eukaryotes contain the glutathione- glutaredoxin system (Newton and Fahey 2002). It belongs to the thioredoxin superfamily and consists of a cysteine-containing tripeptide glutathione (GSH), and small highly conserved thiol-disulphide oxidoreductases (Paget et al. 2001). Glutaredoxin reductase is able to reduce oxidised sulfhydryl thiol groups by the oxidation of the Cys-X-X-Cys motif

(Paget et al. 1998). The glutaredoxin system can reduce these bonds using glutathione (GSH) as an electron donor (Groitl and Jakob 2014).

1.15. Low molecular weight (LMW) thiols

Gram-positive species do not produce glutathione (GSH), but use alternative LMW thiols to maintain the reducing potential of the cell (Ung and Av-Gay 2006). Gram-positive Actinobacteria produce millimolar intracellular concentrations of mycothiol (MSH). The structure is comprised of a cysteine residue (Cys) acetylated at its amine group (*N*-acetylcysteine) and linked at its carboxyl group to glucosamine (GlcN) and a myo-inositol to reduce auto-oxidation (Figure 10) (Newton and Fahey 2002). Mycothiol plays an analogous role to glutathione, acting as a nucleophile donating hydrogen ions, but is structurally unrelated to GSH (Newton and Fahey 2002). The mycothiol system has a partner protein, mycothiol disulphide reductase (MSSM), involved in maintaining MSH in its reduced state within the cytoplasm (Newton and Fahey 2002).

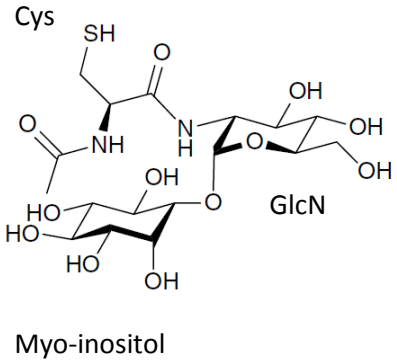


Figure 10- Structure of mycothiol. Mycothiol (MSH) contains a cysteine residue with its amine group acetylated and its carboxyl group linked to glucosamine (GlcN) and myo-inositol (Newton et al. 2009).

There are numerous other systems involved in monitoring and regulating the redox environment of the cell and highlights their importance for the survival of bacteria. These systems use redox sensor cysteine thiol groups or Fe-S clusters within different protein environments, showing flexibility in the signals they can sense and respond to.

Peroxiredoxins play a role in reducing H_2O_2. They contain a cysteine within their active site with a low pKa, which reacts directly with H_2O_2 forming a sulfenic acid intermediate (Groitl and Jakob 2014).

Disulphide bond protein family are involved in the transfer of electrons between the cytoplasm and the periplasm. The transfer of electrons into the cytoplasm enhances the oxidation of cysteine residues. Examples of members of this family are DsbA, B, C and D, which make up two disulphide pathways, oxidative and isomerisation (Heras et al. 2007).

DsbA is a highly oxidising protein that introduces disulphide bonds into proteins through thiol-disulphide exchange (Figure 11). DsbA has a partner, DsbB inner membrane protein that re-oxidises DsbA (Heras et al. 2007). DsbC is involved in the isomerase pathway, which acts as a proof-reading pathway re-arranging disulphide bonds formed by DsbA to form the correct bond. DsbC catalyses this step and becomes re-reduced itself by the inner membrane protein DsbD, which then becomes oxidised. This is linked to the cytoplasm via the thioredoxin-thioredoxin reductase system, which undergoes thiol-disulphide exchange with DsbD to return it to the reduced state (Heras et al. 2007).

DsbA is a member of the thioredoxin-fold family, it contains the Cys-X-X-Cys motif which it uses during thiol-disulphide exchange. DsbB contains a second pair of cysteine residues which it uses to re-oxidise DsbA. DsbD is an inner membrane protein with two periplasmic domains. Its C-terminal thioredoxin-like domain is linked to a transmembrane domain which allows it to interact with the cytoplasmic thioredoxin-thioredoxin reductase antioxidant system, through the transfer of electrons via cysteine pairs to be relayed to the substrate protein (Figure 11) (Heras et al. 2007).

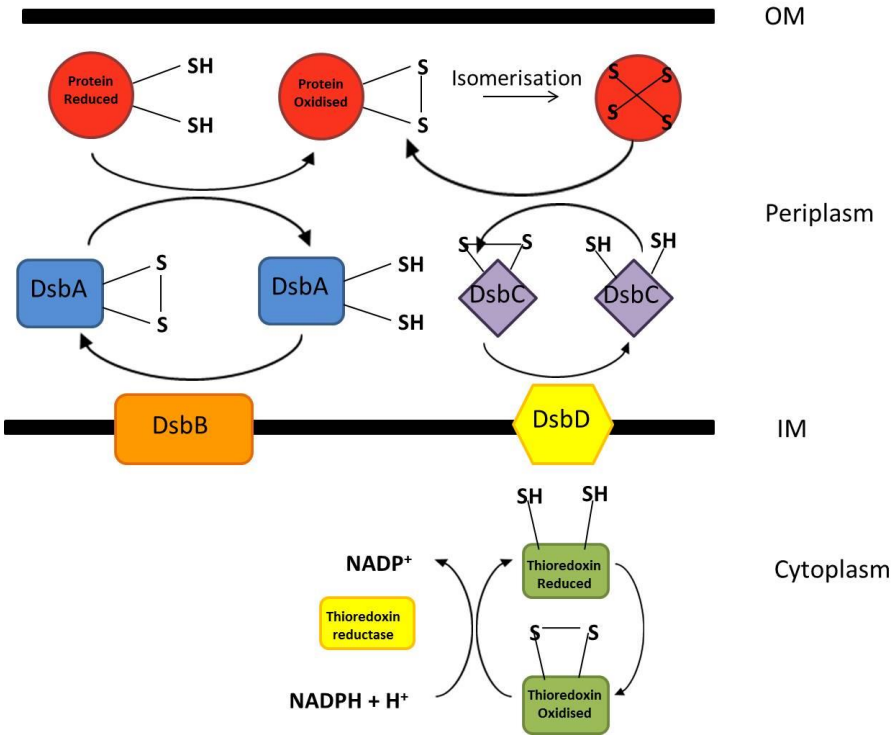


Figure 11- Formation of disulphide bonds within the periplasm by members of the disulphide bond family; DsbA, B, C and D. The oxidoreductase DsbA undergoes thiol-disulphide exchange with proteins containing sulfhydryl groups, becoming reduced itself. DsbA becomes re-oxidised by DsbB in the inner membrane. The disulphide bonds formed in the protein can undergo isomerisation, which is catalysed by DsbC. This step may also involve DsbA working with DsbC to rearrange disulphide bonds to form the correct bond. DsbC is re-reduced by DsbD in the inner membrane. DsbD is reduced itself via disulphide-exchange with cytoplasmic thioredoxin-thioredoxin reductase antioxidant system (Heras et al. 2007).

During oxidative stress in the cytoplasm, levels of ATP decrease, removing the energy source and directly inactivating DnaK and GroEL ATP-dependent chaperones, but activating Hsp33 (Groitl and Jakob 2014). Hsp33 is present in the cytoplasm of Gram-positive and negative bacteria. It plays a role in protecting cytosolic proteins from aggregation during oxidative stress caused exclusively by hypochlorous acid (HOCl), or H_2O_2 along with high temperatures encountered during inflammation (Groitl and Jakob 2014). Hsp33 contains a Cys-X-Cys-Zn-Cys-X-X-Cys motif, which when oxidised causes local unfolding of the protein and two monomers form the activated Hsp33 dimer (Groitl and Jakob 2014). Zinc stabilises Hsp33 from proteolytic degradation and causes a much faster activation by hydrogen peroxide than zinc-free Hsp33 (Paget and Buttner 2003).

Another mechanism in which bacteria rapidly respond to changes in oxidative stress, is by the oxidation of certain redox-sensitive transcription factors, affecting gene transcription (Antelmann and Zuber 2010). OxyR is an oxidative stress response transcription factor in *E. coli.* OxyR directly senses an increase in cytoplasmic peroxide levels and S-nitrosylation of cysteine thiol groups caused by reactive nitrogen species (RNS) like NO. Peroxide exceeding physiological levels of >20 nM (D'Autreaux, and Toledano 2007), causes rapid oxidation of OxyR that initiates transcription of the 20 genes within its regulon, including detoxification enzymes. OxyR can also induce the transcription of thioredoxin and glutaredoxin, to re-reduce the cytoplasm and thiol-groups. Glutaredoxin-1 is responsible for reduction of OxyR and turning off its transcriptional activity by autoregulation (Groitl and Jakob 2014).

SoxR (Superoxide response regulator) is an Fe-S cluster-based sensor of superoxide and nitric-oxide stress in *E. coli*. SoxR contains one $[2Fe\text{-}2S]^{1+}$ cluster per subunit. When exposed to oxidising conditions the cluster becomes oxidised by a single electron to $[2Fe\text{-}2S]^{2+}$. This allows SoxR transcription factor to distort the promoter DNA site of *soxS*, which can then form a complex with RNA polymerase, initiating gene transcription (Green and Paget 2004). In response, SoxR activates the expression of SoxS transcription factor, which transcribes genes involved in DNA and [Fe-S] cluster repair and redox homeostasis (Green and Paget 2004). Once the oxidative stress has been removed, proteolysis degrades SoxS turning off any further gene transcription (Gu and Imlay 2011).

1.16. Sigma anti-sigma complexes in other bacterial species

Sigma-anti-sigma complexes exist in a wide range of bacterial species, with different levels of sequence and structural similarity. These complexes are all activated in response to different environmental signals, undergo different activation mechanisms and transcribe different sets of genes within their regulons.

1.16.1. *Rhodobacter sphaeroides* ChrR-SigE

ChrR from the Gram-negative photosynthetic bacterium *Rhodobacter sphaeroides* is a member of the ZAS (Zinc-anti-sigma) family, involved in the regulation of SigE ECF sigma factor. It contains the ZAS motif and coordinates a zinc ion. The complex responds to singlet oxygen stress, which is a toxic byproduct of aerobic photosynthesis (Campbell et al. 2008). SigE directs the transcription of *cycA* gene, which encodes the periplasmic electron carrier cytochrome c_2, it is also responsible for the transcription of the operon encoding both *chrR* and *sigE* gene (Newman et al. 2001).

ChrR is composed of an N-terminal anti-sigma domain (ASD) and a C-terminal Cupin-like domain (CLD). Both domains coordinate a zinc ion. The N-terminal ASD occludes the RNA polymerase binding sites of SigE by altering the structure of region 4 in an unfavourable conformation. The role of zinc in this domain is to maintain the fold between the N-terminal loop and 3 α-helices on the domain (Campbell et al. 2008) (Figure 12).

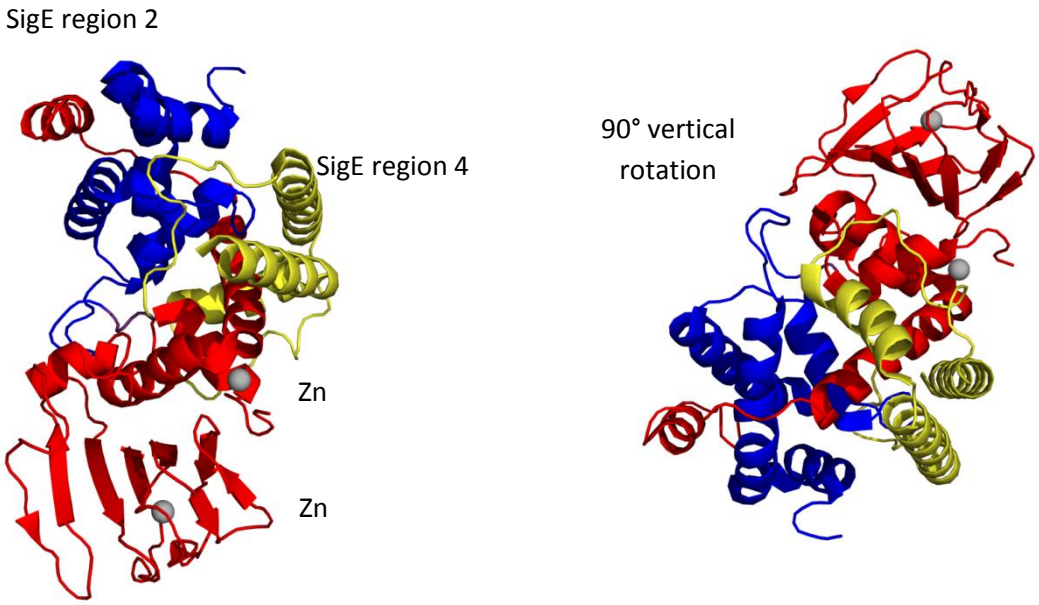


Figure 12- Structure of ChrR-SigE complex. ChrR anti-sigma factor is shown in red, bound to two zinc ions (grey spheres), one in the N-terminus (helical) and one in the C-terminus (β-sheets). SigE ECF sigma factor is shown as region 2 (blue) and region 4 (yellow)(2Q1Z) (Campbell et al. 2007).

The C-terminal CLD has a β-barrel domain, which is sensitive to singlet oxygen and releases SigE. Deletion of any of the C-terminal ligands that coordinate zinc prevents the complex from dissociating, as these residues are necessary for oxygen to promote dissociation (Campbell et al. 2008).

The data of Campbell, Darst and colleagues suggests ~33% of group 4 ECF sigma factors are regulated by anti-sigmas containing an N-terminal cytoplasmic ASD with or without a preceding transmembrane-spanning region (Campbell et al. 2007).

1.16.2. *Mycobacterium tuberculosis* σ anti-σ factors

More than 70 species of *Mycobacteria* exist, they are an acid-fast Gram-positive species usually found in wet environments. They possess a unique cell wall forming an impermeable layer to acids, alkalis, antibiotics and oxidative species, which is vital to their survival (Madigan et al. 2000). They are intracellular pathogens that survive in macrophages inside the human body (World Heath Organisation 2012). Macrophages release a high concentration of superoxides to kill them (Linke and Jakob 2003). The genome of *Mycobacterium tuberculosis* encodes 190 regulators of transcription; there are 11 2-component systems, 5 unpaired response-regulators, 11 protein kinases and 13 σ factors (SigA-SigM), 10 of which are group 4 ECF σ factors (Barik et al. 2010). These allow the cell to respond to stress, enabling their survival particularly within hosts.

1.16.3. *Mycobacterium tuberculosis* RshA-SigH

SigH is an ECF sigma factor that is controlled by RshA, a ZAS anti-sigma. This complex is activated by oxidative, nitrosative and heat stress (~55°C) (Song et al. 2003). SigH transcribes the operon with *sigH* and *rshA* genes in a positive feedback loop for its own expression. SigH transcribes SigE and SigB transcription factors, which are also involved in response to several environmental stresses,

demonstrating the complexity of the sigma anti-sigmas within *Mycobacterium tuberculosis* (Figure 13) (Song et al. 2003).

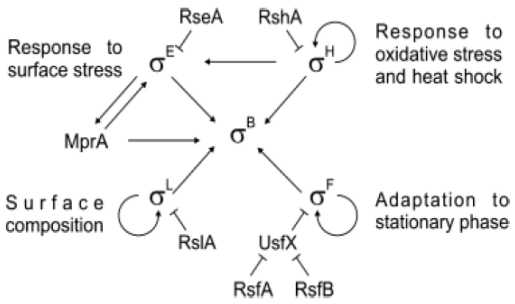


Figure 13- Complexity of sigma factors in *Mycobacterium tuberculosis*. SigH is responsible for the transcription of SigB and SigE transcription factors. These in turn are responsible for the transcription of other sigma factors which express genes in response to different environmental stresses (Rodrigue et al. 2006).

In response to oxidative and heat stress, SigH transcribes the thioredoxin-thioredoxin reductase system to maintain redox homeostasis. *hsp70, clpB* and *dnaK* genes are transcribed in response to heat shock, which repair or degrade proteins that have aggregated as a result of the heat stress and likely to play a role in the pathogenesis of *Mycobacterium tuberculosis* (Song et al. 2003). Activation and response of SigH-RshA to heat shock suggests this complex has a role in establishing an infection, promoting survival in the macrophage against the hosts immune response (Song et al. 2003).

RshA is 32% identical to RsrA and SigH 68% identical to SigR (Kang et al. 1999). 13 of the 30 SigR target genes identified in *Streptomyces coelicolor* have been found to be homologous in *Mycobacterium tuberculosis,* with promoter sequences upstream that resembles that for SigR, including *sigR*, *trxBA, ssrA*, and *rbpA* genes. This suggests that SigH-RshA in *Mycobacterium* aids in the survival of the cell to oxidative killing by the superoxide radicals released by macrophages during infection (Paget et al. 2002).

The mechanism of complex dissociation in response to oxidative or heat stress is unknown. However, the close homology of SigH-RshA to SigR-RsrA complex, the presence of the ZAS motif and response to oxidative stress suggests a similar mechanism of activation. Dissociation is most likely the result of oxidation of the zinc-ligating cysteine residues, forming a trigger disulphide bond that results in a large conformational rearrangement and an inability of RshA to inhibit SigH. The thioredoxin

system expressed by SigH would re-establish redox homeostasis, reduce the disulphide bond and allow the complex to reform (Song et al. 2003).

SigH and RshA have been shown to become phosphorylated by PknB, which causes dissociation of SigH (Park et al. 2008). This kinase-mediated phosphorylation regulation may act in the absence of severe oxidative or heat shock stress to cause dissociation of the complex for a more limited response under certain conditions. This may provide an early activation of SigH to oxidative stress against the immune response, before the level of stress has accumulated to cause much damage (Park et al. 2008).

1.16.4. *Mycobacterium tuberculosis* RslA-SigL

SigL ECF sigma factor has its activity controlled by the RslA ZAS anti-sigma factor. The complex is activated by oxidative stress. SigL regulates the expression of genes involved in cell wall and polyketide secondary metabolite synthesis and modification of secreted proteins (Thakur et al. 2010). RslA is composed of an N-terminal ASD that binds to SigL and a C-terminal domain (CTD) that senses oxidative stress. This is very similar to ChrR from *Rhodobacter sphaeroides* and has a similar mechanism for the inhibition of SigL activity, by sterically occluding the DNA promoter and RNA polymerase binding domains on SigL region 4 (Figure 14).

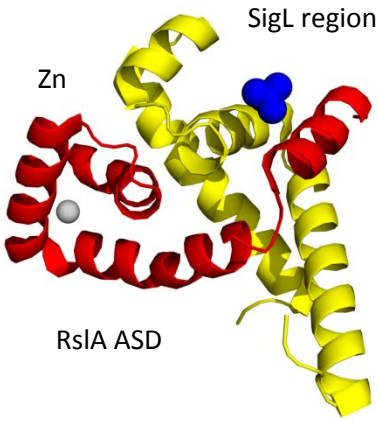


Figure 14- Structure of SigL-RslA complex. Partial RslA anti-sigma ASD (residue 1-108) is shown in red bound to a single zinc ion (grey sphere). Partial SigL ECF sigma factor region 4 (residues 99-177) is shown in yellow bound to its sulphate ion (blue spheres). This is the -35 promoter binding region of SigL blocked by RslA (3HUG) (Thakur et al. 2010).

Structures of the ASDs for RslA and ChrR are superimposable with identical zinc coordination sites, whereas SigL region 4 and SigE region 4 (*R. sphaeroides*) are very different (Thakur et al. 2010). The oxidation mechanism of this complex is similar to SigR-RsrA in *Streptomyces coelicolor;* it responds to oxidative stress by the formation of a disulphide bond in RslA accompanied by the expulsion of zinc, a large conformational change in RslA and dissociation of SigL (Figure 15) (Thakur et al. 2010).

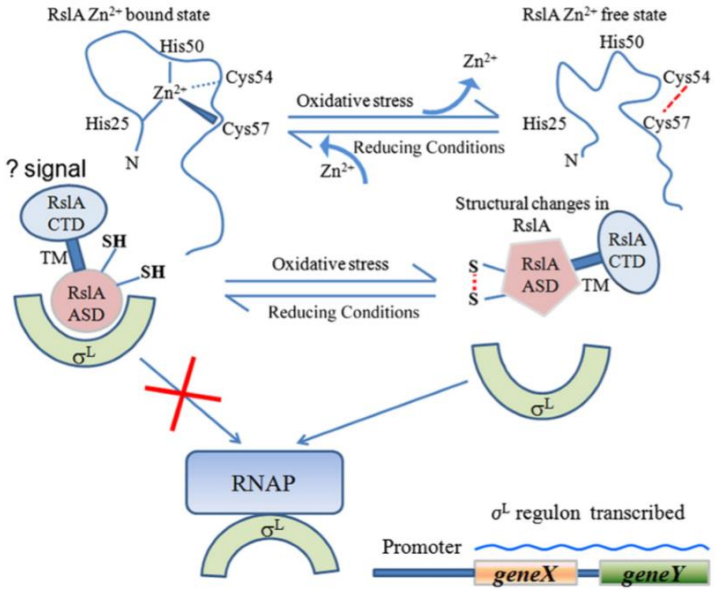
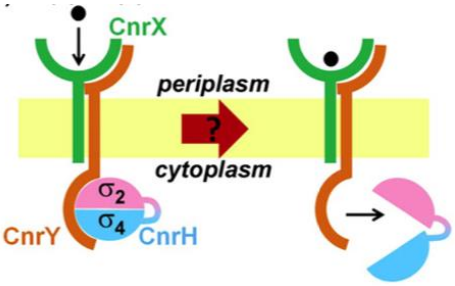


Figure 15- Mechanism of oxidative stress sensing by SigL-RslA. RslA consists of an ASD that binds SigL and a CTD that senses and responds to its activation signal. RslA coordinates a single zinc ion via its ZAS motif, it forms a 1:1 complex with SigL under reducing conditions. This prevents SigL from associating with RNA polymerase, occluding both the DNA promoter and RNA polymerase binding regions of SigL region 4. During oxidative stress a single disulphide bond forms between Cys54 and Cys57 of the ZAS motif causing the expulsion of zinc and a conformational rearrangement of RslA which leads to dissociation of SigL, this is now free to initate transcription of genes within its regulon in response (Thakur et al. 2010).

1.16.5. *Cupriavidus metallidurans* CnrY-CnrH



CnrH ECF sigma factor is regulated by CnrY and CnrX, two transmembrane proteins (Figure 16) (Maillard et al. 2014). The CnrH sigma factor transcribes genes for cobalt and nickel resistance in *Cupriavidus metallidurans*.

Figure 16- Mechanism of CnrY-CnrH complex. CnrY is a transmembrane anti-sigma which binds CnrH ECF sigma, causing a conformational change of region 2 and region 4, preventing their association with RNA polymerase (Maillard et al. 2014).

CnrY is the anti-sigma factor and CnrX is a periplasmic sensor, which senses the presence of Ni^{2+} or Co^{2+} ions within the periplasm. On detection of these ions, CnrH is released into the cytoplasm by an unknown mechanism. In the complex, CnrH region 2 and region 4 contact each other making a hydrophobic patch. It was found that certain helices of both region 2 and region 4 provides a 40 Å-long hydrophobic groove that fits the cytosolic domain of CnrY. In the region 4 hydrophobic pocket, CnrY cytosolic domain forms an α-helix forming a hydrophobic knob (Figure 17) (Maillard et al. 2014). CnrY prevents CnrH region 2 from binding RNA polymerase, CnrY also forces a sigma factor orientation that causes the CnrH sigma region 4 to conceal sigma region 2 DNA binding region.

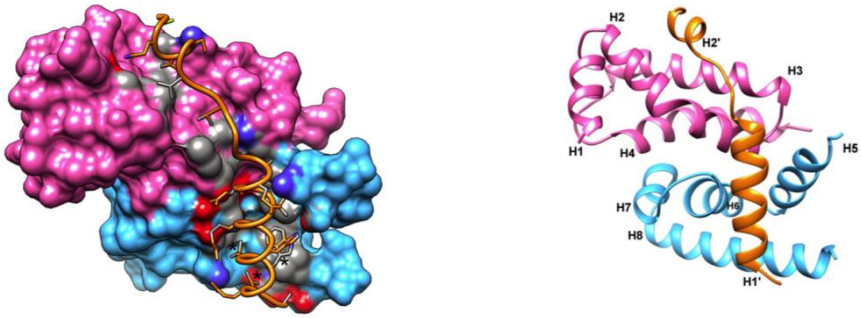


Figure 17- CnrH sigma factor in complex with CnrY anti-sigma cytosolic domain. CnrH region 2 (pink) and region 4 (blue) are forced by CnrY into an orientation that forms a hydrophobic patch. This hydrophobic patch accommodates CnrY cytosolic domain, which prevents sigma region 2 from binding RNA polymerase by competition of the β' subunit, and forces CnrH region 4 to conceal the DNA binding region of region 2 (Maillard et al. 2014).

1.16.6. Escherichia coli RseA-SigE

The ECF sigma factor SigE has its activity controlled by the anti-sigma factor RseA. RseA is composed of an N-terminal cytoplasmic and C-terminal periplasmic domain, and is anchored within the inner membrane. The first ~90 amino acids of the RseA cytoplasmic domain, are sufficient to bind and inhibit the activity of SigE by sterically occluding the RNA polymerase binding domains with a 300-fold tighter

affinity than with RNA polymerase. 50% of RseA surface is involved in this SigE interface, with α-helix 3 almost completely buried between region 2 and 4 of SigE (Figure 18) (Campbell et al. 2003).

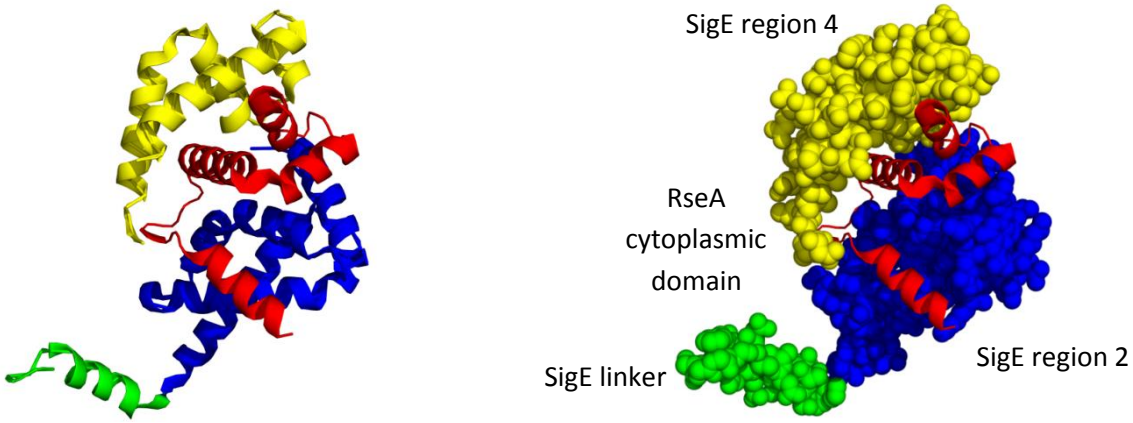


Figure 18- Structure of RseA-SigE complex. RseA anti-sigma factor cytoplasmic domain is shown in red, SigE region 2 (blue) and region 4 (yellow) with the proposed SigE linker region (green). RseA α-helix 3 inserts between region 2 and 4 of SigE. (1OR7) (Campbell et al. 2003).

The periplasmic domain of RseA binds RseB, a co-anti-sigma factor responsible for stabilising the SigE-RseA complex. SigE-RseA responds to cell envelope damage signals in the periplasm, such as misfolding of outer membrane porins in the periplasm, heat shock or overproduction of outer membrane proteins (Ades 2004). The signal activates the periplasmic serine-protease DegS that proteolytically degrades the periplasmic domain of RseA. The membrane-embedded protease YaeL further cleaves RseA near the transmembrane helix, releasing SigE-RseA into the cytosol (Campbell et al. 2003). SigE is released from RseA by its degradation and instability after proteolysis (Figure 19) (Campbell et al. 2003). The mechanism of inhibition by steric occlusion is very similar to RslA-SigL and ChrR-SigE, the mechanism of activation by proteolysis is similar to RsiW-SigW. SigE is essential for normal cellular growth and growth at extreme temperatures. SigE transcribes genes encoding a series of chaperones and proteases that refold or degrade misfolded proteins (Campbell et al. 2003).

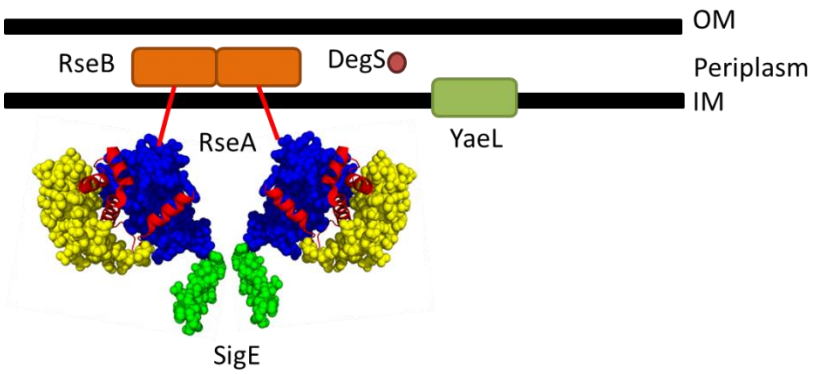


Figure 19- Mechanism of SigE-RseA activation. RseA is composed of a cytoplasmic and periplasmic domain, the cytoplasmic domain binds SigE and sterically occludes the DNA and RNA polymerase binding sites. The periplasmic domain senses the signal for cell envelope damage. RseB is a periplasmic co-anti-sigma factor responsible for the stabilisation of the complex. Under stress, DegS is activated and cleaves the periplasmic domain of RseA, YaeL membrane-embedded protease further cleaves RseA near the transmembrane helix releasing SigE-RseA to the cytosol. SigE is then released from RseA by its degradation and instability after proteolysis.

1.17. Actinobacteria

Actinobacteria are a diverse group of Gram-positive bacteria with a high G+C DNA content that are found in a wide range of environments, from salt water, soil and marine environments. One feature common to all Actinobacteria is the production of mycothiol, which serves as an alternative low molecular weight thiol to glutathione for redox homeostasis (Ventura et al. 2007).

Actinobacteria play an important role in the decomposition of organic material within the carbon cycle. Some are pathogenic and are commonly known for causing certain diseases e.g. Tuberculosis (*Mycobacterium tuberculosis*), Diphtheria (*Corynebacterium diptheriae*) and Leprosy (*Mycobacterium leprae*). They are also known for their production of secondary metabolites of pharmacological interest. Examples include essential amino acids, vitamins, enzymes, probiotics and antibiotics (Ventura et al. 2007).

Streptomyces is a versatile Gram-positive Actinomycete soil bacterium, >500 species have been described. Its genus produces bioactive secondary metabolites for medical use ranging from

antivirals to antibiotics such as streptomycin, chloramphenicol and the cephalosporins (Procopio et al. 2012). The production of antibiotics is species specific within the *Streptomyces* genus, and the antibiotics are produced from the reproductive spores of their aerial hyphae, which produce a characteristic pigment and aroma to stimulate the production of secondary metabolites. 80% of current antibiotics used medically are produced from *Streptomyces*. The antibiotics are produced naturally for survival when the organism encounters other micro-organisms or when colonising plants (Procopio et al. 2012).

Streptomyces coelicolor is the best genetically understood member of this group. Complete genome sequencing identified 965 proteins (12.3% of genome) predicted to have regulatory functions involved in responses to environmental stresses (Bentley et al. 2002). *Streptomyces coelicolor* has been used as a model organism in the study of sigma factors and their regulation in gene transcription.

1.17.1. *Streptomyces coelicolor* SigR-RsrA complex

SigR was one of the earliest ECF σ factors to be identified in *Streptomyces coelicolor*. The anti-sigma factor RsrA (**R**egulator of **S**ig**R**) was the first identified and described anti-sigma factor that was found to regulate an ECF sigma factor (Paget et al. 2002). The genes for *sigR* and *rsrA* are present on the same operon, allowing them to be translationally coupled. This ensures they are co-transcribed and form a 1:1 complex. This is the case for many ZAS and ECF σ factor genes that have not been characterised (Paget et al. 2002).

SigR-RsrA complex has a role in sensing and responding to oxidative stress within *Streptomyces coelicolor*. Its response involves dissociation of the complex and association of free SigR with RNA polymerase to initiate transcription of the genes within its regulon. SigR transcribes the operon encoding genes for *sigR* and *rsrA* (Figure 20). The two promoters for SigR transcription are *sigRp1* and

sigRp2, located 41 bp and 215 bp respectively, upstream of the GTG start codon for the transcription of SigR (Paget et al. 2001).

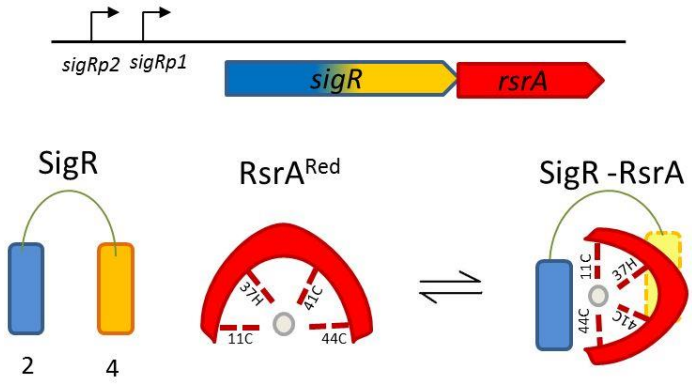


Figure 20- *sigR* and *rsrA* genes are present on the same operon and are translationally coupled. SigR transcribes the operon encoding *sigR* and *rsrA* genes from the *sigRp1* and *sigRp2* promoters. This ensures a 1:1 complex forms with RsrA and the activity of SigR controlled. 2 and 4 represent SigR region 2 and 4, grey sphere represents zinc cooridinated via the HCC motif.

Co-expression ensures there is a constant replacement of SigR-RsrA complex in the cytoplasm and that SigR is transcribed in a 1:1 ratio with its anti-sigma RsrA, so its activity is constantly repressed unless activated. This prevents continuous expression of free SigR and overexpression of its regulon, which can be toxic (Paget et al. 2002).

1.17.2. The SigR regulon

Chromatin immuno-precipitation via chip (ChIP-chip) was used to identify >100 SigR target promoters within the SigR regulon, involved in transcribing >163 genes. Cell cultures were treated with the oxidising agent diamide to activate SigR activity and using anti-SigR antibody serum to locate the promoters. Each proposed target gene was then confirmed by measuring their individual expression in response to diamide (Kim et al. 2012).

SigR target genes have a consensus promoter sequence (-GGAAT-) followed by 18 bp and (-GTT-). The -10 DNA promoter regions of some of the target genes were found to be recognised and

transcribed by other sigma factors. Sequences recognised solely by SigR contained (-TGTT- or -GGTT-), sequences recognised by multiple sigma factors contained (-CGTT-) (Paget et al. 2002). This overlap in DNA promoter sequence recognition allows transcription of certain target genes by multiple sigma factors in response to their different activation signals. A single nucleotide change within this -10 DNA promoter sequence is sufficient to change the σ factor that recognised them (Qui and Helmann 2001). Target genes where classified on the basis of known and predicted functions.

The main function of many genes within the regulon is thiol-redox homeostasis. SigR directs transcription of both the *mshA* enzyme for catalysing mycothiol biosynthesis and the thioredoxin system, Thioredoxin (*trxA*) and thioredoxin reductase (*trxB*) from the *trxBp2* and *trxBp1* transcription promoters upstream of the *trxBA* operon (Paget et al. 2001). Both promoters are induced 70-fold and 50-fold, respectively, in the presence of the artificial oxidant diamide (Paget et al. 1998).

Other SigR target genes modulate ribosome-associated processes and protein degradation. This suggests that under oxidative stress, protein-translation is negatively affected through mRNA truncation. This is demonstrated by the induction of *ssrA* gene, which is involved when a ribosome stalls to tag the interrupted protein for degradation (Kim et al. 2012). Similarly, *relA* expression is induced in response to oxidative stress, which is responsible for sensing the starvation of amino acids and the incorporation of uncharged tRNA molecules into the A site of ribosomes and causing a stall in translation. This results in the production of guanosine tetraphosphate (ppGpp), which inhibits transcription (Kim et al. 2012).

SigR also directs transcription of other sigma factors, acting as a global regulator of cellular transcription and causing a cascade of activated transcription regulators. An example of a sigma factor activated by SigR is HrdB, a major housekeeping sigma factor. This would lead to a dramatic increase in the number of SigR-dependent and independent genes transcribed to act as a collective response to oxidative stress within the cell (Kim et al. 2012).

SigR directs transcription of genes encoding redox-sensitive cofactors, to include CoA, NAD, folic acid and Fe-S clusters. This is thought to replace those in the cytoplasm that have been affected by oxidation. Other functions included oxidoreductases, sulphur, lipid and energy metabolism and DNA damage repair (Kim et al. 2012).

Studies have been undertaken to compare genes within the SigR regulon to other organisms within Actinobacteria to identify common genes and functions required for survival to oxidative stress. Phylogenetic studies comparing the sequences of SigR orthologues identified a high level of conservation for the -10 and -35 DNA promoter regions. This is indicative that orthologues likely recognise similar gene promoter sequences. This has led to the identification of a core-conserved regulon of genes across several actinomycete species that is transcribed in response to oxidative stress (Table 1) (Kim et al. 2012).

Table 1- Core genes within the conserved regulon across actinomycete species that respond to oxidative stress. 14 of the top conserved genes, data adapted from (Kim et al. 2012).

Gene	**Function**
grpE	Co-chaperone, possible integral membrane protein
prfA	Peptide chain release factor 1
Mtb-SigB	SigB sigma factor in Mycobacterium tuberculosis, regulated by SigE
clgR	Activator of cipP and Lon protease synthetic genes
trxC	Thioredoxin
trxB	Thioredoxin reductase
sufA	HesB domain (possible Fe-S cluster assembly protein)
rpbA	RNA polymerase binding protein
sigR	SigR sigma factor
rsrA	RsrA anti-sigma factor
clpC	Clp-family ATP-binding protease
rpmE1	Ribosomal proteins L31
mrxA	Mycoredoxin (glutaredoxin-like protein)
msrA	Methionine S-sulphoxide reductase

1.17.3. Effect of a SigR null mutant

When SigR is deleted in *Streptomyces coelicolor*, no change occurs in the growth, morphological differentiation or secondary metabolite antibiotic production (Paget et al. 1998). However, the cell becomes much more sensitive to oxidising agents and redox-cycling compounds. This is due to the inability to transcribe the thioredoxin system and other redox compounds to re-establish cytoplasmic redox homeostasis. This was demonstrated by comparison of the disulphide reductase activity in reducing disulphide bonds in the wild-type and SigR null mutant strains in response to diamide. Wild-type disulphide reductase was induced by 3.3-fold, whereas SigR null mutant did not respond. This reflects the role of SigR as a sigma factor activated in response to an environmental stress to initiate a response for survival (Paget et al. 1998).

The structure of SigR region 2 has been determined by (Li et al. 2002) by X-ray crystallography to a resolution of 2.4 Å. So far studies to isolate complete SigR for crystal studies have been unsuccessful. SigR region 2 is composed of an anti-parallel 3-helix bundle (Figure 21), which has a 68% α-helical content. It has a high structural similarity to σ^{70}, the eukaryotic signalling molecule Cyclin A and TFIIB transcription factor and to region 2 of other sigma factors.

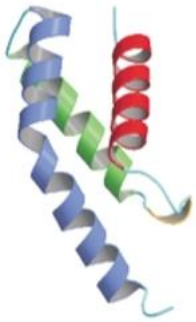


Figure 21- X-ray crystal structure of SigR region 2. SigR region 2 was isolated by tryptic cleavage and structure determined by X-ray crystallography. The structure is composed of residues 23-110 and forms an anti-parallel 3-helix bundle (Li et al. 2002).

Region 2 was shown to interact with RsrA using proteolysis of SigR and pull-down experiments (Li et al. 2002). The complete structure of SigR, or SigR in complex with RsrA remains to be determined.

1.17.4. SigR-RsrA system

SigR-RsrA is a 1:1 complex that is sensitive to oxidative stress. When the cytoplasm becomes more oxidising, SigR-RsrA dissociates due to oxidation of cysteine thiol groups in RsrA, formation of disulphide bond(s), expulsion of zinc ion and (it is presumed) a conformational change in RsrA. This enables SigR to associate with RNA polymerase, directing it to the -10 and -35 DNA promoter regions on the SigR regulon and initiate gene transcription. SigR expresses thioredoxin-thioredoxin reductase genes, which work in a positive feedback loop, re-reducing the oxidised thiol groups of RsrA allowing it to regain its structural and functional ability to bind SigR and turn off further gene transcription (Figure 22).

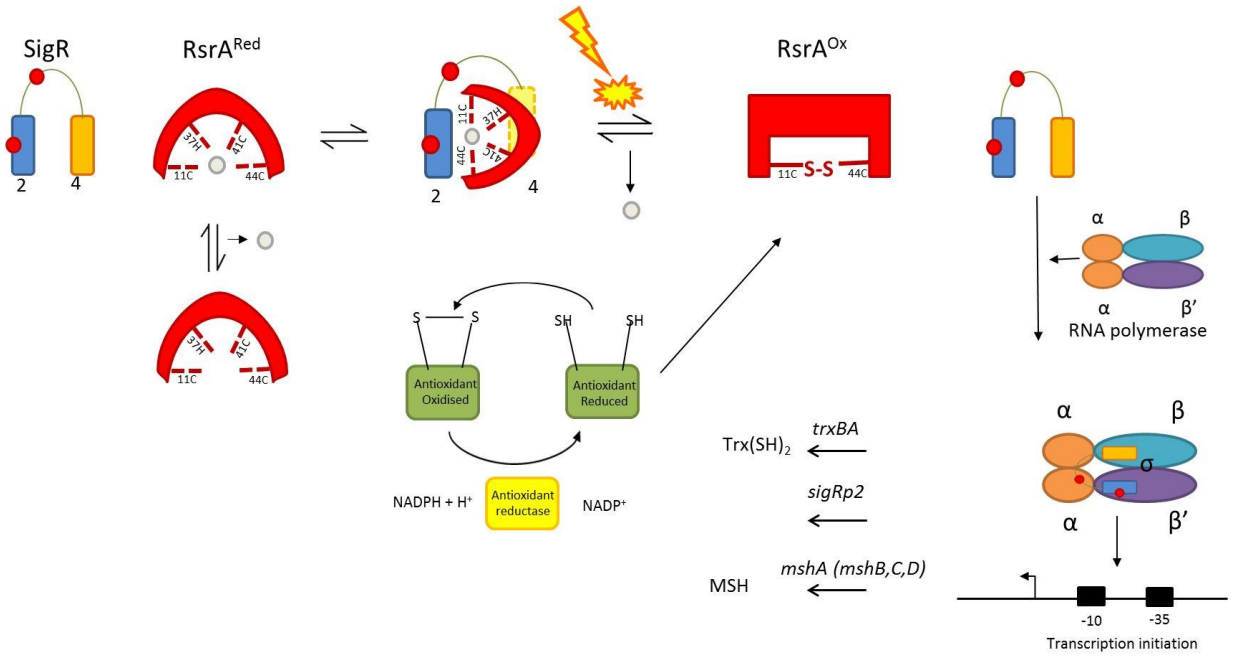


Figure 22- SigR-RsrA system in *Streptomyces coelicolor* and its response to oxidative stress. SigR-RsrA form a stoichiometric complex under reducing conditions. SigR-RsrA is sensitive to changes in the redox status of the cytoplasm, oxidative stress causes the formation of disulphide bonds in RsrA, followed by the expulsion of the zinc ion and a conformational rearrangement of RsrA. This leads to the dissociation of SigR-RsrA complex, leaving SigR to associate with RNA polymerase and form the holoenzyme, initiating transcription of the genes within its regulon. Of the 108 target genes within the SigR regulon, redox regulating proteins like thioredoxin and mycothiol are transcribed. They re-establish the reducing environment of the cytoplasm and reduce the disulphide bonds in RsrA, allowing SigR-RsrA complex to re-form, turning off any further expression. The red circles in SigR represent Trp residues.

SigR does not contain cysteine residues to sense and respond to oxidative stress. This is the function of RsrA anti-sigma factor.

1.17.5. RsrA anti-sigma factor

RsrA is an 11.7 kDa protein containing 105 amino acids, with seven cysteine residues at positions Cys3, Cys11, Cys31, Cys41, Cys44, Cys61 and Cys62. RsrA is a member of the zinc-anti-sigma family (ZAS). Members of this family are all anti-sigma factors that bind ECF sigma factors (Li et al. 2002) and coordinate a zinc ion. They show limited sequence similarity, however they all contain a conserved HXXXCXXC (HCC) motif in their N-terminus, as highlighted in red (Figure 23) (Bae et al. 2004).

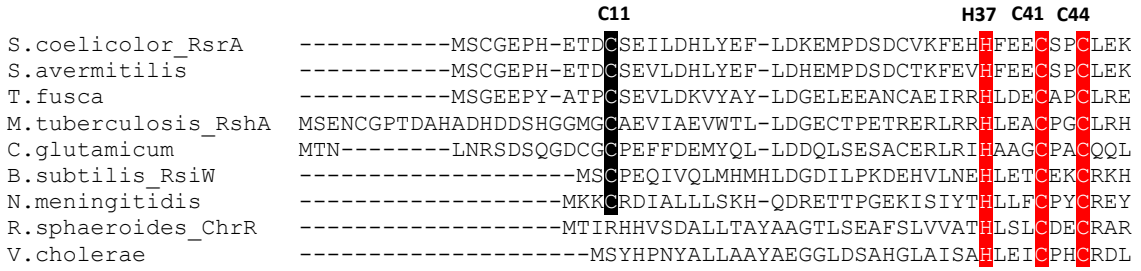


Figure 23- Alignment of several members of the ZAS family by their N-terminus. *Streptomyces coelicolor*; RsrA, *Streptomyces avermitilis*; MA-4680, *Thermobifida fusca*; YX, *Mycobacterium tuberculosis*; RshA, *Corynebacterium glutamicum*; ATCC 13032, *Bacillus subtilis*; RsiW, *Neisseria meningitidis*; MC58, *Rhodobacter Sphaeroides*; ChrR and *Vibrio cholera*; N16961.

ChrR from *Rhodobacter sphaeroides* is a member of this family. It possesses the HCC motif and coordinates a zinc ion. However, this anti-sigma does not respond to oxidative stress, but to singlet oxygen from aerobic photosynthesis, possibly due to the absence of a Cys11, which is replaced by two histidine residues and so prevents the trigger of disulphide bond formation between Cys11 and Cys44 (Zdanowski et al. 2006). The membrane bound RsiW from *Bacillus subtilis* also has a HCC motif, however the complex RsiW-σ^{W} responds to alkaline stress and factors affecting cell wall synthesis. RsiW extracytoplasmic domain senses a signal leading to its proteolysis and release of the sigma factor (Schobel et al. 2004). The similarity in sequence of ZAS family members, centering on the HCC motif, in

comparison to RsrA is very low, suggesting that ZAS factors have a wide range of functions within bacteria (Paget et al. 2002).

1.17.6. Residues important for redox-sensitivity of ZAS proteins

Studies have been undertaken to identify features of the ZAS members that govern redox-sensitivity. Jung et al. (2011) used several redox-sensitive and insensitive ZAS members, the *rsrA* gene was replaced with homologous anti-sigma genes within *Streptomyces coelicolor*. The level of transcription of SigR target genes was measured after treatment of the cells with diamide for each homologue, confirming their sensitivity to oxidation. Multiple sequence alignments identified several conserved residues present only in redox active anti-sigmas, which were located around the conserved HCC ZAS motif from K33 to E46 in RsrA (Figure 24) (Jung et al. 2011).

To confirm these residues determined redox sensitivity, they made recombinant proteins taking the predicted motif from redox-sensitive RsrA and inserting it into redox-insensitive RsiW and *vice versa*. Both proteins were treated with diamide to test expression of their respective target genes. The expression level of RsiW target genes increased and was now redox-sensitive, whilst RsrA became redox-insensitive (Jung et al. 2011).

To narrow down the residues involved, they mutated 15 residues (K33 to E46 of RsrA) and looked at sensitivity to diamide and level of SigR target gene expression. Their ID_{IF50} (concentration of diamide to cause 50% max induction) was calculated and compared to the wild-type. Mutations of K33A, H36A, E39A, E40A, S42A, L45A and E46A had much larger ID_{IF50} values, suggesting they contribute to redox-sensitivity. The residues with the largest effect were L45A, E40A, E46A and E39A; residues found to flank the two conserved cysteines Cys41 and Cys44 of the HCC motif. This could therefore serve as a pattern to predict if members of the ZAS family are redox-sensitive (Jung et al. 2011).

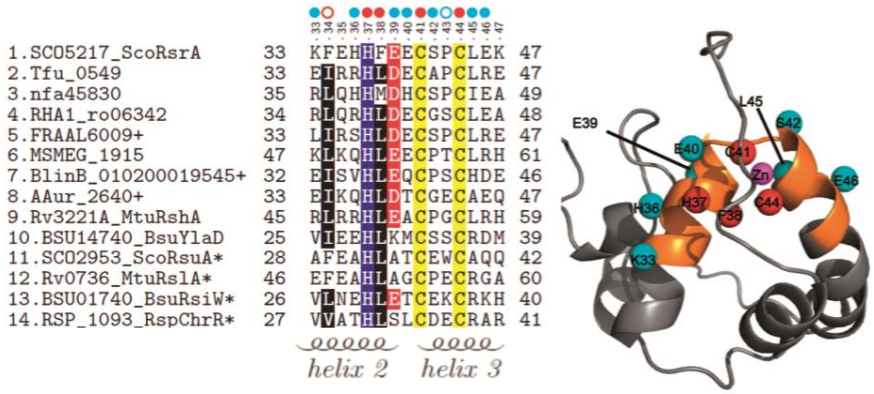


Figure 24- Sequence alignment of redox-sensitive and insensitive members of the ZAS family. ZAS HCC motif residues are highlighted in yellow and blue, the residues found unique to redox-sensitive anti-sigma ZAS members are shown compared to redox-insensitive proteins. Proteins 1-9 are redox-sensitive, and 10-14 redox-insensitive as demonstrated by induction with diamide and transcription level analysis. Mutations of K33A, H36A, and S42A had an effect, with L45A, E40A, E46A and E39A having the most pronounced effect on redox-sensitivity (Jung et al. 2011).

RsrA has been shown by inductively coupled plasma atomic emission spectroscopy (ICP-AES), to co-ordinate a single stoichiometric zinc ion in its reduced state (0.85 (± 0.23) mol zinc mol^{-1}). Although RsrA is a member of the ZAS family, it shows close similarity to features of zinc-finger proteins, which have cysteine residues coordinating a zinc ion and have their activity modulated by oxidation (Paget et al. 2001).

1.17.7. Zinc coordination ligands in RsrA

Two models have been proposed for the coordination of the zinc ion in RsrA. Bae et al. (2004) proposed residues Cys3, His7, Cys41 and Cys44, two of which are present in the HCC conserved motif, as the metal binding residues. This was based on a series of mutations and measuring the amount of zinc bound using the colorimetric PAR assay. They found that H37A mutant from the conserved motif was still able to bind zinc and therefore not involved in zinc coordination (Figure 25).

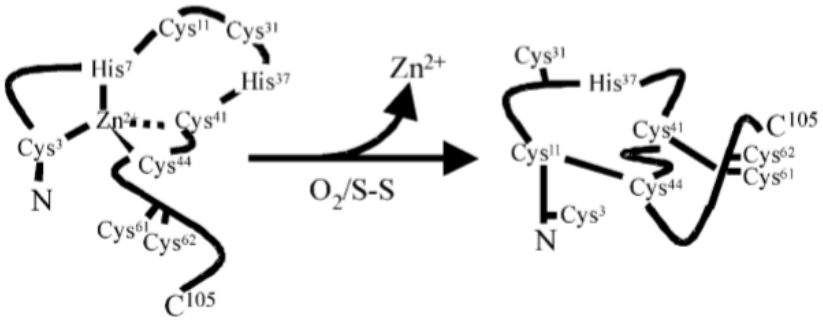


Figure 25- Proposed coordination ligands for zinc, and the residues that form disulphide bonds on oxidation of RsrA. Bae et al. 2004 proposed zinc coordination ligands as Cys3, His7, Cys41 and Cys44, based on mutational studies and measuring the amount of zinc bound. They suggested the residues involved in disulphide bond formation are between Cys11 and Cys41/Cys44 (most likely Cys44), with the secondary disulphide bond between Cys41 and Cys61 (Zdanowski et al. 2006).

Zdanowski et al. (2006) proposed all residues in the conserved ZAS motif; His37, Cys41 and Cys44, were involved in coordinating zinc along with a fourth ligand at position Cys11, in agreement with residues proposed by Paget et al. (2001) and Li et al. (2003). This was based on *in vivo* and *in vitro* studies of a series of RsrA cysteine mutations. Site-directed mutagenesis was used in conjunction with K-edge extended X-ray absorption fine structure (EXAFS) Spectroscopy to determine the coordination ligands. They designed an RsrA mutant with Cys11, Cys41 and Cys44 present, with the remaining predicted non-essential cysteine residues mutated to alanines. This RsrA was still able to bind SigR and was responsive to oxidative stress. The EXAFS data for this RsrA mutant was identical to wild-type RsrA, confirming Cys11, Cys41 and Cys44 as the coordination ligands (Figure 26). These data also confirmed His37 as a ligand, as its mutation caused a change in the EXAFS data. These ligands are not affected by the binding of SigR (Zdanowski et al. 2006).

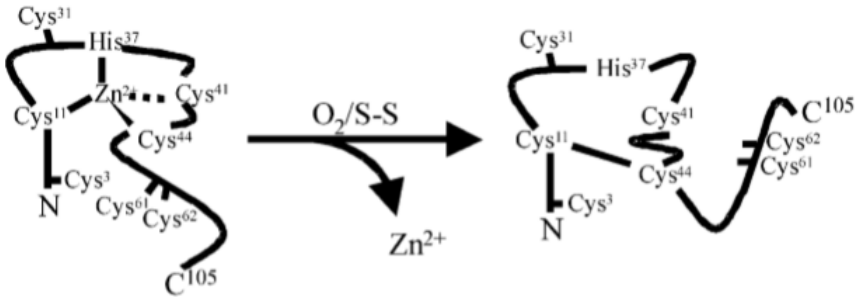


Figure 26- Proposed coordination ligands for zinc. Li et al. (2003) proposed that the zinc coordination ligands were Cys11, His37, Cys41 and Cys44. This was proven based on mutational studies and K-edge EXAFS spectroscopy performed by Zdanowski et al. (2006).

The residues found to be important in RsrA zinc coordination are Cys11, His37, Cys41 and Cys44 as shown in the proposed model of RsrA (Figure 27 kindly provided by Liz Campbell, unpublished).

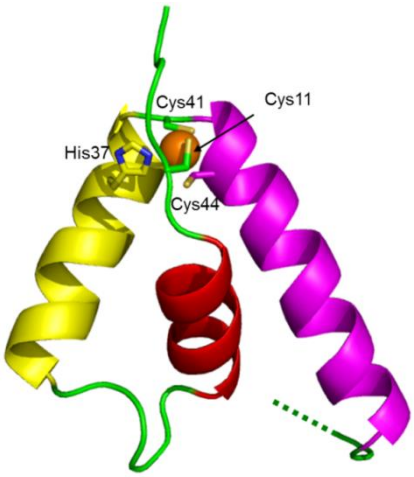


Figure 27- Proposed model of RsrA and its coordination ligands. Model for the structure of zinc-bound RsrA based on the structure of zinc-bound ChrR anti-sigma. The model is based on Cys11, His37, Cys41 and Cys44 residues coordinating a single zinc ion.

1.17.8. Residues involved in disulphide bond formation

On sensing oxidative stress, RsrA forms disulphide bonds leading to the expulsion of zinc and a structural rearrangement that leads to the dissociation of SigR. There has been uncertainty in the cysteine pairs in RsrA involved in forming disulphide bonds and the number of bonds that form in response to oxidative stress. It was found that mixed populations of one and two disulphide bonds form in air-oxidised RsrA and three disulphide bonds in response to strong oxidants (Bae et al. 2004).

Li et al. (2003) isolated air-oxidised RsrA containing a single trigger disulphide and showed that this is sufficient to prevent complex formation between SigR-RsrA. Additional disulphides had no further effect on preventing complex formation. The residues that form the disulphides were mapped using tryptic digestion, and MALDI-TOF mass spectrometry (Li et al. 2003). Cys11 and either Cys41 or Cys44 were involved in forming the trigger disulphide, suggesting the structural rearrangement could be accomplished by either disulphide bond. Formation of the trigger disulphide explains why on oxidation of RsrA, zinc is expelled by formation of a disulphide bond via the ligands coordinating it (Li et al. 2003).

1.17.9. Residues important for SigR-RsrA binding and RsrA activity *in vivo*

A *Streptomyces coelicolor rsrA* null mutant is defective in sporulation, which is due to the increase in free SigR. RsrA null mutant strains also show a higher level (~24-fold) of disulphide reductase activity caused by the overexpression of the thioredoxin system by SigR-dependent transcription (Paget et al. 2001).

To identify residues critical for the anti-sigma factor activity of RsrA, single cysteine mutations were made for all seven residues. Strains carrying *rsrA*^{C3S}, *rsrA*^{C31S} or *rsrA*^{C61S} all had normal sporulation phenotypes suggesting these residues are not important in RsrA activity (Paget et al. 2001). Strains carrying *rsrA*^{C11S}, *rsrA*^{C41S} or *rsrA*^{C44S} all had white phenotypes and therefore defective in sporulation, suggesting that each of these cysteine residues is important for the activity of RsrA in binding and inhibiting SigR. RsrA^{C62S} mutant showed grey colonies, suggesting only partial activity of RsrA *in vivo* (Paget et al. 2001). The reason for the inhibition of sporulation in *rsrA* null mutants, is due to the high level of free SigR outcompeting a known sporulation-specific sigma factor, σ^{WhiG}, for the binding of RNA polymerase and transcriptional activity (Chater 2000).

These RsrA mutants were tested for their ability to sense and respond to disulphide stress in the form of diamide, by measuring transcription from the *trxCp1* promoter (Paget et al. 2001). Results showed that mutations at Cys3, Cys31, Cys61 and Cys62 did not affect the ability of RsrA to sense oxidative stress, dissociate from SigR and allow SigR-dependent transcription of the thioredoxin system. This was followed by the reduction of RsrA by thioredoxin and inhibition of further transcription. Mutation of either Cys11, Cys41 or Cys44 abolished the ability of RsrA to bind SigR and caused transcription of the thioredoxin system even in the absence of diamide oxidising agent (Paget et al. 2001).

This showed that Cys11, Cys41 and Cys44 residues are all essential for the SigR-RsrA complex and the activity of the anti-sigma factor, mutation of a single residue abolished binding and activity. These residues were confirmed *in vitro*, by the purification of each RsrA mutant protein and evaluating

their ability to inhibit SigR-dependent transcription from *sigRp2* promoter, in the presence and absence of DTT reducing agent (Paget et al. 2001). This suggests that the residues important for RsrA activity are Cys11, Cys41 and Cys44, the same residues involved in coordinating zinc and formation of the trigger disulphide bond.

1.17.10. Importance and role of zinc in RsrA

SigR-RsrA is bound stoichiometrically to a single zinc ion, however complex can form in the absence of zinc, as demonstrated via native PAGE migration and gel filtration chromatography (Li et al. 2003). Zinc is essential for the functional activity of RsrA to bind and inhibit SigR-dependent transcription, which was demonstrated by *in vitro*-transcription assays. Recent molecular dynamic simulations by Heo et al. (2013) have suggested the possibility of a role for multiple zincs affecting the redox activity of RsrA.

Zinc binds tightly to RsrA with a K_d of $0.5x10^{-12}$ pM (Bae et al. 2004). The loss of functional activity of RsrA in the absence of zinc, was suggested to be due to weaker binding between SigR-RsrA and an inability of RsrA to effectively compete with RNA polymerase for the binding of SigR (Li et al. 2003). Zinc also plays a role in protecting RsrA cysteine thiol coordination ligands and modulating their reactivity to oxidation; apo-RsrA is rapidly oxidised while Zn-RsrA is relatively resistant to oxidation. Interestingly, the rate of zinc release and oxidation does not appear to be affected by the presence of SigR (Li et al. 2003).

1.17.11. Structural rearrangement of RsrA on oxidation

The oxidation of RsrA and expulsion of zinc on disulphide bond formation accompanies a large structural change. Li et al. (2003) used CD to compare apo-RsrA and Zn-RsrA under reducing conditions, showing that the absence of zinc with reduced thiol groups had only a minor change in CD spectra. Apo-RsrA under oxidising conditions showed a much more significant change in CD spectrum,

with RsrA increasing its α-helical content from 23% to 30%, due to the formation of a disulphide bond. This change in structure could be used to measure the kinetics of air-oxidation of RsrA, $2x10^{-4}$ s^{-1}, which was identical to the rate measured by gel filtration chromatography Li et al. (2003).

Aim of this work

Many questions remain to be answered as to how ZAS proteins such as RsrA bind SigR and respond to oxidative stress. In addition, there is controversy as to how many zinc ions are bound to the protein and their role in redox sensing. The binding affinity of SigR-RsrA has been determined previously by SPR, but little follow on work has been carried out on the thermodynamics and kinetics of complex formation, for this or other ZAS-ECF complexes. The structure of the complex has not been determined, however use of a homology model and development of a fluorescence-based assay using tryptophan fluorescence to monitor complex formation, will allow further work in determining the association and dissociation kinetics for SigR-RsrA.

Determining the thermodynamics and kinetics of the complex under reduced and oxidised conditions, will allow a better understanding of the mechanism by which the complex senses and responds to oxidative stress. This knowledge can then be applied to developing a better understanding of other related ZAS-ECF complexes and their response to environmental stress.

Objectives

- Develop a fluorescence-based-assay to monitor SigR-RsrA complex formation
- Define the thermodynamics of interaction between SigR-RsrA and determine its binding affinity by isothermal titration calorimetry (ITC)
- Determine the association and dissociation kinetics of SigR-RsrA using pre-steady-state fluorescence stopped-flow
- Determine the role of zinc in the thermodynamics and kinetics of RsrA
- Develop an oxidation-based assay to determine the association and dissociation kinetics of SigR-RsrA in response to a change in redox state
- Develop expression strategies for other novel sigma anti-sigma proteins for future structural studies (Appendix)

2- Materials and Methods

2.1. Microbiology

2.1.1. Bacterial strains and growth conditions

All strains and plasmids used in the following work are listed in table 2. For molecular biological methods or protein expression, strains were routinely grown at 37°C in LB (Lysogeny broth) containing 10 g Tryptone, 10 g NaCl and 5 g yeast extract per litre of medium (Miller, J. H., 1972). Selective media were supplemented where necessary with appropriate antibiotics (Table 3).

2.1.2. Plasmids and strains

Table 2- Plasmids and strains used in this study.

Strain	**Genotype**		**References**
XL1-Gold Ultracompetent cells	TetrD(mcrA)183 D(mcrCB-hsdSMR-mrr)173 endA1 supE44 thi-1 recA1 gyrA96 relA1 lac Hte [F´ proAB lacIqZDM15 Tn10 (Tetr) Amy Camr]		Agilent
DH5α	F– Φ80lacZΔM15 Δ(lacZYA-argF) U169 recA1 endA1 hsdR17 (rK–, mK+) phoA supE44 λ– thi-1 gyrA96 relA1		Invitrogen
BL21 (DE3)	F– *ompT hsdS*$_B$(r_B– m_B–) *gal dcm* (DE3)		Novagen
BL21 (DE3) pLysS	F–, *omp*T, *hsd*S_B (r_B–, m_B–), *dcm*, *gal*, λ(DE3), pLysS, Cm^r		Life technologies
Rosetta 2 pLysS	F^- *ompT hsdS*$_B$(r_B^- m_B^-) *gal dcm* (DE3) PLysSpRARE2[3] *(*CamR)		Novagen
Plasmid	**Strain**	**Properties**	**Source**
pET-21a			Novagen
pET-21a-SigR	BL21 (DE3)	Expression construct for wild-type SigR and template vector for SigR mutants, T7 promoter (IPTG inducible), Amp^R	Kleanthous lab; pKR07
pET-21a-SigR W88I	BL21 (DE3)	Trp-to-Ile mutant at position 88	This work; pMLF01
pET-21a-SigR W119I	BL21 (DE3)	Trp-to-Ile mutant at position 119	This work; pMLF02
pET-21a-SigR W88I W119I (SigR*)	BL21 (DE3)	Trp-to-Ile mutant at positions 88 and 119	This work; pMLF03
pET-21a-SigR W88I W119I F171W (SigR* F171W)	BL21 (DE3)	Triple mutant at positions 88, 119 and 171	This work; pMLF04
pET-21a-SigR W88I W119I F159W (SigR* F159W)	BL21 (DE3)	Triple mutant at positions 88, 119 and 159	This work; pMLF05
pET-15b-RsrA	Rosetta 2 pLysS	Expression vector for RsrA, with N-term. Thrombin-cleavable His_6-tag, T7 promoter (IPTG inducible), $AmpCam^R$	Kleanthous lab
pCDFDuet-1 SigH	BL21 (DE3)	Expression vector for SigH, T7	This work; pMLF06

		promoter (IPTG inducible), $Strep^R$	
pET-21a-SigH	BL21 (DE3)	Expression vector for SigH, T7 promoter (IPTG inducible), Amp^R	Kleanthous lab; Colin Seepersad; pCES004
pET-21a-RshA	BL21 (DE3)	Expression vector for RshA, T7 promoter (IPTG inducible), Amp^R	Kleanthous lab; Colin Seepersad; pCES003
pCDFDuet-1 ECF1-ZAS1	BL21 (DE3)	Expression vector for ECF1-ZAS1, T7 promoter (IPTG inducible), $Strep^R$	Kleanthous lab; Colin Seepersad; pCES024
pCDFDuet-1 ECF2-ZAS2A	BL21 (DE3)	Expression vector for ECF2-ZAS2A, T7 promoter (IPTG inducible), $Strep^R$	Kleanthous lab; Colin Seepersad; pCES025
pCDFDuet-1 ECF2-ZAS2B	BL21 (DE3)	Expression vector for ECF2-ZAS2B, T7 promoter (IPTG inducible), $Strep^R$	Kleanthous lab; Colin Seepersad; pCES026
pCDFDuet-1 ECF3-ZAS3	BL21 (DE3)	Expression vector for ECF3-ZAS3, T7 promoter (IPTG inducible), $Strep^R$	Kleanthous lab; Colin Seepersad; pCES027

Table 3- Antibiotics and chemicals used and their concentrations for plasmid selection and maintenance in cultures, for growth and expression of proteins.

	Stock solution	**Working concentration**
Chloramphenicol (Cam)	20 mg/ml	20 µg/ml
Ampicillin (Amp)	100 mg/ml	100 µg/ml
Streptomycin (Str)	50 mg/ml	50 µg/ml
IPTG	1 M	1 mM
$ZnCl_2$	100 mM	10 µM (expression), 0.1 mM (purification)

2.2. Molecular Biology

2.2.1. Purification of plasmid DNA

QIAGEN QIAprep spin Miniprep

Plasmids containing DNA for purification were prepared from DH5α cells. Strains were streaked on LB agar plates containing the appropriate antibiotics (as listed in table 3), and incubated overnight at 37°C for ~16 hours. A single colony was picked and re-suspended in 5 ml LB broth with the appropriate antibiotics and grown overnight at 37°C with shaking for ~16 hours. DNA was purified following the manufacturer's protocol. Concentrations were determined by absorbance at 260 nm using the Beer-Lambert Law (Section 2.3.4).

QIAGEN Plasmid Plus Midi Kit

For purification of large quantities of plasmid DNA, a single colony was picked and re-suspended in 50 ml LB broth with appropriate antibiotics and grown overnight at 37°C with shaking for 12-14 hours. DNA was purified using the Midi kit following the manufacturer's protocol.

2.2.2. Polymerase chain reaction (PCR)

QuikChange Lightning Site-directed Mutagenesis by Agilent

Site-directed mutagenesis was used to mutate tryptophans (W) to isoleucines (I) and phenylalanines (F) to tryptophans (W) in SigR plasmid pET-21a. PCR reactions were assembled as described in table 4 and run according to the program in table 5. Mutagenesis primer sets were designed and purchased from Eurofins MWG Operon (Table 6). Their design was aimed to be between 18-30 nucleotides, contain the mismatch in the centre of the sequence and to display a melting temperature greater than 60°C, calculated using the formula $T_m = 4(G + C) + 2(A + T)$ °C. The GC content was designed to have 40-68% GC content with the 3' end ending with C/G. The plasmid pET-21a encoding SigR WT (pKR07) was the template for region 2 mutant SigR W88I, linker region mutant SigR W119I, and SigR W88I W119I (SigR*). SigR* was the template for region 4 mutant SigR* F171W and SigR* F159W.

Table 4- Composition of a PCR reaction for whole plasmid site-directed mutagenesis using the Agilent QuikChange Lightning Site-directed Mutagenesis kit.

	SigR W to I			**SigR F to W**	
Reagent	W88I	W119I	SigR*	F171W	F159W
10x reaction buffer	5µl	5 µl	5 µl	5 µl	5 µl
100 ng dsDNA template	4.6 µl	4.6 µl	4.6 µl	8.9 µl	8 µl
125 ng oligonucleotide forward primer	3.5 µl	4.3 µl	3.5 µl (88) 4.3 µl (119)	7.1 µl	8.8 µl
125 ng oligonucleotide reverse primer	3.9 µl	4.6 µl	3.9 µl 4.6 µl	8.4 µl	8.6 µl
1 µl dNTP mix	1 µl	1 µl	1 µl	1 µl	1 µl
1.5 µl QuikSolution reagent	1.5 µl	1.5 µl	1.5 µl	1.5 µl	1.5 µl
ddH_2O to final volume 50 µl	30.4 µl	28.9 µl	21.5 µl	17 µl	16.1 µl
QuikChange Lightning Enzyme	1 µl	1 µl	1 µl	1 µl	1 µl

Table 5- PCR programme for whole plasmid site-directed mutagenesis using the Agilent QuikChange Lightning Site-directed Mutagenesis kit.

			SigR W88I, SigR W119I, SigR*, SigR* F171W, SigR* F159W
Step	**Cycles**	**Temp. (°C)**	**Time (mins)**
Initial denaturation	1 cycle	95°C	1 minute
Denaturation	30 cycles	95°C	1 minute
Annealing		60°C	1 minute
Extension		68°C	3.1 minutes (30s/kb plasmid)
Final extension	1 cycle	68°C	5 minutes
	Hold	4°C	Hold

Table 6- List of primers used in this study.

Template	**Primer**	**Mutagenesis primer sequence**	**Primer Tm (°C)**
pET-21a-SigR WT	W88I Forward	5'-ACCAACCTCAAGGCG**ATT**CTGTACCGCATCCTC-3'	102
pET-21a-SigR WT	W88I Reverse	3'-TGGTTGGAGTTCCGC**TAA**GACATGGCGTAGGAG-5'	102
pET-21a-SigR WT	W119I Forward	5'-GAGGAGATCGAGGAC**ATT**CAGCTCGCCCGTGCC-3'	108
pET-21a-SigR WT	W119I Reverse	3'-CTCCTCTAGCTCCTG**TAA**GTCGAGCGGGCACGG-5'	108
pET-21a-SigR* (W88I W119I)	F171W Forward	5'-CGTCGAGGGC**TGG**GCCTACAAGG-3'	78
pET-21a-SigR* (W88I W119I)	F171W Reverse	3'-GCAGCTCCCG**ACC**CGGATGTTCC-5'	78
pET-21a-SigR* (W88I W119I)	F159W Forward	5'-CCCCGAGGAA**TGG**CGTATCGCCG-3'	78
pET-21a-SigR* (W88I W119I)	F159W Reverse	3'-GGGGCTCCTT**ACC**GCATAGCGGC-5'	78

To digest the parental plasmid template DNA after the PCR reaction, the samples were incubated with 2 µl *DpnI* restriction enzyme at 37°C for 1 hour. 2 µl per reaction was used to transform XL1-Gold Ultracompetent cells and incubated overnight.

Mutations were confirmed by DNA sequencing (Source Bioscience Sequencing). The primers used for sequencing are shown in table 7.

Table 7- Sequencing primers used in this study.

	Sequencing primers	
Plasmids	**Forward**	**Reverse**
SigR pET-21a	(T7 forward) 5'-TAATACGACTCACTATAGGG-3'	(T7 terminator) 5'-GCTAGTTATTGCTCAGCGG-3'
RsrA pET-15b	(T7 forward) 5'-TAATACGACTCACTATAGGG-3'	(T7 terminator) 5'-GCTAGTTATTGCTCAGCGG-3'
SigH pCDFDuet-1	(ACYCDuetUP1) 5'-GGATCTCGACGCTCTCCCT-3'	(T7 terminator) 5'-GCTAGTTATTGCTCAGCGG-3'
RshA pET21-a	(T7 forward) 5'-TAATACGACTCACTATAGGG-3'	(T7 terminator) 5'-GCTAGTTATTGCTCAGCGG-3'

Transformation of SigR mutants into XL1-Gold Ultracompetent cells

Transformation followed the manufacturer's protocol.

2.2.3. Preparation of competent cells

Rosetta 2 pLysS and BL21 *E. coli* derivatives DE3, (DE3) pLysS and DH5α cells, were made competent by growing cells in a 50 ml culture to an OD_{600} of 0.5-0.6 in LB medium, before harvesting by centrifugation (10 minutes at 5000 xg, 4°C). The cells were re-suspended in 20 ml of competent cell solution 1 (20 mM Tris pH 7.5, 50 mM $CaCl_2$) and incubated at 4°C for 1 hour. Cells were pelleted by centrifugation (10 minutes at 5000 xg, 4°C), and re-suspended in 2 ml competent cell solution 2 (20 mM Tris pH 7.5, 50 mM $CaCl_2$, 20% v/v glycerol). Aliquots of 200 µl were flash frozen in liquid nitrogen and stored at -80°C.

2.2.4. Transformation of competent cells (DH5α, BL21 (DE3), (DE3) pLysS, Rosetta 2 pLysS)

Transformation competent cells were thawed on ice, mixed with 100 ng of plasmid DNA per 100 µl of competent cells and incubated on ice for 30 minutes. Cells were subjected to a heat shock at 42°C for 1 minute, ice for 5 minutes, followed by the addition of 1 ml LB medium and incubated for 1 hour at 37°C with shaking, before plating 100 µl onto LB-Agar and incubating at 37°C for ~16 hours.

2.3. Biochemical methods

2.3.1. Polyacrylamide gel electrophoresis (PAGE)

Gels were prepared using a stock of 30% (w/v) acrylamide and 0.8% bis-acrylamide (Protogel, National Diagnostics) which was diluted into 375 mM Tris-HCl pH 8.8 and 0.1% (w/v) sodium dodecyl sulphate (SDS) to give final acrylamide concentration of 15% as required for the running gel. Ammonium persulfate (APS) and N, N, N', N'-tetramethyl ethylenediamine (TEMED) were added to a final concentration of 0.08% w/v and 0.13% v/v, respectively. Stacking gels were prepared similarly but contained 5% acrylamide and 250mM Tris-HCl pH 6.8.

Expression samples for SDS-PAGE were made up in 200 µl; 150 µl water, 50 µl 4x sample loading buffer (200 mM TrisHCl pH 6.8, 8% (w/v) SDS, 0.4% (w/v) bromophenol blue, 40% (w/v) glycerol, 400 mM (14 M) (10% v/v) β-ME). Protein samples were made up in 20 µl; 10 µl water, 10 µl 2x sample loading buffer (100 mM TrisHCl pH 6.8, 4% (w/v) SDS, 0.2% (w/v) bromophenol blue, 20% (w/v) glycerol, 200 mM (14 M) (10% v/v) β-ME). Samples were boiled for 5 minutes prior to gel loading in 8 µl aliquots. Unstained protein molecular weight marker with a range of 14.4 to 116 kDa (Fermentas #SM0431) was run alongside samples to enable approximate molecular weight determination of protein samples. Gels were run in 250 mM Tris, 192 mM glycine, 0.1% (w/v) SDS at a constant current of 30 mA per gel for 30 minutes.

Proteins were visualised by staining the gel with 0.2% (w/v) Coomassie brilliant blue R250 (Pierce) in 10% v/v acetic acid and 10% v/v ethanol for 30 minutes and de-stained in the same solution but without added Coomassie brilliant blue dye.

2.3.2. Native PAGE gels

Native PAGE gels were prepared as above with omission of SDS and stacking gel. Native PAGE (16% polyacrylamide (w/v)) was used to follow complex formation between SigR Wild-type and SigR

mutants. The running buffer contained 250 mM Tris and 192 mM glycine using the pH as made (pH 9.43 at room temperature). Protein concentrations were 50 µM, in 50 mM Tris pH 7.5, 100 mM NaCl, 2 mM DTT. Complexes were formed on ice and left for 15 minutes, before addition of loading dye (#BN20032 Invitrogen) using non-reducing, non-denaturing loading buffer. Samples were not boiled prior to loading and gels were run at 20 mA per gel for 3 hours at 4°C, using cold buffer so as not to denature the proteins or complexes, before staining in Coomassie blue solution.

2.3.3. Oxidative and reducing Native PAGE

Concentrations of proteins were 15 µM SigR and 30 µM complex in the presence and absence of zinc. All proteins were buffer exchanged into 50 mM Tris pH 7.5, 100 mM NaCl. Hydrogen peroxide (H_2O_2), diamide and oxidised DTT oxidants were diluted in 50 mM Tris pH 7.5, 100 mM NaCl and adjusted to pH 7.5 at room temperature. Concentrations of oxidants were 250 µM, 2 mM and 10 mM. Protein samples were incubated on ice with each oxidant for 15 minutes, 1 hour, 2 hours or 4 hours.

Native PAGE (12% polyacrylamide (w/v)) was used to follow reduced and oxidised samples and SigR-RsrA complex dissociation. Reduced samples contained 2 mM DTT. The running buffer contained 250 mM Tris, 192 mM glycine pH 9.43, and 2 mM hydrogen peroxide or oxidised DTT where indicated. Pre-run 12% native PAGE gels were pre-run with buffer containing 2 mM of each oxidant for 2 hours at 4 mA, and left sitting in the buffer for a further 30 minutes. Gels were run with samples at room temperature for 30 minutes or 1 hour at 20 mA before staining in coomassie blue solution.

2.3.4. Measurement of protein concentrations

Protein concentrations were determined using the Beer-Lambert law ($A=\varepsilon c l$, where A = absorbance, ε = molar extinction coefficient (M^{-1} cm^{-1}), c = concentration (M) and l = pathlength (1 cm)) at 280 nm,

where absorbance values were measured on either a nanodrop or biophotometer, in combination with sequence based theoretical extinction coefficients.

The theoretical molar extinction coefficients were calculated according to the formula:

$\varepsilon_{protein} = N_{Tyr} . \varepsilon_{Tyr} + N_{Trp} . \varepsilon_{Trp} + N_{Cys} . \varepsilon_{Cys}$

Where $N_{Tyr, Trp, Cys}$ is the number of tyrosine, tryptophan or cysteine residues in the protein sequence, and $\varepsilon_{Tyr, Trp, Cys}$ are the molar extinction coefficients for tyrosine, tryptophan and cysteine (1280, 5690, and 120 M^{-1} cm^{-1} respectively, as determined by Gill and Von Hippel, 1989).

Theoretical extinction coefficients were used at 280 nm calculated from their amino acid sequences using http://protcalc.sourceforge.net/ (table 8).

Table 8- Theoretical extinction coefficients for proteins used in this study.

Protein	**ε Theoretical extinction coefficients (M^{-1} cm^{-1})**
SigR	21620
SigR W88I	15930
SigR W119I	15930
SigR*	10240
SigR* F171W	15930
SigR* F159W	15930
RsrA	2560
SigR-RsrA	24180
SigH	22900
RshA	6970

2.3.5. Test expressions

From a 5 ml overnight LB culture, 750 µl was diluted into 10 ml LB, supplemented with the appropriate antibiotics and grown to OD_{600} 0.6. Expression was then induced using 1 mM IPTG for 3 hours at 37°C or overnight at 20°C, taking samples at different time intervals. Cells were pelleted by centrifugation at 6238 x g for 2 minutes and then re-suspended in 150 µl water, 50 µl 4x loading buffer and boiled for 5 minutes, of which 8 µl was analysed by SDS-PAGE.

2.3.6. RsrA expression and purification

RsrA expression

A single colony of pET-15b-RsrA plasmid transformed into *E. coli* Rosetta 2 pLysS cells, was used to inoculate 50 ml LB, which was grown to mid-log (OD_{600} ~0.6) at 37°C with the appropriate antibiotics. The culture was then diluted between 6 flasks of 800 ml LB (4800 ml) and supplemented with 10 µM $ZnCl_2$, 100 µg/ml Amp 20 µg/ml Cam antibiotics per flask. The culture was grown to OD_{600} 0.6 with shaking at 120 rpm, using 2.5 L flasks at 37°C before inducing expression with 1 mM IPTG for 2.5 hours at 37°C. The cells were harvested by centrifugation at 6238 x g for 20 minutes at 4°C.

RsrA purification

For the purification of N-terminal His-tagged RsrA, the cell pellet were re-suspended in 50 ml lysis buffer (50 mM Tris pH 7.5, 300 mM NaCl, 0.1 mM $ZnCl_2$, 1 mM PMSF, 1 PIK tablet (Roche Complete, EDTA-free)). The suspension was sonicated (Misonix S4000) on ice for 2 minutes (3 seconds pulse on, 7 seconds pulse off) at 60% amplitude. The cell lysate was centrifuged for 30 minutes at 22,658 x g at 4°C, to pellet cellular debris and collect the supernatant, which contained RsrA. The pellet was washed before re-suspending in 25 ml lysis buffer for SDS-PAGE analysis.

The lysate containing His-RsrA was filtered (0.45 µm), before loading via a 50 ml superloop onto a 5 ml HisTrap HP nickel column (GE Healthcare) equilibrated with binding buffer (50 mM Tris pH 7.5, 100 mM NaCl, 0.1 mM $ZnCl_2$, 1 mM imidazole), manually at a rate of 1 ml/min. The column was washed in 20 column volumes of binding buffer to remove any unbound protein and then washed with 10 column volumes 2% elution buffer (20 mM imidazole) to remove non-specifically bound protein (50 mM Tris pH 7.5, 100 mM NaCl, 0.1 mM $ZnCl_2$, 1 M imidazole). Bound His-RsrA was eluted at 1 ml/min using a linear gradient of 20-500 mM imidazole over 20 column volumes. Protein elution was monitored by UV absorbance at 280 nm. Eluted fractions were selected from the profile before running on SDS-PAGE gels to locate fractions of protein to pool.

Protein fractions were concentrated to 5 ml (using Vivaspin 20 5000 MWCO) and buffer exchanged into Thrombin cleavage buffer (20 mM Tris pH 7.5, 150 mM NaCl, 2.5 mM $CaCl_2$), either via overnight dialysis in 4 Litres using Spectra/Por membrane with a molecular weight cut off (MWCO) of 3500 kDa, or PD-10 desalting gel filtration column.

The PD-10 column was prepared by equilibrating with thrombin cleavage buffer (20 mM Tris pH 7.5, 150 mM NaCl, 2.5 mM $CaCl_2$). 2.5 ml of concentrated protein was added to the column, before the addition of 3.5 ml of elution thrombin cleavage buffer to the column and collecting the 3.5 ml eluate.

10 µl (20 units) of Thrombin protease enzyme was added to 5 ml RsrA, dialysed in thrombin cleavage buffer, and incubated overnight at 4°C to cleave the His-tag.

His-tag cleaved RsrA protein solution was loaded onto a 5 ml HisTrap HP Nickel column (GE Healthcare) to separate cleaved RsrA from the His-tag. The column was washed using the same buffer as the initial nickel column (50 mM Tris pH 7.5, 100 mM NaCl, 0.1 mM $ZnCl_2$, 1 mM imidazole). Cleaved RsrA was collected in the flow-through and washing stages, un-cleaved RsrA required high imidazole concentration to elute from the column. Eluted fractions were selected from the profile before running on SDS-PAGE gels to locate fractions to pool and concentrate to 5 ml (using Vivaspin 20 5000 MWCO).

RsrA was further purified by gel filtration using a Superdex S75 HL 26/60 column (GE Healthcare) equilibrated with gel-filtration buffer (50 mM Tris pH 7.5, 100 mM NaCl, 0.1 mM $ZnCl_2$, 10 mM DTT) on an AKTA FPLC. 5 ml of cleaved RsrA from the second nickel column purification was loaded onto the size exclusion column using a 10 ml superloop manually at a rate of 1 ml/min. RsrA was eluted using an isocratic gradient at a flow-rate of 1 ml/min, 0.5 MPa pressure. Eluted fractions were selected from the profile before running on SDS-PAGE gels to locate fractions to pool, concentrate (using Vivaspin 20 5000 MWCO) and freeze at -80°C.

2.3.7. SigR expression and purification

A single colony of SigR plasmids pMLF01, pMLF02, pMLF03, pMLF04 and pMLF05 transformed into *E. coli* BL21 (DE3), was inoculated and grown overnight in 50 ml LB at 37°C. The culture was diluted between 6 flasks of 800 ml LB (4800 ml) and supplemented with 100 µg/ml Amp antibiotic and grown to mid-log phase OD_{600} 0.6 with shaking at 37°C. Expression was then induced with 1 mM IPTG for 3 hours at 37°C, before cells were harvested by centrifugation at 6238 x g for 20 minutes at 4°C.

Cell pellets were re-suspended in 25 ml lysis buffer (50 mM Tris pH 7.5, 100 mM NaCl, 1 mM PMSF, 1 PIK). The suspension was sonicated (Misonix S4000) on ice for 2 minutes (3 seconds pulse on, 7 seconds pulse off) at 60% amplitude. The cell lysate was centrifuged for 30 minutes at 22,658 x g at 4°C, to pellet cellular debris and collect supernatant containing SigR protein. The pellet of cellular debris was washed before re-suspending in 25 ml lysis buffer for SDS-PAGE analysis.

All SigR constructs were produced without purification tags because it was found during the course of this work that the flexible linker between regions 2 and 4 was very susceptible to proteolysis during cleavage of the tags. Ammonium sulphate was therefore used as an additional purification step. Ammonium sulphate powder (Fisher chemical, 99.9% purity) was added to the protein lysate in fractions calculated by their total volume of lysate using Encor Biotechnology calculator http://www.encorbio.com/protocols/AM-SO4.htm. The first fraction was 20% saturation, which for 30 ml total volume required 3.3 g ammonium sulphate. This was added slowly to the lysate with stirring at 4°C to avoid localised precipitation. This was stirred for 15 minutes, before centrifuging for 15 minutes at 4°C at 12,000 rpm (17,418 x g) to pellet proteins that have precipitated within the 20% fraction. The pellet was kept, and supernatant treated further by the addition of ammonium sulphate for the 40% fraction, allowing the precipitation of proteins between 20-40% saturation. After 15 minutes the lysate was centrifuged at 12,000 rpm (17,418 x g) for 15 minutes, to pellet the precipitate formed from the 40% fraction where SigR was expected. The pellet from the 40% fraction was re-suspended in 25 ml SigR dialysis Buffer (50 mM Tris pH 7.5, 20 mM NaCl, 1 mM EDTA, 0.1 mM PMSF),

and sample taken for SDS-PAGE analysis. The re-suspended pellet was dialysed in 2 L SigR dialysis buffer overnight at 4°C with a 3 hour buffer change to remove ammonium sulphate.

The lysate containing SigR was filtered (0.45 µm), before loading via a 50 ml superloop onto a 30 ml Q-Sepharose column manually at a rate of 1 ml/min. The column containing GE Healthcare Q Sepharose Fastflow resin, was equilibrated with Q-Sepharose buffer A (50 mM Tris pH 7.5, 20 mM NaCl, 1mM EDTA, 0.1 mM PMSF). The column containing SigR (Theoretical pI ~5.38 at pH 7.5 and charge of ~-7.8 (http://protcalc.sourceforge.net/cgi-bin/protcalc)) bound to Q Sepharose using buffer A to remove any unbound protein, and then washed with 5% elution buffer (50 mM NaCl) to remove non-specifically bound protein (50 mM Tris pH 7.5, 1 M NaCl, 1 mM EDTA, 0.1 mM PMSF). Bound SigR was eluted at 1 ml/min using a linear gradient of 50-150 mM NaCl over 20 column volumes. Eluted fractions were selected from the profile before running on SDS-PAGE gels to locate purest SigR. Protein was concentrated to 5 ml (using Vivaspin 20 5000 MWCO) for further purification by size exclusion.

Proteins were subsequently purified using gel-filtration using essentially the same method as described above for RsrA, but using SigR S75 Buffer (50 mM Tris pH 7.5, 100 mM NaCl, 0.1 mM PMSF).

2.3.8. HiTrap desalting column; buffer exchange of SigR and RsrA proteins

1 ml of RsrA and SigR proteins were loaded via a 2 ml sample loop onto a 5 ml HiTrap desalting column (GE Healthcare), prepacked with Sephadex G-25 Superfine resin that was equilibrated using buffers as specified in the text. This column was used to buffer exchange proteins for ITC, stopped-flow, fluorescence and oxidation Native PAGE experiments. The protein was injected via the sample loop onto the column at 1 ml/min, collecting 1.4 ml fractions. The first 1.4 ml fraction collected contained buffer from the column void, the second 1.4 ml contained the protein in the new buffer.

2.4. Biophysical methods

2.4.1. Electrospray-Ionisation Mass spectrometry

The mass of all the proteins purified during this study was verified by electrospray ionisation mass spectrometry (ESI-MS) (Dr David Staunton, Molecular Biophysics Suite, University of Oxford).

2.4.2. Isothermal Titration Calorimetry (ITC)

To investigate the thermodynamics and binding affinity of the interaction between SigR and RsrA, calorimetric analysis was performed using isothermal titration calorimetry (ITC, Microcal iTC200). Purified proteins were buffer exchanged using a Hi-Trap column (as described in section 2.3.8) into fresh ITC buffer, all the titrations were conducted in 50 mM Tris pH 7.5, 100 mM NaCl and 2 mM DTT. Protein concentrations were quantified using a biophotometer as described in section 2.3.4.

Titrations were performed between 40 µl of 100 µM wild-type and mutant SigR proteins in the syringe, and 200 µl of 10 µM for RsrA in the sample cell. The titration was performed at 35°C and SigR was injected in 26 increments of 1.5 µl, with a spacing of 180 seconds between consecutive injections at a stirring speed of 1000 rpm. The initial injection was 1 µl for 2 seconds, the baseline signal reference power was 6 µcal/sec, with high feedback. Controls included the titration of SigR into buffer, buffer into RsrA, and buffer into buffer, to determine the heats of dilution and effect of solution mixing.

For data analysis, the raw data peaks were integrated and fit to a single set of identical sites model by non-linear regression using Microcal Origin 7 software, from which the K_a and hence the equilibrium K_d were obtained. The fitting equation implemented by Origin to fit data is shown below.

$$Q = \frac{nM_t \Delta HV_o}{2}\left[1 + \frac{X_t}{nM_t} + \frac{1}{nKM_t} - \sqrt{\left(1 + \frac{X_t}{nM_t} + \frac{1}{nKM_t}\right)^2 - \frac{4X_t}{nM_t}}\right]$$

(Q= total heat content, K= binding constant, n= number of sites, V_o= active cell volume, M_t and [M] are bulk and free concentration of macromolecule in V_o, X_t and [X] are bulk and free concentration of ligand, Θ= fraction of sites occupied by ligand X.)

The variation of Gibbs free energy was calculated using;

$\Delta G^0 = - RT \ln K_A$

K_a= ([LM]/[L][M]), a dissociation constant can also be defined using K_d= ([L][M]/[LM])

Entropy changes were then calculated using;

$\Delta G = \Delta H - T\Delta S$

2.4.3. Steady-state Tryptophan Fluorescence emission quenching

RsrA (+Zn) and SigR were buffer exchanged using a Hi-Trap column into 50 mM Tris pH 7.5, 100 mM NaCl, 2 mM DTT (Section 2.3.8). SigR was diluted to 1 µM in a 3 ml quartz cuvette with a 10 mm path length and placed in a FluoroMax-4 spectrophotometer (HORIBA Scientific).

An initial excitation scan was performed using a 343 nm emission wavelength and a scanning excitation wavelength of 200-300 nm. An emission scan was also performed to determine emission λ_{max} for SigR using an excitation of 295 nm wavelength and a scanning emission wavelength of 310-450 nm. The CPS (counts per second) score of each protein at 343 nm was increased to 1 million by increasing the slit widths of both excitation and emission monochromators to normalise the data and allow comparison of fluorescence intensity changes during fluorescence quenching titrations. SigR used 3.8 nm slit widths, SigR W88I used 4.7 nm, SigR W119I used 4.3 nm, SigR* used 3.8 nm, and SigR* F159W used 4.1 nm slit widths for excitation and emission monochromators.

Fluorescence measurements were performed at 25°C, the temperature maintained by a circulating water bath. Tryptophan excitation was performed at 295 nm and emission was scanned between 310-450 nm. After the initial fluorescence intensity of each SigR protein was recorded, RsrA was titrated at 0.1 µM per titration into the quartz cuvette of SigR. The solution was thoroughly mixed

before placing the cuvette in a thermostatically controlled cell holder in the fluorometer, with a 5 minute temperature equilibration time to reach 25°C. Fluorescence intensity was then measured with three accumulations per addition to obtain an average, and repeated for each titration from 0.1 µM to 1.2 µM RsrA in 0.1 µM increments, in which saturation of SigR was observed and no further fluorescence intensity change measured. 1.2 µM to 2.0 µM RsrA was then titrated into the solution at 0.2 µM increments to ensure no further change.

The emission spectrum of the buffer used (50 mM Tris pH 7.5, 100 mM NaCl, 2 mM DTT) was obtained using an excitation of 295 nm and emission scanning of 310-450 nm and slit widths cited for the respective SigR proteins. This was to obtain the correction for buffer contribution and inelastic Raman scattering peak of the solvent to be removed from each fluorescence intensity emission scan. The wavelength of the peak is dependent on the excitation wavelength used, calculated using; $1/\lambda_{RA}=1/\lambda_{EX}-0.00033$. So 1/295 nm-0.00033=$1/\lambda_{RA}$ =327 nm.

Steady-state fluorescence intensity data were normalised using F/F_0, where F is the fluorescence intensity at that RsrA titration concentration, and F_0 is the initial fluorescence intensity.

2.4.4. Association kinetics of SigR-RsrA complex formation

Stopped-flow fluorescence experiments were performed to study pre-equilibrium fluorescence changes on complex formation on an Applied Photophysics SX20 stopped-flow spectrofluorometer (Instrument dead time ~2 ms). RsrA, with and without zinc, and SigR were buffer exchanged using a Hi-Trap column into 50 mM Tris pH 7.5, 100 mM NaCl, 2 mM DTT (as described in section 2.3.8). SigR was diluted to a cell concentration of 0.125 µM in 2 ml and RsrA+/-Zn diluted to 10-20-fold excess concentrations (1.25 µM, 1.5 µM, 1.75 µM, 2 µM, 2.25 µM, and 2.5 µM) per 2 ml to allow the reaction to proceed under pseudo-first order conditions. To detect tryptophan fluorescence emission, an excitation wavelength of 295 nm was used while the fluorescence emission was monitored above 320

nm in the case of the SigR-RsrA complex, using a cut-off filter and a voltage of 500V. The manual entrance and exit monochromator slits were set to 2 mm (with a bandpass of 4.6 nm/mm). Experiments were carried out at both 25°C and 35°C, which was maintained using a circulating water bath. The time course of fluorescence quenching on complex formation was recorded, collecting between 2000-5000 points.

Each injection of the two proteins was measured over 1.5 seconds in prodata SX software, with 5 injections performed to obtain an average, this was repeated a total of 15 times per RsrA concentration to obtain 3 averages. The pseudo-first-order kinetic traces were fitted using the Pro-Data software from Applied Photophysics Ltd. to a single-exponential rate equation: $F=\Delta F_1 \exp(+k_{obs1} t)+Fe$

Where F is the fluorescence at time t, ΔF is the total fluorescence change, k_{obs} is the observed rate constant, and Fe is the end-point fluorescence (by nonlinear least-squares regression analysis using the Workstation software (Applied Photophysics Ltd.)).

Three values were obtained; k_{obs}, a, and c. c is the end point of fitted data (*F*e), a is the amplitude/total intensity of signal change (ΔF_1), and k_{obs} is the apparent rate constant per second. The software also gives residuals of data minus the fit. Data fitting involved plotting the pseudo-first-order k_{obs} against the excess RsrA concentrations used and fitting to the equation of a straight line, providing a slope-intercept linear equation; y=mx+ b. This gives a value for the 'on'-rate (m or slope) and 'off' rate (b or Y-axis intercept) for the binding of SigR and RsrA in a pre-steady state before equilibrium is reached. A reliable 'off' rate could not be obtained by this method, and was therefore determined by competition stopped-flow (see below). Binding affinity was determined using the following equation; $K_d = k_{off}/ k_{on}$.

2.4.5. Dissociation kinetics by competition fluorescence Stopped-flow

SigR-RsrA complex with zinc was pre-formed and run through a gel filtration column to ensure no excess of either protein in the complex. SigR-RsrA complex without zinc was formed using RsrA that had been stripped of its zinc by incubating with 1 mM EDTA on ice for 15 minutes, and buffer exchanged to remove EDTA and zinc. Complexes were then formed and run through a gel filtration column, and buffer exchanged into its respective buffer.

Competition experiments were performed under the same experimental conditions as association rate data above at both 25°C and 35°C. Complex with and without zinc was held constant at 0.5 µM cell concentration against SigR* (SigR in which both tryptophans had been substituted for isoleucine) at 5 µM, a 10-fold excess ensuring any RsrA that dissociated from the complex would bind SigR*. The two proteins were injected and the time course of fluorescence change on competition between SigR* and SigR for binding RsrA recorded over time. All dissociation reactions were carried out in triplicate. Data were fitted to a single exponential rate equation as association rate above ($F=\Delta F_1 \exp(-k_{obs1}t)+Fe$), assuming k_{on} is larger than k_{off}, then k_{obs} is equal to k_{off}. Controls were performed by injecting buffer, SigR, RsrA and complex against buffer.

2.4.6. Circular Dichroism (CD) Spectroscopy

CD spectra were obtained using a Jasco J-815 CD spectrometer, at both far-UV (260-190 nm) and near-UV (350-250 nm) regions under constant nitrogen flush. 1 ml of ~350 µM SigR, SigR* F171W and SigR* F159W were dialysed into 10 mM Tris pH 7.5 overnight at 4°C using dialysis membrane with a MWCO of 12-24 kDa. For Far UV, 250 µl of each protein at 5 µM (0.124 mg/ml) was loaded into a 1 mm path length quartz cuvette. Scans were performed from 260-190 nm at a temperature of 20°C, 25°C and 35°C, with an ellipticity scanning speed of 100 nm/min, a data pitch of 0.5 nm and a multiplicity of 4 accumulations. The baseline was measured using Tris pH 7.5 buffer, which was subtracted from the average of the 4 accumulative scans. For near UV, 2 ml of each protein at 40 µM (0.98 mg/ml) was

loaded into a 1 cm pathlength quartz cuvette. Scans were performed using the same parameters as far UV, but measuring from 350-250 nm at a temperature of 20°C.

3- Establishing a fluorescence-based assay to monitor SigR-RsrA complex formation

SigR-RsrA complex formation has previously been monitored using native PAGE and gel filtration chromatography (Li et al. 2003). SPR has been used to determine the K_d of SigR-RsrA as 11 nM (Kang et al. 1999), however no further thermodynamic or kinetic work has been undertaken. A fluorescence resonance energy transfer (FRET) based system has been developed by Wei et al. (2014) for SigR-RsrA, using Cyan Fluorescent Protein (CFP) and Yellow Fluorescent Protein (YFP) to determine the K_d as 81 nM for the complex in the absence of zinc.

The first aim of this research was to develop an intrinsic fluorescence-based-assay to monitor complex formation, which could be used to investigate the kinetics of the SigR-RsrA complex.

SigR contains two naturally occurring tryptophan residues which could be exploited to observe changes in fluorescence on complex formation. A series of SigR tryptophan mutants was designed and purified as described below, to identify if either tryptophan residue was sensitive to the binding of RsrA and therefore binding interaction.

3.1. SigR Tryptophan mutagenesis and purification

SigR group 4 ECF sigma factor is a 24.8 kDa protein with 224 amino acids. It is composed of region 2 and region 4 DNA binding domains connected by a flexible linker region. SigR has two tryptophan residues, one at residue 88 in the region 2 domain, and one at residue 119 in the linker region (Figure 28).

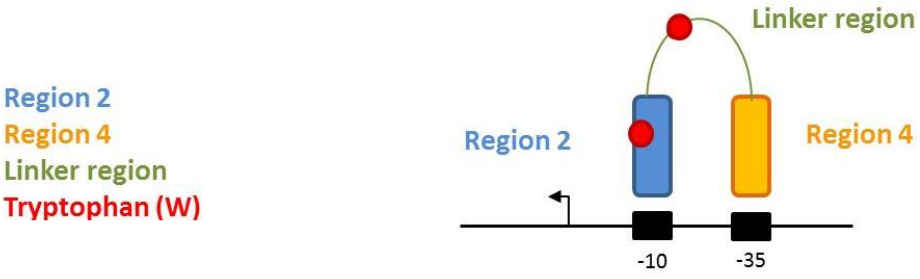


Figure 28- SigR structure. SigR is composed of 224 amino acids with a molecular weight of 24.8 kDa. The sequence encodes a highly conserved region 2 (light blue) and a region 4 (yellow) connected by a flexible linker region (green). The sequence contains two tryptophans (red circles) in region 2 and the linker region.

Site-directed mutagenesis was performed using PCR to mutate each of SigR's tryptophans to isoleucine, using the protocol and primers shown in Materials and methods section 2.2.2. Three SigR mutants were created; SigR W88I, SigR W119I single mutants and SigR W88I W119I double mutant, referred to as SigR* (Figure 29).

In addition, two further SigR mutants were created, mutating two phenylalanine residues in region 4 to tryptophan residues at position F171 and F159 using SigR* as a template. Mutations were confirmed by DNA sequencing.

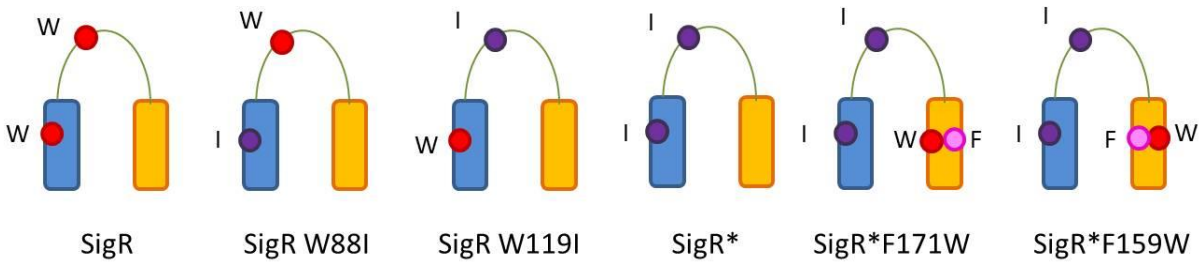


Figure 29- SigR mutants generated in this study. SigR tryptophan (W) to isoleucine (I) mutations for region 2 SigR W88I, linker region SigR W119I and SigR* double mutant. SigR region 4 phenylalanine (F) to tryptophan (W) mutations using SigR* as a template. Tryptophans are red circles, isoleucines are purple circles and phenylalanines are pink circles.

The two phenylalanine (F) residues in region 4 at position F159 and F171, were chosen based on a homology model generated by Dr Karthik Rajasekar, based on the structure of ChrR-SigE (Figure 30). Residues were chosen on opposite sides of region 4 in the proposed model of SigR.

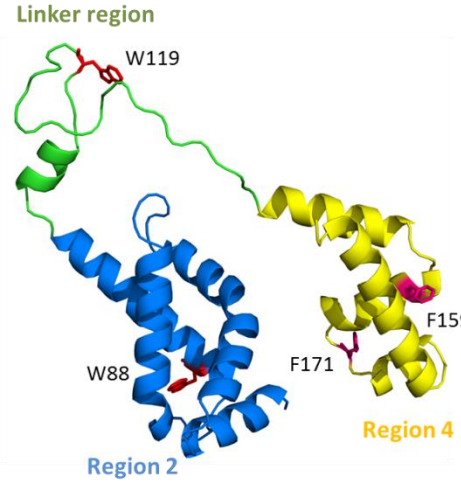


Figure 30- Homology model of SigR. Model was based on the structure-based sequence alignments of ChrR-SigE (2Q1Z) from *Rhodobacter sphaeroides*. From this, a preliminary model of SigR in complex was made using swiss model and energy minimised using Kobamin software. The alignment of the two protein structures was used to design several homology models of SigR, of the models suggested, the top scoring model was chosen. The two natural tryptophans at position 88 and 119 are highlighted in red, and the two phenylalanines in region 4 are highlighted in pink (Rajasekar and Kleanthous, unpublished data).

3.1.1. SigR mutant test expressions

The mutant *sigR* genes cloned into a pET-21a plasmid were then transformed into *E. coli* BL21 (DE3) and BL21 (DE3) pLysS cells to test for expression. For each SigR mutant, SDS-PAGE showed highest expression in BL21 (DE3) cells, after induction with 1 mM IPTG for 3 hours (Figure 31) (as described in Materials and methods section 2.3.5). Hence BL21 (DE3) cells were used for the expression of all SigR mutants.

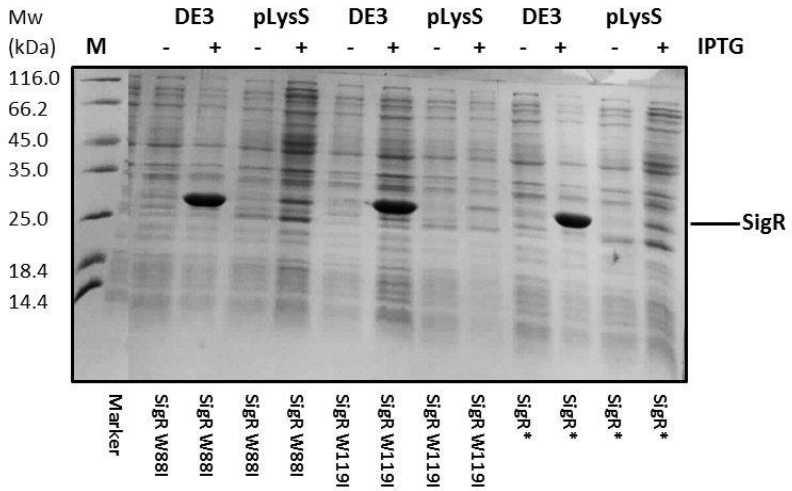


Figure 31- SDS-PAGE gel test expression of SigR tryptophan mutants using BL21 (DE3) and BL21 (DE3) pLysS cells. Cells were grown in the presence of appropriate antibiotics in LB to OD_{600} 0.6, and expression was induced using 1 mM IPTG at 37°C for 3 hours. Samples were taken for both induced and non-induced cultures for subsequent 16% SDS-PAGE analysis.

3.1.2. Large-scale SigR protein expression

Large scale protein expressions of SigR, SigR W88I, SigR W119I, SigR*, SigR* F159W and SigR* F171W mutants were performed in BL21 (DE3) cells. All SigR constructs were purified by the same methods without purification tags (Materials and methods section 2.3.7.). The purification of SigR* is shown below as a representative example.

3.1.3. Ammonium sulphate precipitation

SigR* in sonicated cell lysates (Misonix S4000) was first fractionated using ammonium sulphate (20%-40% saturation). SDS-PAGE demonstrated the precipitation of SigR* (24.8 kDa) within these ammonium sulphate cuts (Figure 32). The pellet of the 40% cut was re-suspended and dialysed to remove ammonium sulphate.

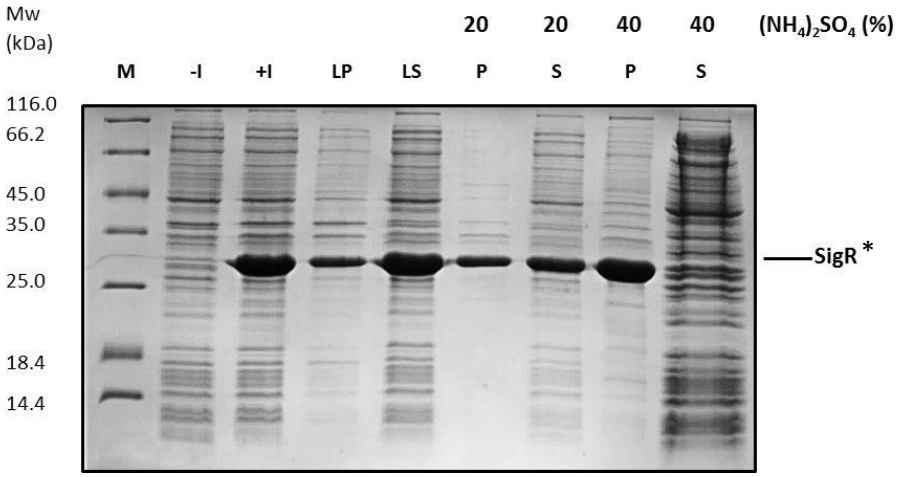


Figure 32- SigR* ammonium sulphate precipitation purification. 16% SDS-PAGE Coomassie gel showing the Marker (M) and expression of SigR* in BL21 (DE3) cells before (-I) and after IPTG (+I) induction. Lanes show the cellular lysed pellet (LP) and lysed supernatant (LS) fractions, and pellet (P) and supernatant (S) after 20% and 40% ammonium sulphate precipitation.

The dialysate was loaded onto a Q-Sepharose Anion exchange column equilibrated in 50 mM Tris pH 7.5, 20 mM NaCl, 1 mM EDTA, 0.1 mM PMSF. SigR* was eluted from the column using a linear gradient of 50-150 mM NaCl, in which it eluted at 150 mM. Non-specific bound proteins and impurities that were eluted during the 50 mM NaCl step gave a small peak (Figure 33). SDS-PAGE was used to

determine the elution position of SigR (Figure 34). Fractions corresponding to elution volume 165-230 ml were pooled and concentrated (using Vivaspin 20 5000 MWCO) for gel filtration chromatography.

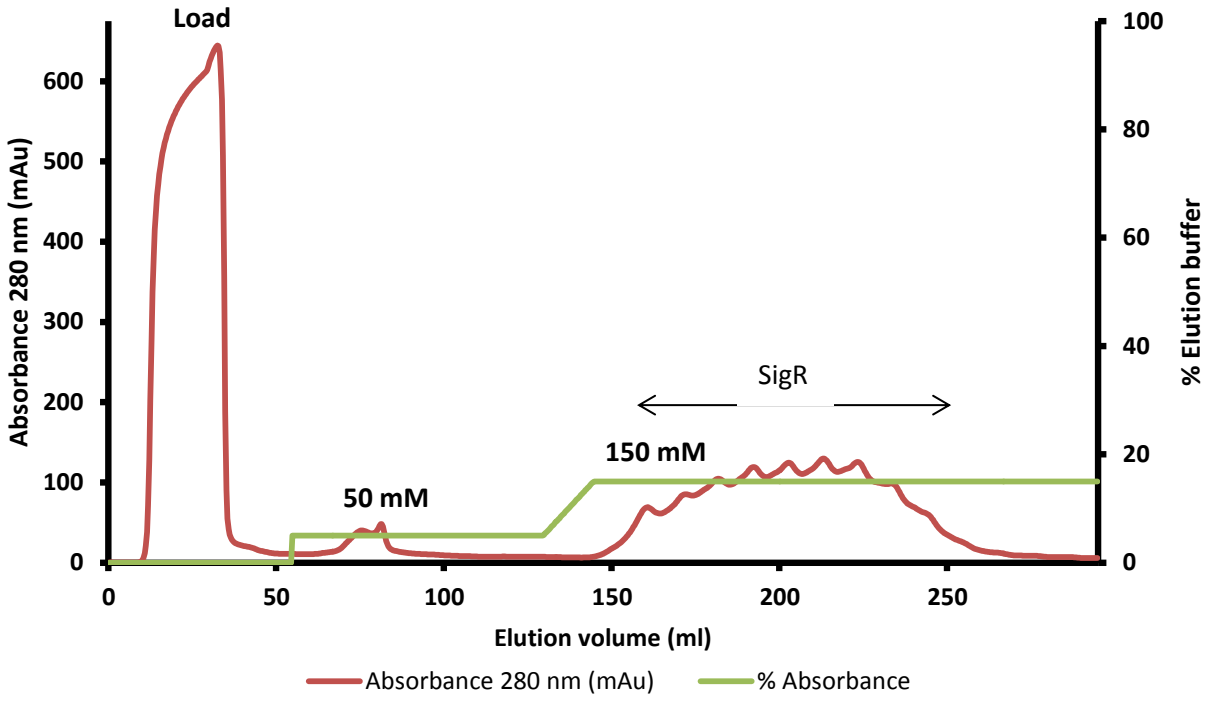


Figure 33- SigR* Q Sepharose Anion Exchange chromatography purification. SigR* was eluted at 1 ml/min using 50 mM Tris pH 7.5, 1 M NaCl, 1 mM EDTA, 0.1 mM PMSF buffer. Elution profile of SigR* at 150 mM NaCl concentration. Fractions of the load, 50 mM and 150 mM elution were run on 16% SDS-PAGE to locate SigR* and demonstrate its purity. The black arrow represents SigR* elution at 150-250 ml elution volume.

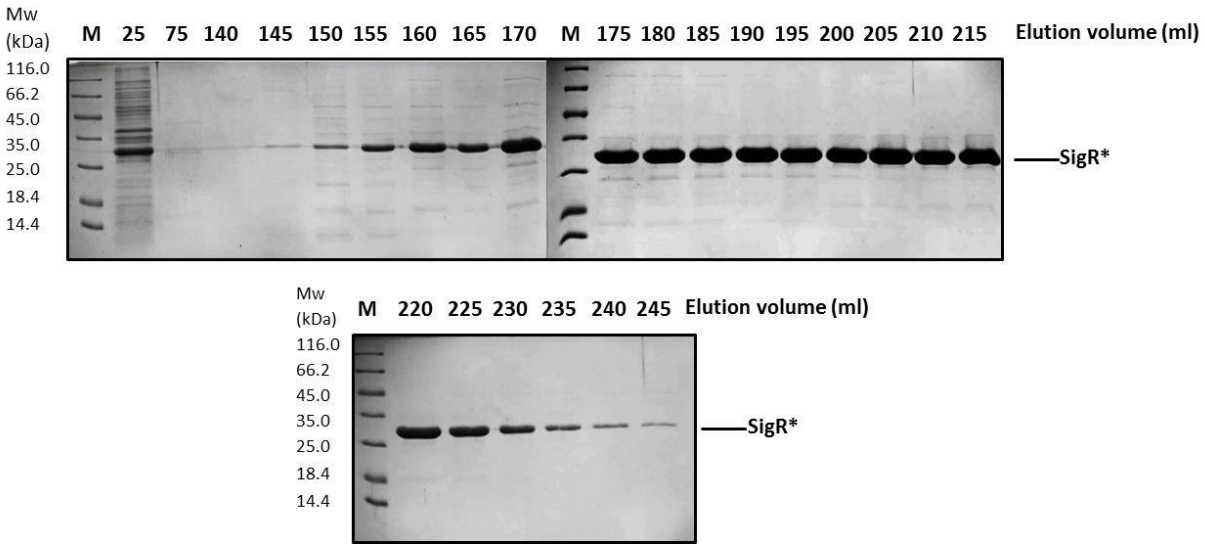


Figure 34- 16% SDS-PAGE of samples from SigR* Q-Sepharose Anion exchange chromatography. Samples from elution volume 165-230 ml containing the purest SigR* were pooled and concentrated.

3.1.4. SigR size exclusion purification

Each SigR protein was further purified by size-exclusion gel filtration chromatography on a HiLoad 26/60 Superdex 75 column at 4°C (See Materials and methods section 2.3.7.). SigR* was concentrated (using Vivaspin 20 5000 MWCO) to 5 ml, loaded and eluted isocratically using 50 mM Tris pH 7.5, 100 mM NaCl, 0.1 mM PMSF (Figure 35). SDS-PAGE identified eluted fractions containing SigR* and demonstrating its purity (Figure 36). Fractions corresponding to 120-175 ml were pooled and concentrated (using Vivaspin 20 5000 MWCO) to 0.22 mM (5.46 mg/ml), flash frozen and stored at -80°C for later experiments.

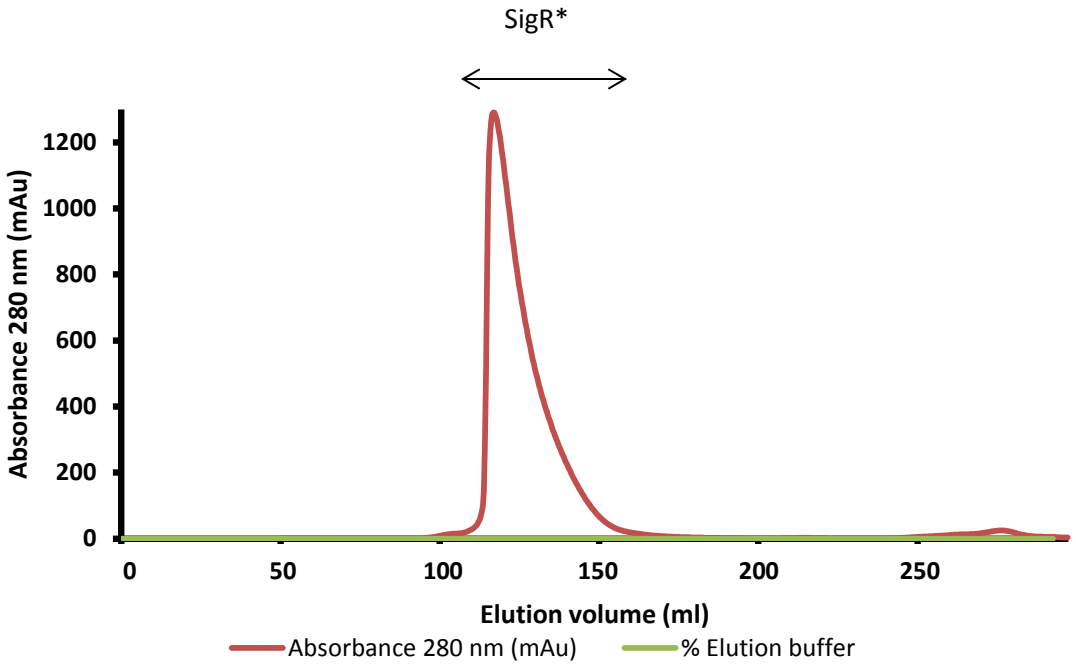


Figure 35- SigR* Size exclusion chromatography purification. Elution profile of SigR* from a HiLoad 26/60 Superdex 75 column equilibrated in 50 mM Tris pH 7.5, 100 mM NaCl, 0.1 mM PMSF, eluted at 1 ml/min. Fractions corresponding to 100-175 ml were run on SDS-PAGE to locate SigR* and demonstrate its purity. The black arrow represents SigR* elution.

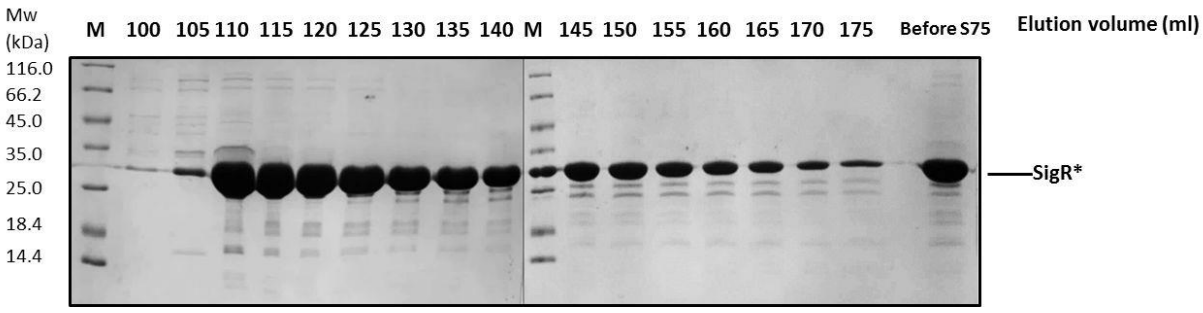


Figure 36- 16% SDS-PAGE of samples from SigR*size exclusion chromatography. Samples from elution volume 120-175 ml containing the purest SigR* were pooled and concentrated.

Each SigR protein used in this study was purified using the same protocol as shown above. SDS-PAGE gels of the final Size exclusion purification showing the purity of each protein are shown in Figure 37. All proteins were concentrated (using Vivaspin 20 5000 MWCO) typically at a concentration of 5.46-31.8 mg/ml, and flash frozen at -80°C. Final stock concentrations are listed in table 9. The masses of all purified proteins were confirmed by ESI-MS (Table 9).

Table 9- Final SigR protein concentrations, predicted and observed molecular weights used in this study. Comparison of the predicted molecular weight and observed molecular weight as determined using ESI-MS for each construct.

SigR protein	Stock concentration (5 ml) mg/ml	Total yield (mg)	Predicted mW (Da)	Observed mW (Da)
SigR	8.6	43	24,960	24,968
SigR W88I	23.6	118	24,891	24,894
SigR W119I	31.8	159	24,891	24,894
SigR*	5.46	27.3	24,818	24,822
SigR* F171W	16.6	83	24,891	N.D.
SigR* F159W	7.9	39.5	24,891	N.D.
RsrA	7.8	39	11,962	11,962

3.1.5. Final Size exclusion purifications of all SigR proteins

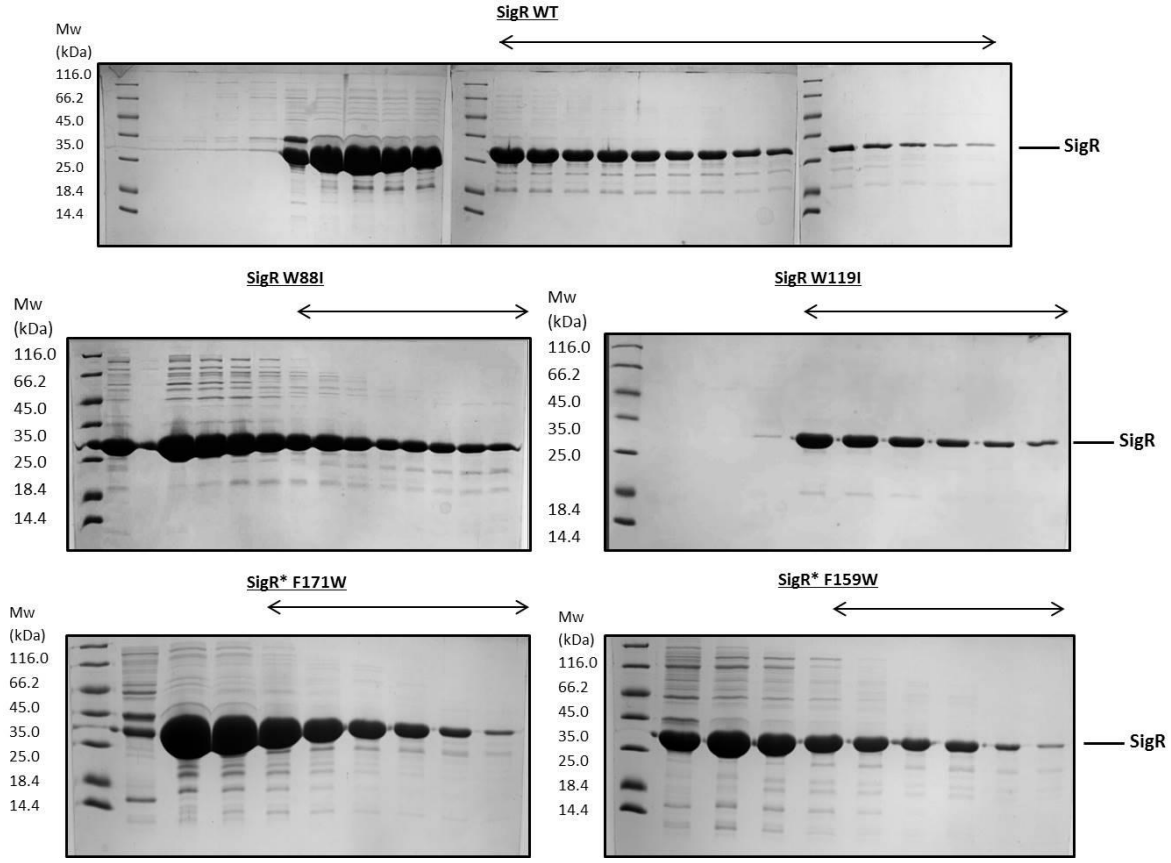


Figure 37- Final SigR Size exclusion chromatography purifications. 16% SDS-PAGE gels showing the final Size exclusion purifications of SigR WT, SigR W88I, SigR W119I, SigR* F171W, and SigR* F159W used for further kinetic and thermodynamic characterisation. Lanes show the Marker (M), and fractions from size exclusion elution profiles. Fractions highlighted with arrow containing the purest SigR were pooled and concentrated.

3.2. RsrA purification

3.2.1. RsrA test expression

RsrA pET-15b plasmid was transformed into *E. coli* Rosetta 2 pLysS cells, a test expression was performed to determine optimal expression conditions. SDS-PAGE showed optimal expression using 1 mM IPTG for 2.5 hours at 37°C in the presence of zinc (Figure 38).

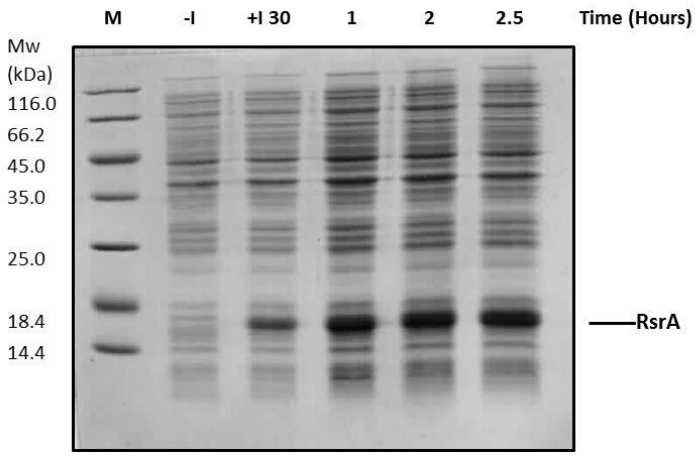


Figure 38- 16% SDS-PAGE test expression of RsrA in Rosetta 2 pLysS cells. Cells were grown in the presence of 10 µM $ZnCl_2$ in LB to OD_{600} 0.6, and expression was induced using 1 mM IPTG at 37°C for 30 minutes, 1, 2 and 2.5 hours. Samples were taken for SDS-PAGE analysis as indicated.

3.2.2. Large-scale RsrA protein expression and Nickel affinity purification

Large-scale expression of RsrA was performed in Rosetta 2 pLysS cells (as described in Materials and methods section 2.3.6.). RsrA has an N-terminal (hexa)polyhistidine tag, allowing purification by immobilised metal ion affinity chromatography (IMAC) column charged with nickel ions. The sonicated lysate (Misonix S4000) was loaded onto a 5 ml nickel column and RsrA eluted using a linear gradient of 20-500 mM imidazole. Non-specifically bound proteins and impurities that eluted during the 20 mM imidazole step gave a large peak (Figure 39). SDS-PAGE identified eluted fractions containing RsrA (Figure 40), fractions corresponding to 179-207 ml were pooled and dialysed into thrombin cleavage buffer to remove imidazole. The protein solution was then concentrated (using Vivaspin 20 5000 MWCO) to ~1 mg/ml in 10 ml and incubated with 20 Units thrombin for cleavage of the His-tag overnight at 4°C.

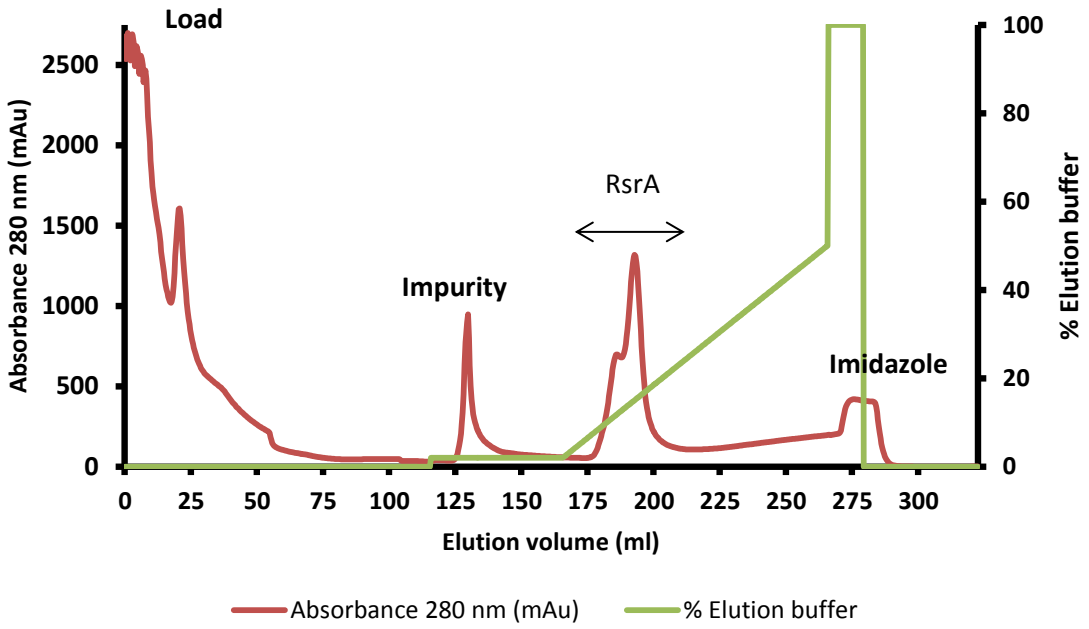


Figure 39- RsrA IMAC nickel affinity purification using a 2-50% 1M imidazole gradient (20-500 mM). The first peak corresponds to the loading. SDS-PAGE identified elution position of RsrA 179-207 ml. The black arrow represents RsrA elution.

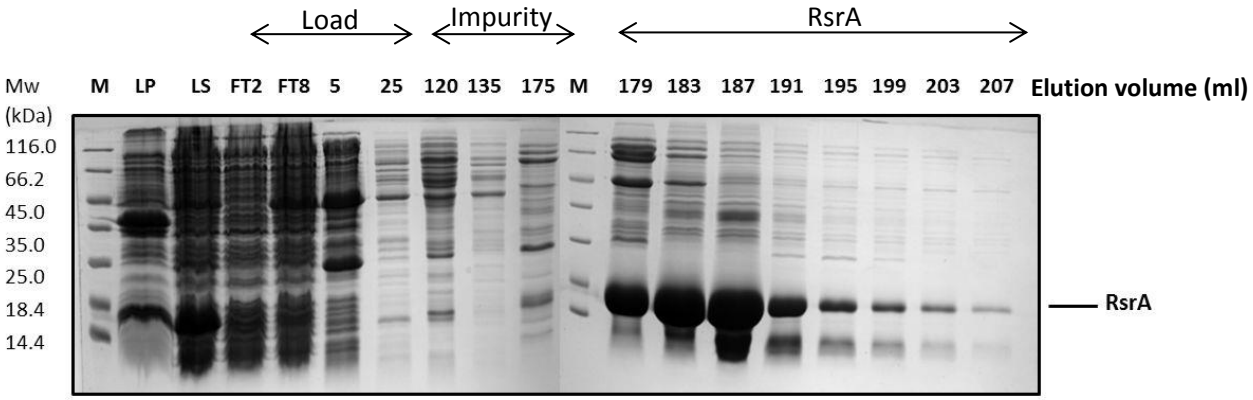


Figure 40- RsrA Immobilised metal affinity chromatography (IMAC) nickel column purification. 16% SDS-PAGE Coomassie gel showing the marker (M), the cellular lysed pellet (LP) and lysed supernatant (LS) fractions, the flow-through (FT) from the loading of the column and fractions from nickel column elution profile. Samples from elution volume 179-207 ml were pooled and concentrated.

3.2.3. RsrA nickel affinity column re-bind

Following thrombin cleavage the protein solution was re-loaded onto the nickel affinity column, with cleaved protein eluting in the flow-through and un-cleaved RsrA binding to the column. Un-cleaved protein was then eluted using buffer containing 1 M imidazole (Figure 41 & 42). The flow-through and

first 8 ml was then pooled and concentrated (using Vivaspin 20 5000 MWCO) for gel filtration chromatography. Unexpectedly, un-cleaved RsrA migrates further than cleaved in SDS-PAGE gels (Figure 42).

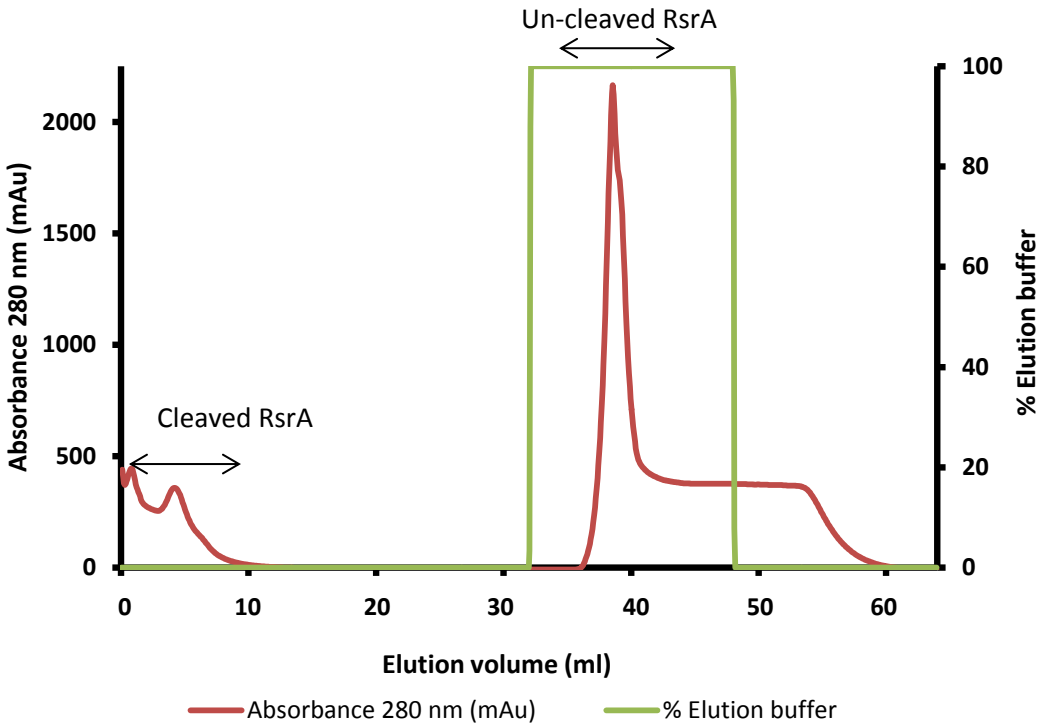


Figure 41- Second RsrA IMAC nickel affinity purification. The first peak corresponds to thrombin cleaved RsrA. The large peak at ~40 ml corresponds to a small amount of un-cleaved RsrA and other impurities. Fractions were run on SDS-PAGE gel to locate RsrA and demonstrate its purity. The black arrow represents RsrA elution.

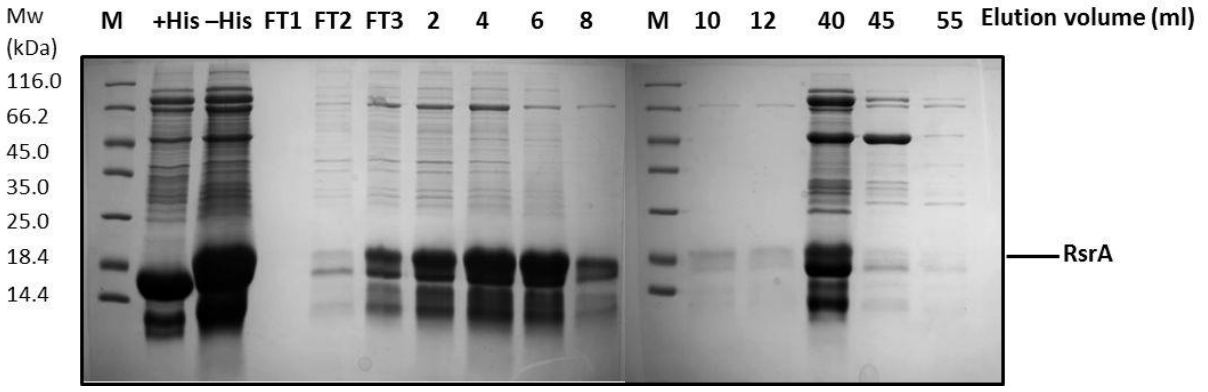


Figure 42- RsrA IMAC nickel column re-bind purification. 16% SDS-PAGE Coomassie gel showing the marker (M), RsrA before (+His) and after (-His) His-tag cleavage, the flow-through (FT) from the loading of the column and fractions from nickel column elution profile. Flow-through (FT) and 2-8 ml containing the purest RsrA were pooled and concentrated for gel filtration chromatography.

3.2.4. RsrA size exclusion purification

RsrA was further purified by size-exclusion gel filtration chromatography using a HiLoad 26/60 Superdex 75 column equilibrated in 50 mM Tris pH 7.5, 100 mM NaCl, 0.1 mM $ZnCl_2$, 10 mM DTT at 4°C (See Materials and methods section 2.3.6.). RsrA was concentrated (using Vivaspin 20 5000 MWCO) to 5 ml, loaded and eluted isocratically (Figure 43). SDS-PAGE identified eluted fractions containing RsrA and demonstrated its purity (Figure 44). Fractions corresponding to 154- 186 ml were pooled and concentrated (using Vivaspin 20 5000 MWCO) (7.8 mg/ml), flash frozen and stored at -80°C for later use in kinetic and thermodynamic experiments.

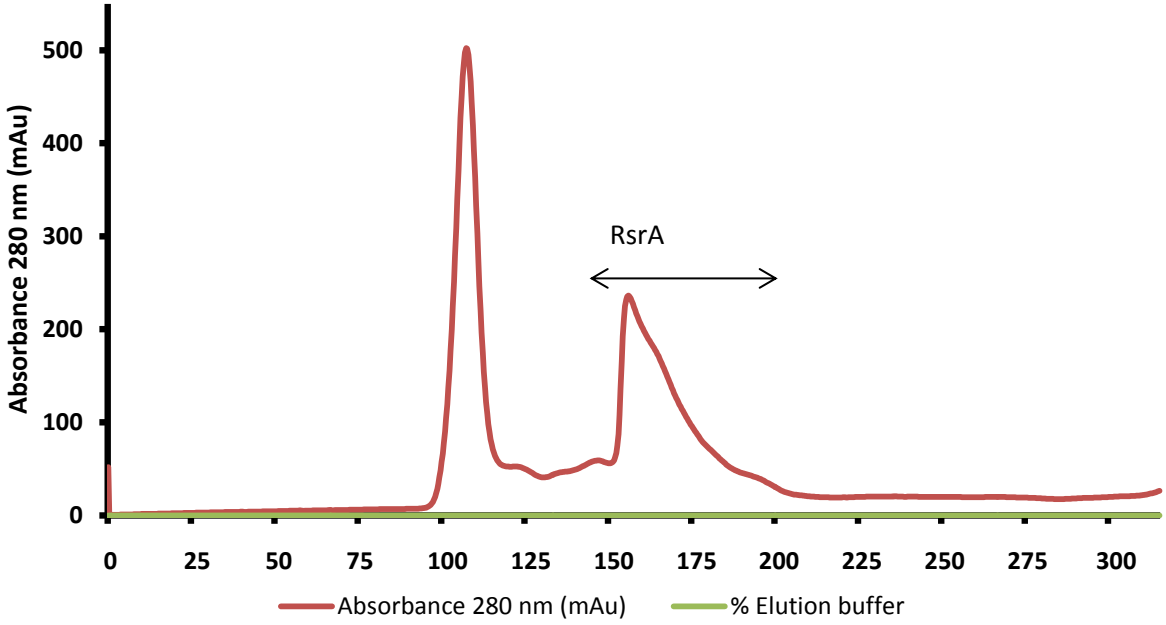


Figure 43- Size exclusion chromatography purification elution profile of RsrA. The first peak corresponds to impurities and higher molecular weight proteins, the second peak corresponds to RsrA. Samples were run on 16% SDS-PAGE to locate RsrA and demonstrate its purity. The black arrow represents RsrA elution.

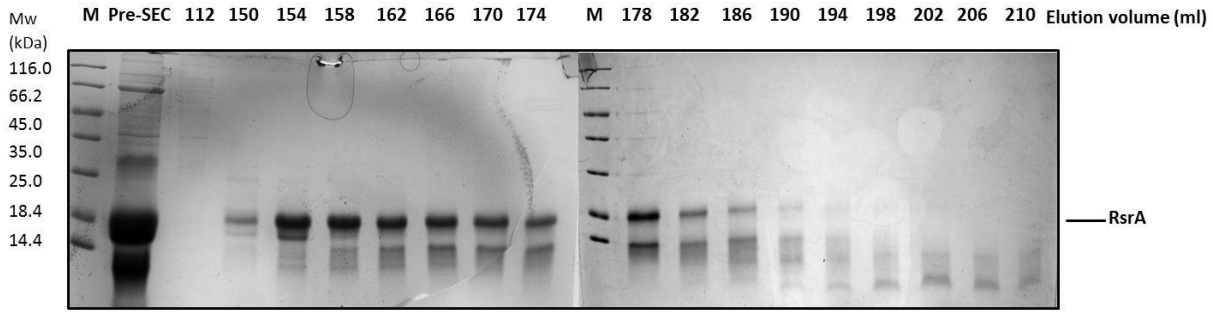


Figure 44- RsrA Size exclusion chromatography purification. 16% SDS-PAGE Coomasie gels showing the Marker (M), a sample of RsrA before size exclusion purification (Pre-SEC) and fractions from HiLoad 26/60 Superdex 75 column elution profile, samples from elution volume 154-186 ml containing the purest RsrA was pooled and concentrated to 0.67 mM (7.8 mg/ml). RsrA is seen as two bands of different intensities, the lower molecular weight band corresponds to the degradation product of RsrA.

3.3. Complex formation between SigR-RsrA by Native PAGE

16% native PAGE was used to confirm all SigR mutants bound RsrA, 50 µM of SigR proteins, were incubated with 50 µM RsrA on ice for 15 minutes. 8 µl of 50 µM of each of the single proteins and complexes were then loaded onto a 16% polyacrylamide gel and the gel was run at 20 mA for 3 hours at 4°C. Complexes had different mobilities to the individual proteins.

Results showed single proteins of SigR and its mutants ran at similar migrations, RsrA migrated further. On complex formation, an intermediate migration between those of the single proteins was formed, confirming SigR, SigR W88I, SigR W119I and SigR* form complexes with RsrA (Figure 45).

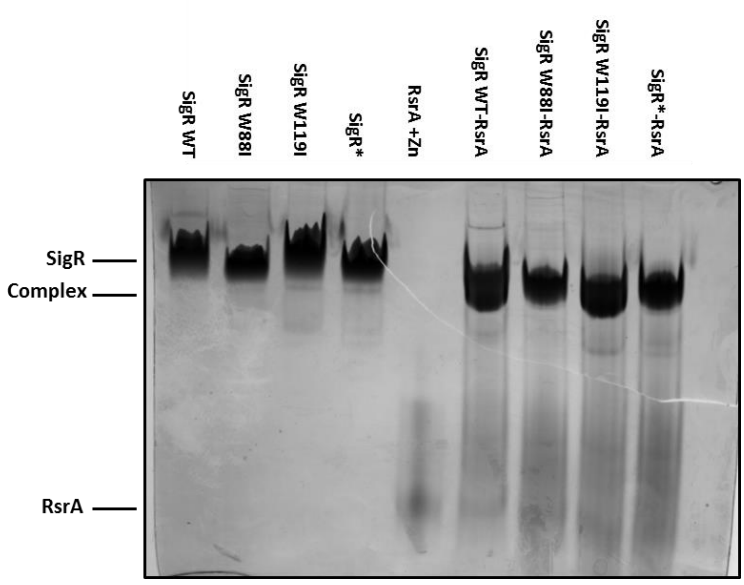


Figure 45- Complex formation between RsrA+Zn and SigR mutants at 50 µM. Gel was run in tris-glycine buffer at pH 9.4, for 3 hours at 20 mA at 4°C. Gel shows that SigR and mutants form complexes with RsrA. RsrA appears as a smear as it runs poorly on native PAGE.

3.4. Development of a tryptophan fluorescence-based assay for monitoring SigR-RsrA complex formation

SPR has been used to determine the K_d for SigR-RsrA as well as the kinetics of interaction for similar homologous complexes (Kang et al. 1999). SPR requires the immobilisation of a protein onto a chip. SigR-RsrA associate by movement in the cytoplasm, immobilising either SigR or RsrA on a chip does not mimic natural conditions. Similarly, sites of interaction are not fully characterised for this complex, therefore their immobilisation could interfere with these sites.

A fluorescence resonance energy transfer (FRET) based system has been developed by Wei et al. (2014) for monitoring SigR-RsrA complex formation, using Cyan Fluorescent Protein (CFP) and Yellow Fluorescent Protein (YFP). This FRET-based method has been used to monitor complex formation and determine a K_d of 81 nM in the absence of zinc only, not in the presence of zinc or for determining kinetic parameters. Using this FRET-based assay Wei et al. (2014) monitored the sensitivity of the SigR-RsrA complex in the presence and absence of zinc to various ROS, by measuring the FRET emission ratios, monitoring changes that occurred to help understand the regulatory mechanism. Their results showed that disulphide bond formation, zinc expulsion and SigR dissociation can be induced by ROS directly.

The uncertainty with this is that the method uses very large tags, which may affect either the structure of the protein or interfere with the interaction with its partner, thereby affecting the end result. This method allows monitoring of the complex *in vivo*, however it is performed in *E. coli* instead of *S. coelicolor*, therefore the result may not be a true representation of what is naturally occurring.

Intrinsic protein fluorescence quenching experiments were used as an approach to develop a fluorescence-based assay for use in monitoring the SigR-RsrA complex and ultimately for dissecting the kinetics of complex formation. The assay also provided indirect structural information about the regions of SigR involved in binding RsrA.

The structure of SigR region 2 DNA binding domain has been solved individually by X-ray crystallography (Li et al. 2002). The complete structure of SigR, or SigR in complex with RsrA has not been determined. There have been direct binding studies showing that RsrA binds to SigR region 2 (Li et al. 2002) and the binding affinity of the complex has been determined by SPR, K_d 11 nM (Kang et al. 1999). There is evidence from other sigma factors, the structures of which have been solved in complex with their anti-sigma factors, that the anti-sigma binds region 2 and region 4 during complex formation. For example, ChrR-SigE from *Rhodobacter sphaeorides*, FlgM-Sig^{28} from *Aquifex aeolicus* (Campbell et al. 2008) and RseA-SigE from *Escherichia coli* (Campbell et al. 2003).

During the course of this work I developed an intrinsic protein fluorescence method to monitor complex formation between RsrA and SigR, that could be adapted for pre-steady state experiments. I discovered that RsrA quenches the fluorescence emission of tryptophan residues in SigR in a concentration-dependent manner (Figure 47). This method allowed direct monitoring of RsrA binding SigR and in addition provided information about the environment and exposure of the tryptophans in SigR.

Fluorescence quenching titrations were performed between SigR, SigR W88I, SigR W119I, SigR* and SigR* F159W, with RsrA (which has no tryptophans). The mutants were purified using the same protocol as for SigR (See Materials and methods section 2.3.7.). RsrA+Zn and SigR were buffer exchanged into 50 mM Tris pH 7.5, 100 mM NaCl, 2 mM DTT.

To selectively excite SigR's tryptophan residues, 295 nm excitation was used. An emission scan was performed for SigR using a scanning emission wavelength of 310-450 nm at 25°C (Figure 46).

Emission fluorescence spectra of each SigR mutant were also obtained for direct comparison to the wild-type protein (Figure 46).

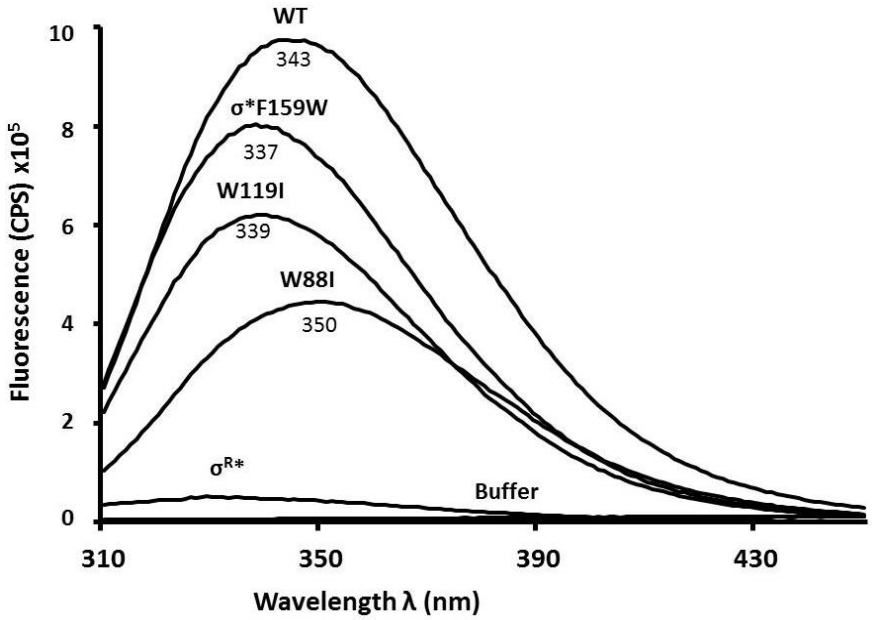


Figure 46- Fluorescence emission spectra of SigR, SigR W88I, SigR W119I, SigR* and SigR* F159W. The scan was performed at 25°C using 295 nm excitation, 310-450 nm emission using 3.8 nm slit widths. Proteins were used at a concentration of 1 µM in 3 ml in 50 mM Tris pH 7.5, 100 mM NaCl, 2 mM DTT. The maximum fluorescence intensity (CPS) of each SigR protein differs based on the number of tryptophans present and the location and environment of the tryptophans. The wavelength max (λ_{max}) of each SigR protein is indicated.

Comparison of the tryptophan fluorescence spectra for SigR and the various mutants (Figure 46), demonstrated that each of SigR's tryptophans contributes to the fluorescence intensity of the wild-type protein. The initial fluorescence intensity emission scans of each SigR protein (Figure 46) also provided indirect structural information about the location and environment of the tryptophans. Wild-type SigR W88 and W119 has a λ_{max} of 343 nm. The SigR W88I mutant, which has a single tryptophan in the linker region, has a λ_{max} of 350 nm and ~40% intensity of the wild-type protein. This emission is red-shifted in comparison to the wild-type, suggesting that this tryptophan is more solvent-exposed, as expected in the flexible linker region. SigR W119I has a single tryptophan in region 2 and has a λ_{max} of 339 nm and ~60% fluorescence intensity. This emission is blue-shifted in comparison to the wild-type, suggesting that this tryptophan is more buried within the hydrophobic region of protein structure of

region 2, as suggested by the homology model. SigR* F159W, which has a single tryptophan in region 4, has a λ_{max} of 337 nm and ~80% fluorescence intensity of the wild-type. This emission is blue-shifted in comparison to the wild-type, similarly suggesting that this residue is buried within the protein.

After the tryptophan emission fluorescence spectrum of each SigR protein was recorded, RsrA was titrated into the cuvette. RsrA caused a quench in the tryptophan fluorescence of SigR, saturating at a 1:1 molar ratio, with the emission maxima remaining at 343 nm (Figure 47 & 48).

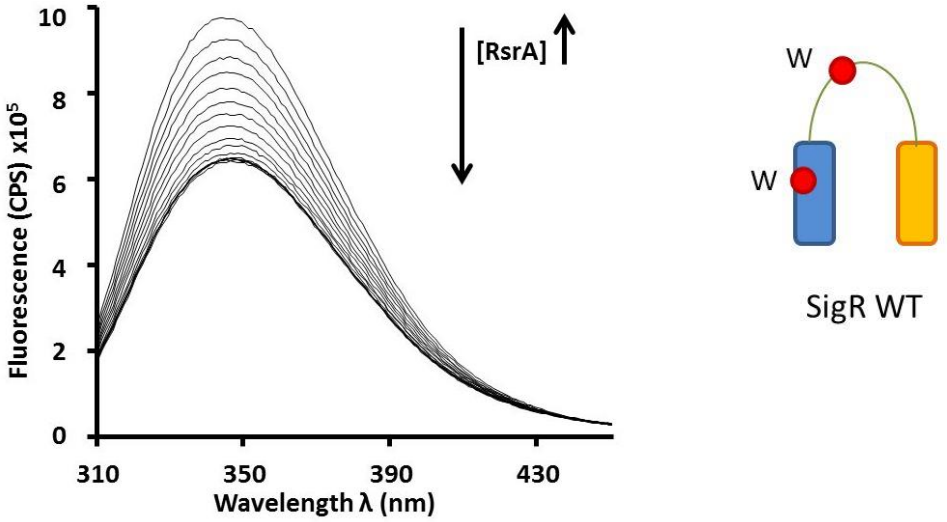


Figure 47- Quenching of SigR tryptophan fluorescence on titration with RsrA. 0.1 µM RsrA was titrated into 1 µM SigR in 50 mM Tris pH 7.5, 100 mM NaCl, 2 mM DTT at 25°C. Excitation at 295 nm and emission maximum at 343 nm. RsrA causes a concentration-dependent quenching of the intrinsic protein tryptophan fluorescence. SigR fluorescence was fully quenched when a 1:1 complex was formed after 10 titration points, further RsrA caused no change in the fluorescence intensity. Arrows represent the decrease in fluorescence intensity as the concentration of RsrA increases.

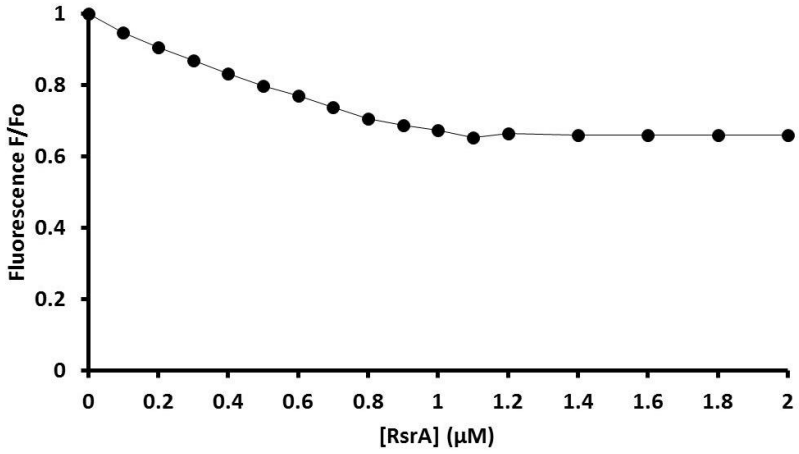


Figure 48- Quenching of SigR Wild-type tryptophan fluorescence upon addition of RsrA. Data from Figure 47.

Importantly, when RsrA was titrated into SigR W88I no significant change was seen in the tryptophan fluorescence emission relative to the protein alone (Figure 49 & 50).

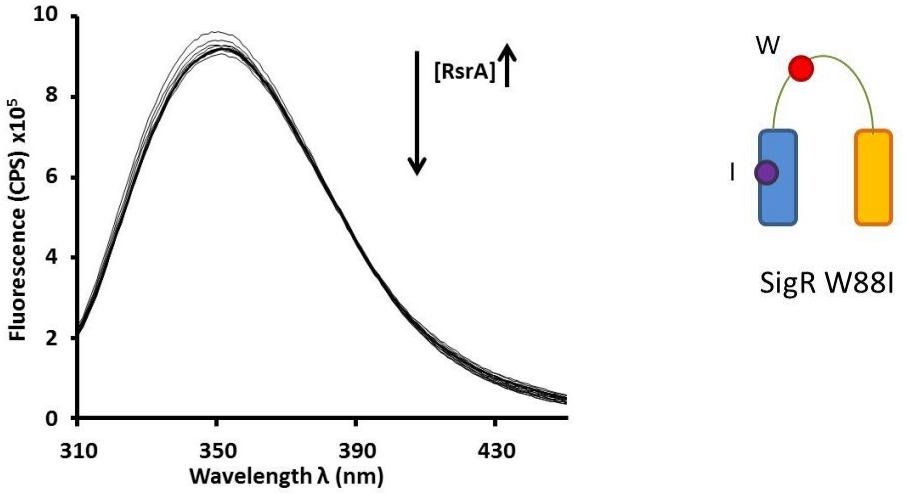
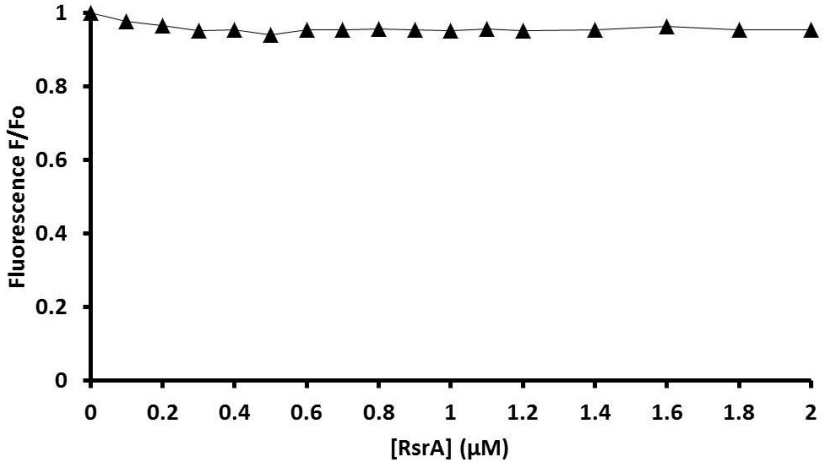


Figure 49- Tryptophan fluorescence of SigR W88I when titrated with RsrA. 0.1 µM RsrA was titrated into 1 µM SigR in 50 mM Tris pH 7.5, 100 mM NaCl, 2 mM DTT at 25°C. Excitation at 295 nm and emission maximum at 350 nm. RsrA does not cause a concentration-dependent quenching of the intrinsic protein tryptophan fluorescence. Arrow represents the direction of fluorescence intensity on addition of RsrA.



F**igure 50- Representative change in fluorescence intensity of SigR W88I at 350 nm**. On each addition of RsrA into SigR, there was no change in fluorescence intensity. Data from Figure 49.

When RsrA was titrated into SigR W119I, the fluorescence emission decreased as for the wild-type protein (Figure 51 & 52). The wavelength of maximum emission was at 339 nm, making it more blue-shifted than the wild-type, suggesting the side chain was more buried in comparison to the wild-type. The SigR W119I max emission at 339 nm shifted to 336 nm in the complex.

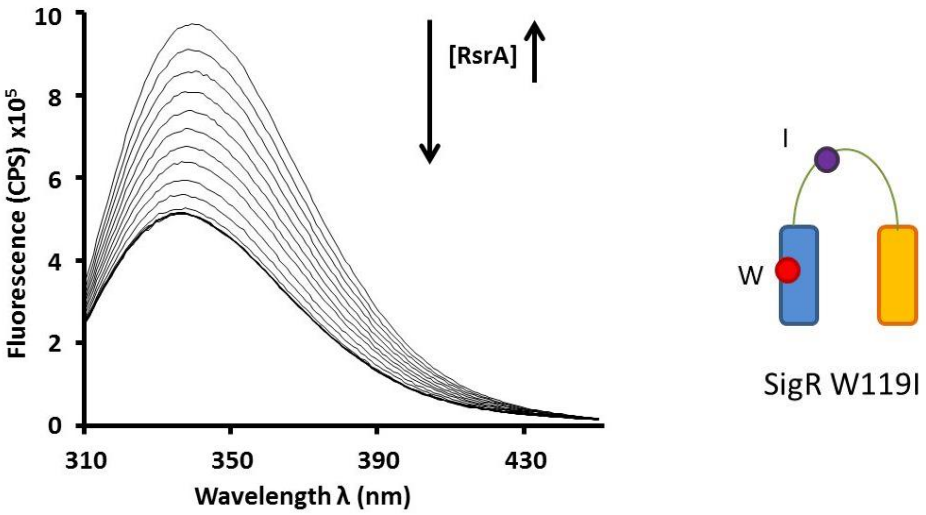


Figure 51- Quenching of SigR W119I tryptophan fluorescence on titration with RsrA. 0.1 µM RsrA was titrated into 1 µM SigR in 50 mM Tris pH 7.5, 100 mM NaCl, 2 mM DTT at 25°C. Excitation at 295 nm and emission maximum at 339 nm. RsrA causes a concentration-dependent quenching of the intrinsic protein tryptophan fluorescence. SigR fluorescence was fully quenched when a 1:1 complex was formed after 10 titration points, further RsrA caused no change in the fluorescence intensity. Arrows represent the decrease in fluorescence intensity as the concentration of RsrA increases.

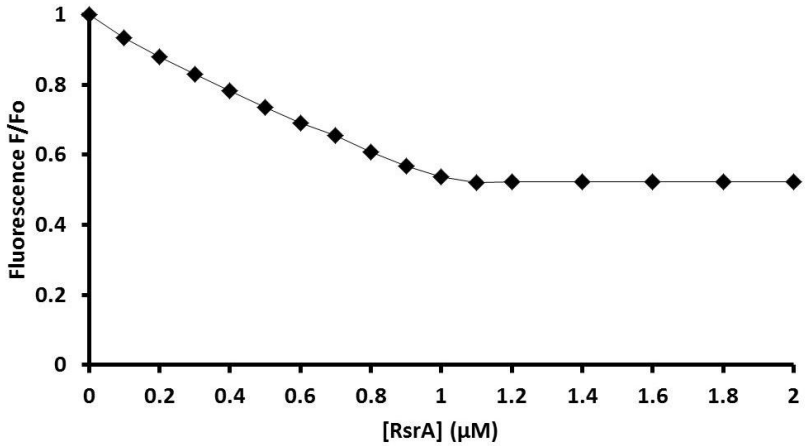


Figure 52- Quenching of SigR W119I tryptophan fluorescence upon addition of RsrA. Data from Figure 51.

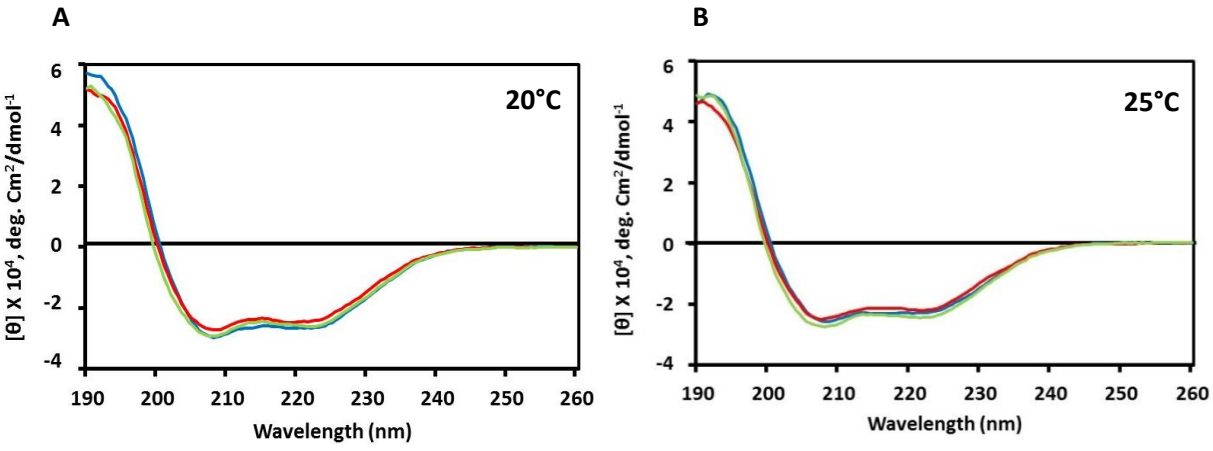
As expected, control titrations of RsrA into SigR* and RsrA into buffer showed no fluorescence emission in the tryptophan wavelength.

3.5. Introducing tryptophans into SigR region 4

On generation of SigR region 4 mutants, SigR* F171W and SigR* F159W, their thermodynamic characteristics were determined. The binding affinity of SigR* F171W was found to be reduced compared to the other SigR mutants. Circular dichroism (CD) was performed to identify if this was due to a structural change in the protein.

Far-UV (260-190 nm for peptide bond) circular dichroism was used to determine if mutation of the SigR phenylalanine residues at 159 and 171 to tryptophan resulted in a change to the secondary structure and stability of the protein. CD spectra were recorded at 20°C, 25°C and 35°C to allow comparison of SigR structures at temperatures used for both fluorescence and ITC. All spectra showed maxima at 191 and minima at 208 and 222 nm (Figure 53), indicating high alpha (α)-helical content (Kelly et al. 2005).

Each protein had a comparable far-UV CD spectrum at all three temperatures (Figure 53), which indicated that the mutations in SigR* F171W and SigR* F159W region 4 had no drastic effect on the secondary structure in comparison to the wild-type.



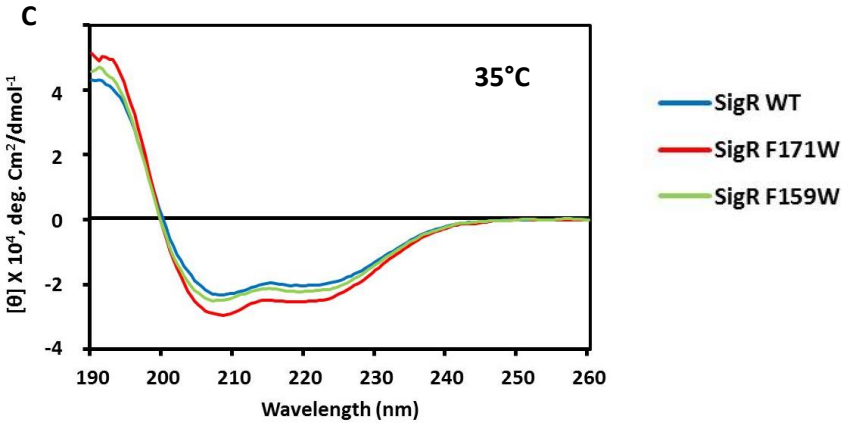


Figure 53- Circular dichroism spectroscopy far UV spectra for SigR wild-type, SigR* F171W and SigR* F159W mutant at 20°C, 25°C and 35°C in 10 mM Tris pH 7.5. CD spectra of SigR Wild-type (blue), SigR* F171W (red) and SigR* F159W (green) at 20°C (A), 25°C (B) and 35°C (C) with four scans averaged for each spectrum. Proteins were prepared as described in Materials and methods section 2.4.6.

Near-UV data (250-350 nm for aromatic amino acids) was used to analyse the tertiary structure of the SigR proteins (Data not shown). Each protein had comparable spectra with slight differences in intensities due to the difference in number of each aromatic amino acid.

When RsrA was titrated into SigR, in which all its native tryptophans had been replaced with isoleucines and a single tryptophan was engineered into region 4 (SigR* F159W), a fluorescence enhancement was observed which saturated when a 1:1 complex was formed (Figure 54 & 55). The increase in fluorescence intensity suggests that region 4, directly or indirectly, is involved in complex formation and is suggestive of a conformational change. The wavelength λ_{max} of this SigR* F159W mutant is 337 nm, which is blue-shifted in comparison to the wild-type. This suggests this residue is more buried in SigR than the tryptophan in the linker region.

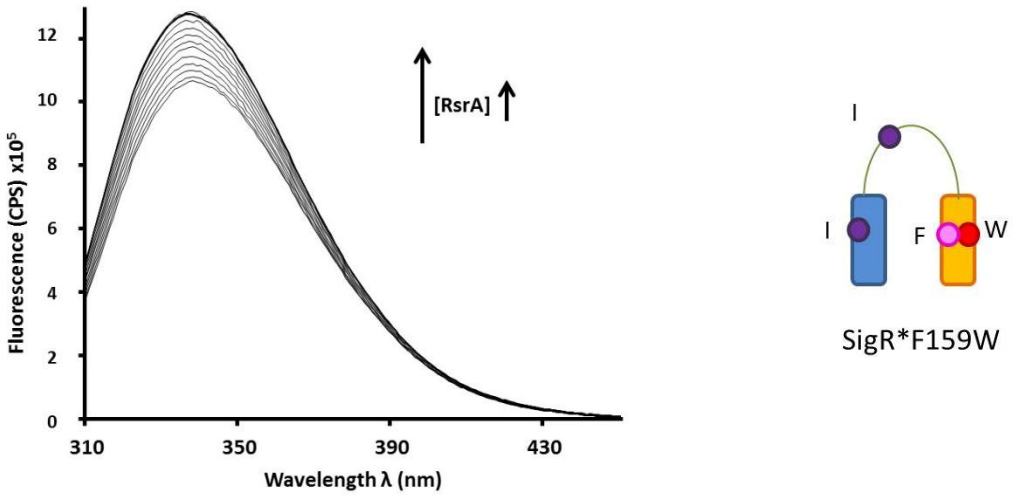


Figure 54- Fluorescence intensity change on complex formation between SigR* F159W-RsrA. 0.1 µM RsrA was titrated into 1 µM SigR in 50 mM Tris pH 7.5, 100 mM NaCl, 2 mM DTT at 25°C. Excitation at 295 nm and emission maximum at 337 nm. On titration of RsrA, fluorescence intensity increased consistently with each increment of RsrA until a 1:1 complex was formed after 10 titrations, and any further titration saw no change in fluorescence. Arrows represent the increase in fluorescence intensity as the concentration of RsrA increases.

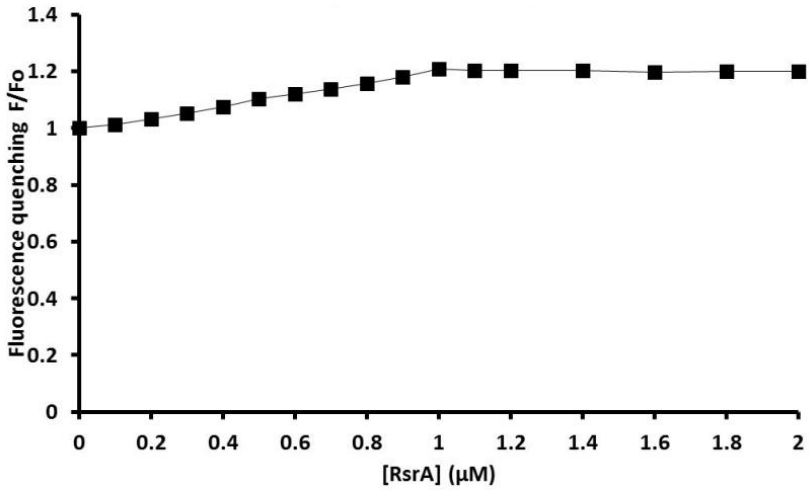


Figure 55- Representative change in fluorescence intensity of SigR* F159W at 337 nm. Data from Figure 54.

When RsrA was titrated into the various SigR mutants, the region 2 tryptophan W88 and region 4 tryptophan W159 were sensitive to the binding of RsrA, as seen by a change in the fluorescence intensities. There was no effect on the W119 tryptophan in the linker region. These data

indicate that RsrA likely binds to both region 2 and region 4 of SigR during complex formation, which would be consistent with the structure of other ZAS-ECF complexes such as ChrR-SigE.

Several homologous ZAS-ECF complexes have shown that the anti-sigma binds to either one or both of sigma region 2 and region 4, as found within this study between SigR-RsrA. As it does so, a large conformational change accompanies this. An example of this is ChrR-SigE from *Rhodobacter sphaeroides*, in which the N-terminal anti-sigma domain alters the structure of region 4 into an unfavourable conformation and occludes the RNA polymerase binding sites (Campbell et al. 2008). This is a common mechanism seen in Gram-positive and negative species to control the activity of sigma factors.

The observation of a change in fluorescence intensity on complex formation between SigR-RsrA has allowed the development of a fluorescence-based assay to monitor complex formation. This allowed further work to determine the kinetics of SigR-RsrA complex formation by fluorescence stopped-flow.

4- Results

Determining the thermodynamics and kinetics of SigR-RsrA complex formation

Interactions between homologous sigmas and anti-sigmas have been studied by SPR. Binding affinities for the complexes are generally seen to be ~15-20 nM in the presence of zinc, and ~7-8-fold weaker in the absence of zinc. Limited thermodynamic information is available for SigR-RsrA. The only published data is restricted to reporting binding affinity between SigR-RsrA. Kang et al. (1999) used SPR to obtain a K_d of 11 nM in the presence of zinc, Bae et al. (2004) repeated this in the presence and absence of zinc, and observed a ~8.7-fold weaker binding in the absence of zinc (although no value is stated). Wei et al. (2014) used FRET to obtain a K_d of 81 nM in the absence of zinc, but no value in the presence of zinc. This highlights the importance of zinc in affecting the binding affinity between SigR and RsrA but also the lack of specific biophysical information on the complex.

Determining the thermodynamics of the sigma-anti-sigma complexes, in combination with structural and kinetic information, will give a better understanding of the mechanism of binding between sigmas and anti-sigmas.

4.1. Characterisation of interaction by Isothermal Titration Calorimetry (ITC)

Calorimetry is commonly used to investigate protein-protein interactions (Pierce et al. 1999). The thermodynamic information provided by ITC, combined with structural data can help define the interactions of these molecules (Campbell 2012). The parameters determined by ITC are stoichiometry (n), Gibbs free energy (ΔG), binding affinity (K_d), enthalpy (ΔH) and entropy (ΔS).

On titration of ligand into macromolecule in a series of volume increments at fixed time intervals, depending on whether the reaction is endothermic (+ΔH) or exothermic (-ΔH), the change in heat associated with binding causes a change in the temperature of the sample cell. This is detected by

the linked reference cell, and modifies the input of power required to correct for the change. As the titration continues, the macromolecule starts to become saturated with ligand. When macromolecule saturation is reached there is no further change in heats with further titrations, as there is no more free protein to interact. The signal recorded is a direct measurement of both the reaction rate and enthalpy for the reaction. The time-dependent input of power required to compensate for the change in heat is recorded, and this appears as a sigmoidal curve demonstrating the transition to saturated macromolecule. Control experiments of protein into buffer were performed to correct for heats of dilution.

4.1.1. Thermodynamic analysis of SigR binding RsrA

ITC was used to characterise the thermodynamics of the interaction between SigR-RsrA in order to determine its binding affinity and all the thermodynamic parameters associated with binding (ΔH, ΔS, n). ITC was performed with SigR, SigR W88I, SigR W119I, SigR*, SigR* F171W and SigR* F159W, to confirm their interaction with RsrA, as visualised by native PAGE (Figure 45). ITC was performed between SigR-RsrA in the presence and absence of zinc. RsrA was incubated and purified in the presence of zinc and after buffer exchange any excess zinc was removed. RsrA had zinc removed using EDTA. Table 10 summarises the thermodynamic values observed.

4.1.2. Thermodynamic analysis of RsrA binding to SigR wild-type and tryptophan-to-isoleucine mutants

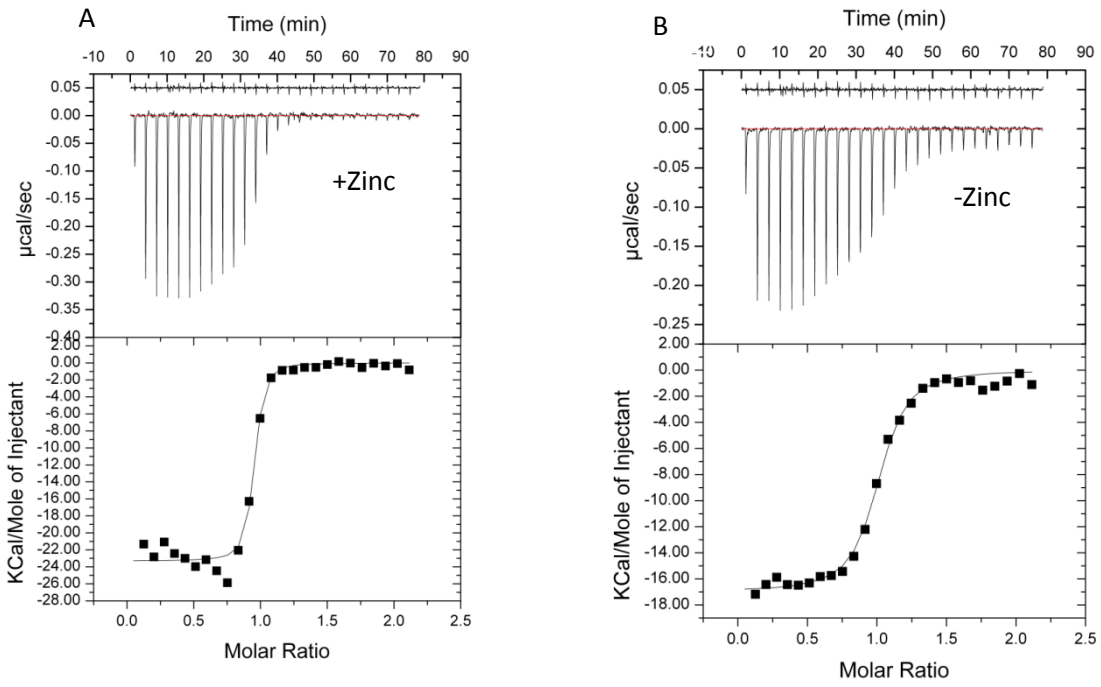


Figure 56- Representative ITC data of SigR-RsrA binding. Titration of 100 µM of SigR protein into 10 µM RsrA in the presence and absence of zinc in 50 mM Tris pH 7.5, 100 mM NaCl and 2 mM DTT at 35°C. Control data was performed by the titration of SigR into buffer to determine the heats of dilution. These have not been subtracted from the data and are displayed above the heats of complex formation. A) Titration of 100 µM of SigR protein into 10 µM RsrA in the presence of zinc. n =0.91± 0.13, K_d =<10.5 ± 0.9 nM (0.78 nM by competition ITC), Δ*H*= -23 ± 1.14 kcal mol^{-1}, Δ*S*=-38.3 ± 3.54 cal/mol/deg. B) Titration of 100 µM of SigR protein into 10 µM RsrA in the absence of zinc. n =1.01 ± 0.08, K_d = 101.7 ± 27.5 nM, Δ*H*=-14.8 ± 2.78 kcal mol^{-1}, Δ*S*= -18.6 ± 4.74 cal/mol/deg.

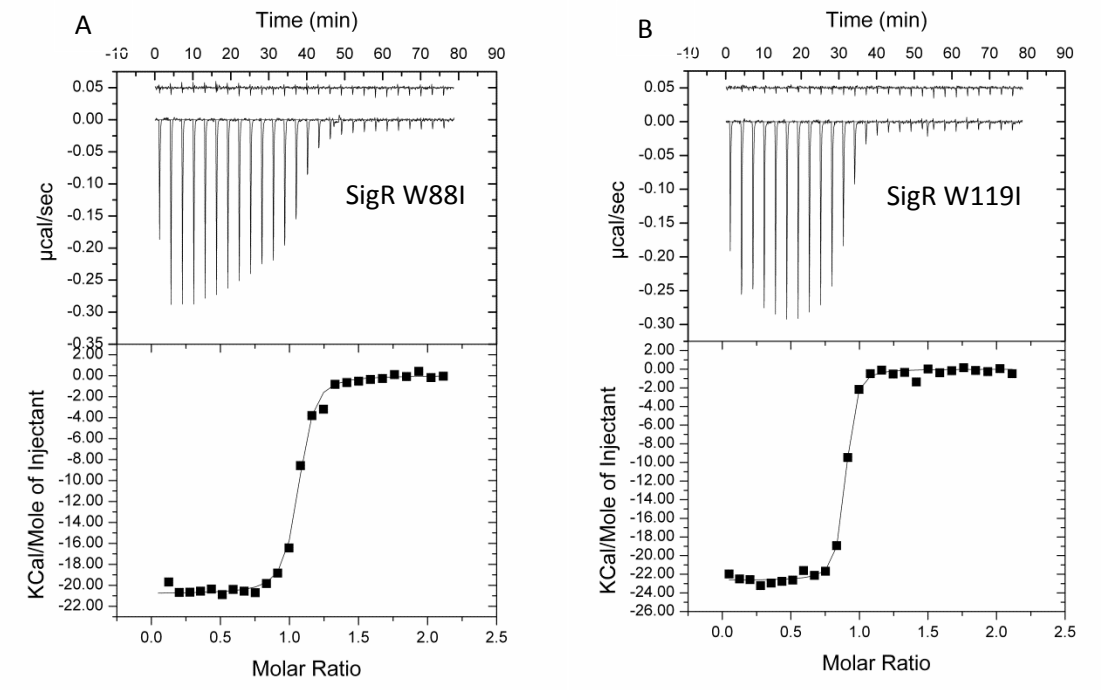


Figure 57- Representative ITC data of SigR-RsrA binding using SigR W88I and SigR W119I. Titration of 100 µM of SigR protein into 10 µM RsrA in the presence of zinc in 50 mM Tris pH 7.5, 100 mM NaCl and 2 mM DTT at 35 °C. Control data was performed by the titration of SigR into buffer to determine the heats of dilution. These have not been subtracted from the data and are displayed above the heats of complex formation. A) Titration of 100 µM of SigR W88I protein into 10 µM RsrA in the presence of zinc. n =0.97 ± 0.06, K_d =20.5 ± 4.7 nM, Δ*H*= -23.9 ± 4.6 kcal mol^{-1}, Δ*S*= -34.8 ± 2.33 cal/mol/deg. B) Titration of 100 µM of SigR W119I protein into 10 µM RsrA in the absence of zinc. n =0.96 ± 0.21, K_d = 17.3 ± 9.5 nM, Δ*H*= -22.8 ± 3.14 kcal mol^{-1}, Δ*S*= -34.2 ± 5.98 cal/mol/deg.

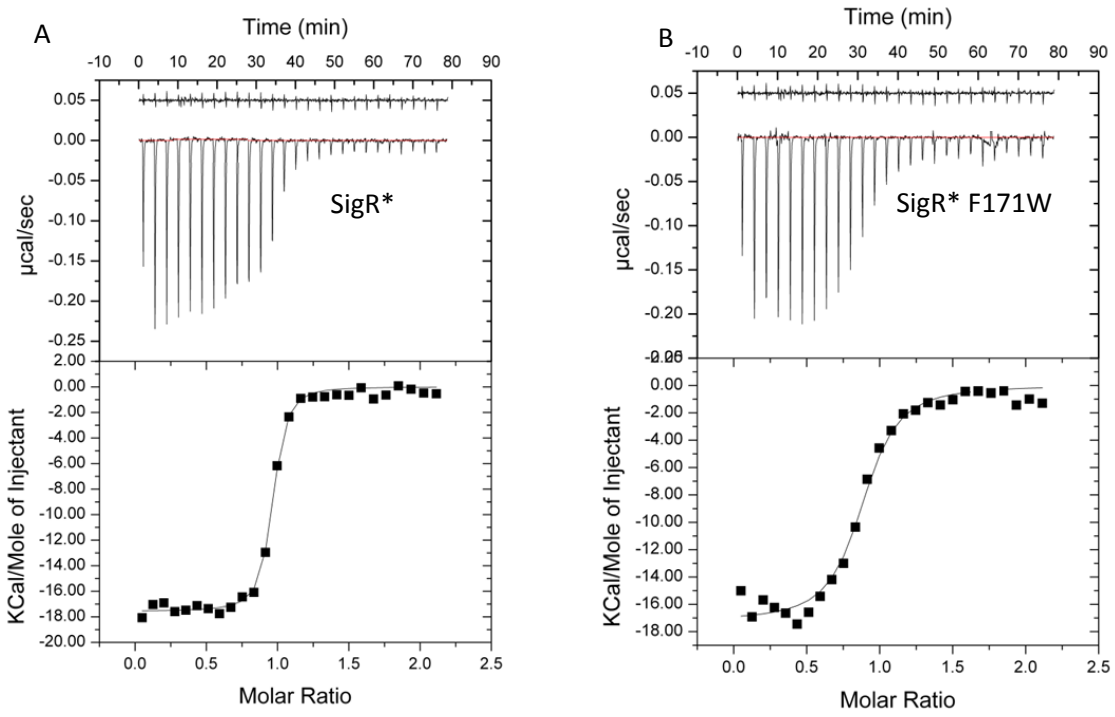


Figure 58- Representative ITC data of SigR-RsrA binding using SigR* and SigR* F171W. Titration of 100 µM of SigR protein into 10 µM RsrA in the presence of zinc in 50 mM Tris pH 7.5, 100 mM NaCl and 2 mM DTT at 35 °C. Control data was performed by the titration of SigR into buffer to determine the heats of dilution. These have not been subtracted from the data and are displayed above the heats of complex formation. A) Titration of 100 µM of SigR* protein into 10 µM RsrA in the presence of zinc. n =0.94 ± 0.11, K_d =24.1 ± 4.2 nM, Δ*H*= -15.6 ± 1.07 kcal mol^{-1}, Δ*S*=-16 ± 3.18 cal/mol/deg. B) Titration of 100 µM of SigR* F171W protein into 10 µM RsrA in the absence of zinc. n = 0.99 ± 0.23, K_d = 265.8 ± 62.7 nM, Δ*H*= -17.2 ± 2.13 kcal mol^{-1}, Δ*S*= -23.6 ± 5.46 cal/mol/deg.

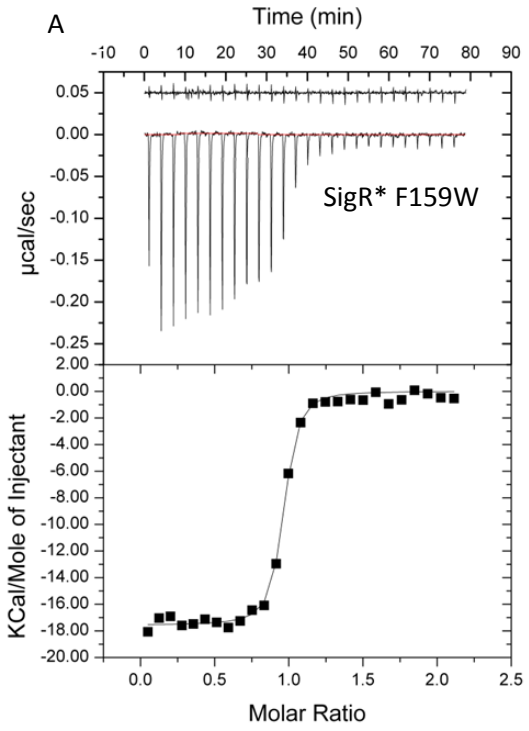


Figure 59- Representative ITC data of SigR-RsrA binding using SigR* F159W. Titration of 100 µM of SigR protein into 10 µM RsrA in the presence and absence of zinc in 50 mM Tris pH 7.5, 100 mM NaCl and 2 mM DTT at 35 °C. Control data was performed by the titration of SigR into buffer to determine the heats of dilution. These have not been subtracted from the data and are displayed above the heats of complex formation. A) Titration of 100 µM of SigR* F159W protein into 10 µM RsrA in the presence of zinc. n =0.99 ± 0.01, K_d =43.4 ± 3.9 nM, Δ*H*= -19.6 ± 0.9 kcal mol^{-1}, Δ*S*= -29.8 ± 3.1 cal/mol/deg.

Table 10- Thermodynamic parameters for wild-type and mutant SigR-RsrA complexes in the presence and absence of zinc. RsrA was incubated and purified in the presence of zinc, after buffer exchange excess zinc was removed.

Protein	**Zn^{2+}**	**Δ*H* (kcal mol^{-1})**	**TΔ*S* (kcal mol^{-1})**	**K_d (nM)**	***n***
SigR *versus* RsrA	+	-23.0 ± 1.14	-11.8 ± 1.09	10.5 ± 0.9	0.91 ± 0.13
SigR *versus* RsrA	-	-14.8 ± 2.78	-5.7 ± 1.45	101.7 ± 27.5	1.01 ± 0.08
SigR W88I *versus* RsrA	+	-23.9 ± 4.60	-10.7 ± 0.7	20.5 ± 4.7	0.97 ± 0.06
SigR W119I *versus* RsrA	+	-22.8 ± 3.14	-10.5 ± 1.84	17.3 ± 9.5	0.96 ± 0.21
SigR* *versus* RsrA	+	-15.6 ± 1.07	-4.9 ± 0.97	24.1 ± 4.2	0.94 ± 0.11
SigR* F171W *versus* RsrA	+	-17.2 ± 2.13	-7.3 ± 1.69	265.8 ± 62.7	0.99 ± 0.23
SigR* F159W *versus* RsrA	+	-19.6 ± 0.90	-9.2 ± 0.96	43.4 ± 3.9	0.99 ± 0.01

Stoichiometry of binding (n), dissociation constant (K_d), enthalpy change (Δ*H*), and entropy change (Δ*S*) upon binding are presented for each titration pair. The values represent means of experiments

repeated four times (N=4). The errors for the average values represent the standard deviation between replicates.

The ITC thermodynamic parameters and binding isotherms for each SigR-RsrA titration, showed that all of the SigR region 2, linker region and region 4 mutants were able to form a complex with RsrA. The thermodynamic parameters verified the 1:1 binding stoichiometry of all the SigR proteins observed by native PAGE. The enthalpic values show that binding of all SigR proteins to RsrA was exothermic, in the range of -14.8 to -23.9 kcal mol^{-1}, and entropy ranged from -16 to -42.2 (cal/mol/deg).

SigR bound RsrA in the presence of zinc with a K_d <10.5 ± 0.9 nM. However, this affinity is unreliable as determined by the current ITC experiments, as there are few points in the transition region of the binding isotherm (Figure 56), a point which I return to below.

Region two and linker region SigR W88I, SigR W119I (Figure 57) and SigR* (Figure 58) were all shown to bind RsrA in the presence of zinc with similar high affinities of 20.5 ± 4.7, 17.3 ± 9.5 and 24.1 ± 4.2 nM respectively. Hence, given the limitations of the current methods, the mutants did not grossly affect binding to RsrA, however see below.

The region four SigR mutants also bind RsrA in the presence of zinc. However, SigR* F159W (Figure 59) binds with an average affinity of 43.4 ± 3.87 nM and SigR* F171W (Figure 58) with an average affinity of 265.8 (±62.7) nM. SigR* F159W still has a strong binding affinity but is two-fold weaker than the other SigR region two mutants for binding RsrA.

SigR* F171W is a much weaker binding protein than the other SigR mutants. The large decrease in binding affinity by the mutation of this phenylalanine suggests either that this residue is important in binding RsrA, or the mutation has had an adverse effect on the stability of SigR, causing a structural change that reduced complex affinity.

Due to the very high affinity of SigR wild-type with RsrA in the presence of zinc, reaching the lower detection limit capable using the iTC200 calorimeter, fitting of the data is much more difficult as there are fewer points in the transition region. This causes the thermodynamic values from the fit to become less reliable. It is therefore conceivable that SigR binds RsrA with a higher affinity than 10 nM. This interpretation was confirmed by competition ITC experiments performed by Dr Karthik Rajasekar (This laboratory). In this experimental set-up a high affinity ligand was titrated into a solution of a complex formed with a weaker ligand. The thermodynamics of the high-affinity ligand to the macromolecule are subsequently calculated from the displacement. This experiment required a weaker binding complex to be generated using 41C-RsrA (with 1 Cys present at position 41, the other cysteines mutated) with SigR the result was a K_d of 0.78 (±0.033) nM.

The affinity of SigR for RsrA in the absence of zinc was also measured. RsrA was treated with 1 mM EDTA on ice to chelate the zinc ion, it was then buffer exchanged to remove any trace of zinc, and ITC was performed in the same manner. The average affinity was 101.7 ± 27.5 nM (Figure 56), which is 130-fold weaker binding than the cognate interaction in the presence of zinc. This highlights the importance of zinc bound RsrA in the formation of the complex with SigR.

These data therefore confirm that each of my SigR tryptophan mutants are able to bind and form a complex with RsrA, with a 1:1 stoichiometry and with tight binding affinities. The exception to this was SigR* F171W, with its decreased binding affinity suggesting an impact on RsrA binding. The data highlight the importance of zinc in the thermodynamics of the complex.

4.2. Kinetics of the association and dissociation of SigR and RsrA in the presence and absence of zinc

There is currently little kinetic information available for the SigR-RsrA complex. Previous kinetic studies have been published for homologous complexes by SPR such as SigH-RshA (Jeong et al. 2006) and SigL-RslA (Thakur et al. 2010). For SigR-RsrA, published kinetic information is limited to the rate of zinc release on oxidation by PAR assay and the rate of air-oxidation of apo-RsrA by gel filtration chromatography and change in secondary structure by circular dichroism (Bae et al. 2004).

To shed light on the kinetics of SigR-RsrA complex, I measured the individual association (k_{on}) and dissociation (k_{off}) rate constants and obtained the equilibrium dissociation constant (K_d) from this (Figure 60). Pre-steady state fluorescence stopped-flow was used to look at the association of SigR-RsrA.

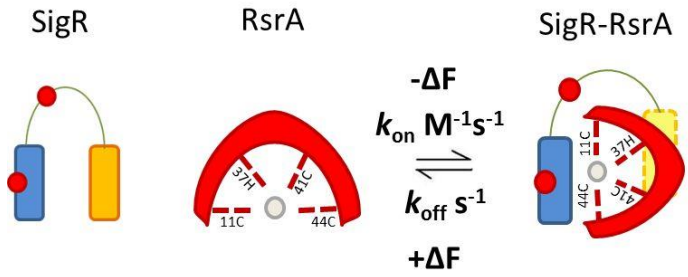


Figure 60 – Formation of complex between SigR and RsrA. The association (k_{on}) and dissociation (k_{off}) rate constants of the SigR-RsrA complex can be measured using fluorescence stopped-flow. +/-ΔF means the positive or negative change in fluorescence intensity for each rate constant.

The kinetics of association and dissociation of complex were followed using stopped-flow spectrofluorimetry (Materials and Methods section 2.4.4. and 2.4.5.), by monitoring the change in tryptophan fluorescence emission on complex formation over time, using the fluorescence-based assay previously developed.

Association and dissociation controls were performed to show the quench and enhancement of fluorescence intensity of complex association and dissociation respectively. For association controls,

samples were measured for two seconds, recording 4000 points and 40 samples. A fluorescence voltage of 1.3V from a photomultiplier of 500F was used to collect the fluorescence data. Samples were excited at 295 nm, and emission measured using a 320 nm cut-off filter. A 2 ml syringe concentration of 0.125 µM SigR, 1.25 µM RsrA and 0.125 µM complex (+ zinc) were used (Figure 61), similar results were obtained using RsrA in the absence of zinc (data not shown).

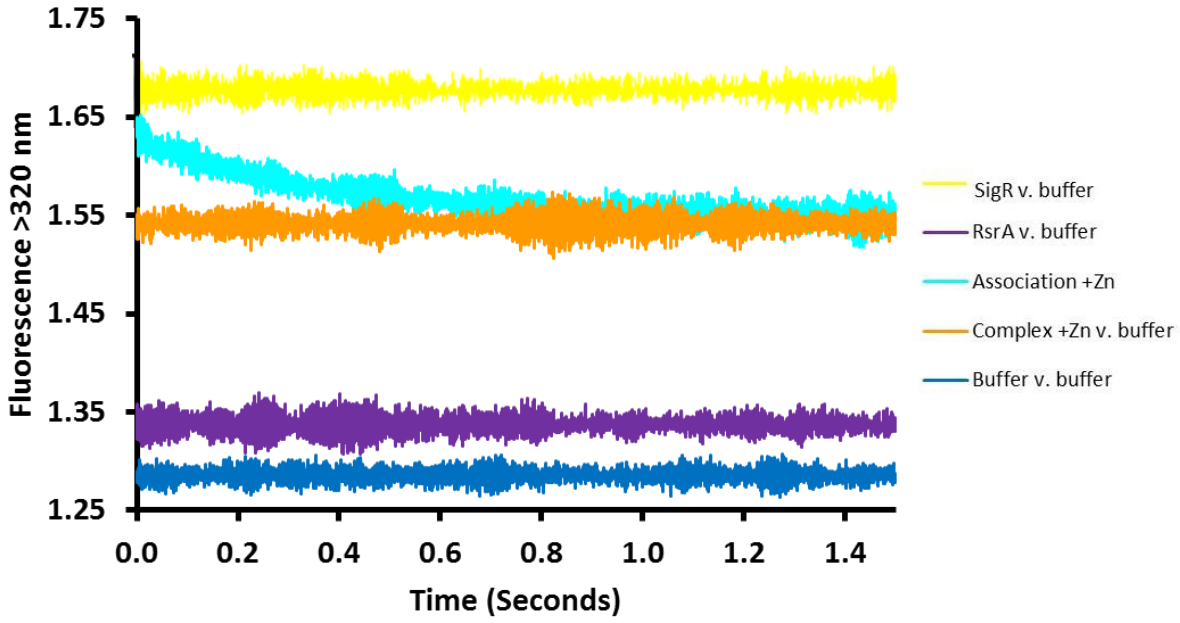


Figure 61- Fluorescence controls for the association of SigR-RsrA. Samples were measured for two seconds, recording 4000 points and 40 samples. A fluorescence voltage of 1.3V from a photomultiplier of 500F was used to collect the fluorescence data. Samples were excited at 295 nm, and emission measured using a 320 nm cut-off filter. 0.125 µM SigR, 1.25 µM RsrA and 0.125 µM complex (+ zinc) were used.

Controls showed that buffer did not contribute to the signal change and that RsrA measured against buffer had minimal fluorescence due to the tyrosine residues. SigR had a high fluorescence due to the presence of the two tryptophans and that complex had a lower fluorescence intensity. The association of SigR with both RsrA with zinc and without zinc (data not shown), showed a change in fluorescence starting from just below the intensity of free SigR, quenching to the intensity of the complex. This showed that the association of free SigR and RsrA completely quenches the fluorescence

of free SigR to the levels of SigR in complex, demonstrating an absence of reaction in the dead time (Figure 61).

These controls were repeated looking at the dissociation of SigR-RsrA to identify if fluorescence was restored, moving from the intensity of the quenched complex to that of free SigR. Samples were measured for 1,600 seconds, recording 4000 points and 40 samples. A fluorescence voltage of 1.3V from a photomultiplier of 500F was used to collect the fluorescence data. Samples were excited at 295 nm, and emission measured using a 320 nm cut-off filter. Concentrations of 0.125 µM SigR, 1.25 µM RsrA and 0.125 µM complex (+ zinc) and without zinc (data not shown), and 1.25 µM SigR* (10-fold excess) were used. On mixing of complex with SigR* at a 10-fold excess means that RsrA binds SigR* as it dissociates and a change in fluorescence from the level of complex to free SigR (Figure 62).

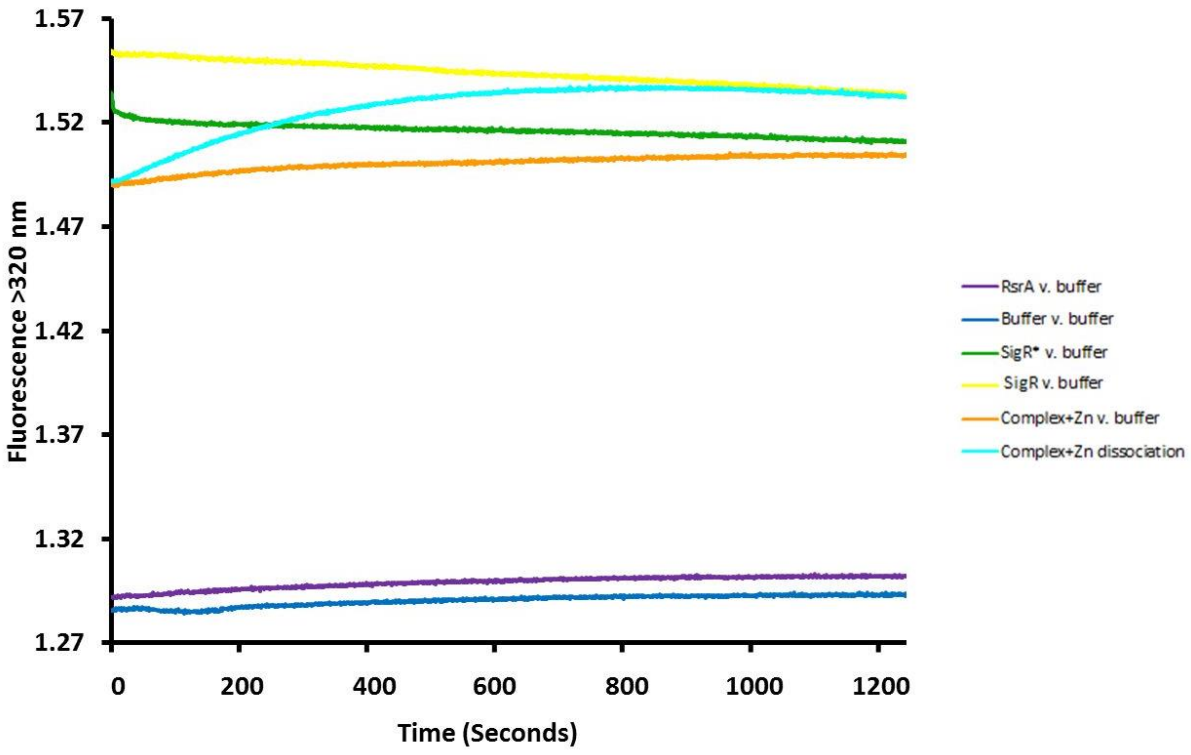


Figure 62- Fluorescence controls for the dissociation of SigR-RsrA. Samples were measured for 1,600 seconds, recording 4000 points and 40 samples. A fluorescence voltage of 1.3V from a photomultiplier of 500F was used to collect the fluorescence data. Samples were excited at 295 nm, and emission measured using a 320 nm cut-off filter. A 2 ml syringe concentration of 0.125 µM SigR, 1.25 µM RsrA and 0.125 µM complex (+ zinc) were used.

This demonstrates that fluorescence quenching observed is due to complex formation as seen by the restoration in fluorescence. This also shows that the complex completely dissociates and does so in a single step. These data demonstrated that intrinsic protein tryptophan fluorescence could be used as an assay to monitor the binding of RsrA to SigR in stopped-flow experiments.

4.2.1. Association kinetics

The association of SigR-RsrA in the presence of zinc at 25°C (24.2°C actual sample handling unit temperature), resulted in a rapid quench in fluorescence intensity (Figure 63). The data showed a monophasic exponential decay in fluorescence intensity, corresponding to the bimolecular association of SigR-RsrA. The fluorescence kinetic traces were fitted from 2 ms to 1.5 seconds to a single-exponential rate equation: $F=\Delta F_1 \exp(-k_{obs1}\, t)+F$e

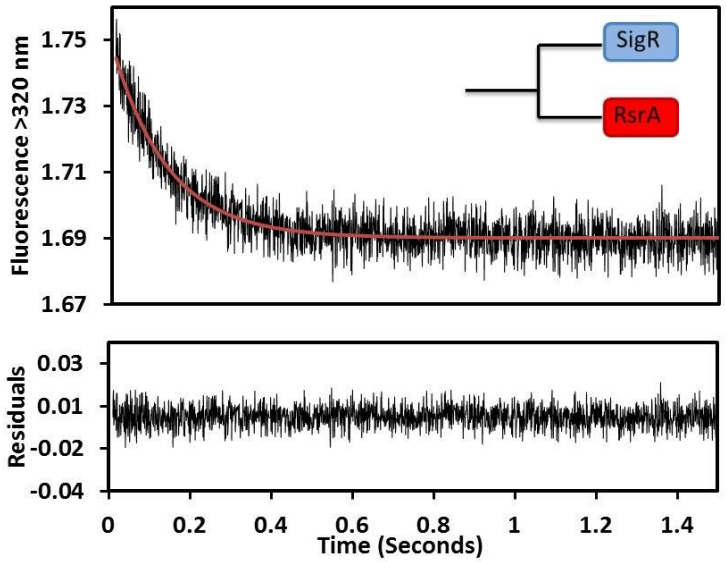


Figure 63- Representative association kinetic trace of SigR-RsrA complex using pre-steady state tryptophan fluorescence stopped-flow. SigR was used at a cell concentration of 0.125 µM and measured against 1.25-2.5 µM RsrA (10-20 fold excess). This trace is an example of the association using 0.125 µM SigR and 2.5 µM RsrA (20-fold excess), in the presence of zinc at 25°C. Excitation at 295 nm, and emission measured using a 320 nm cut-off filter, 5000 points with 24 samples collecting range. The red line and lower panel show the fit and residuals respectively, of single-exponential fits to produce an average k_{obs}=8.4 s^{-1} for RsrA+Zn binding.

Association reactions were repeated using several RsrA concentrations 1.25-2.5 µM RsrA (10-20 fold excess). The pseudo-first-order k_{obs} values were plotted against the excess RsrA concentrations, from which k_{on} and k_{off} for binding were obtained (k_{obs}= [RsrA] k_{on} + k_{off}) (Figure 64).

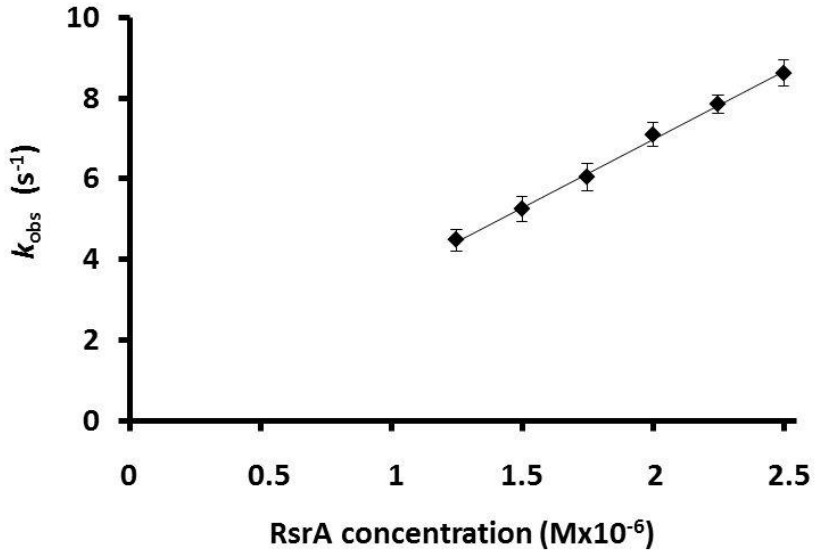


Figure 64- Linear concentration dependence of the observed rates, k_{obs}, between SigR and RsrA under pseudo-first order conditions, at 25°C in the presence of zinc. Data were fitted to equation y=mx+b (R^2>0.96). Error bars correspond to the averages of 3 measurements per sample with 4 repeats.

This was repeated four times, using different protein stocks to obtain an average bimolecular association rate k_{on} of 3.55 (± 0.4) x10^6 $M^{-1}s^{-1}$ for SigR-RsrA in the presence of zinc at 25°C.

Due to the fast rates of association under these conditions, the concentration dependence of the association rates could only be determined over a limited concentration range (10-20 fold excess RsrA). Nevertheless, the data clearly show a monophasic exponential decay that has a linear concentration dependence on RsrA (Figure 64), consistent with this phase reporting the bimolecular association of SigR and RsrA at 25°C in the presence of zinc.

RsrA was treated with 1 mM EDTA for 15 minutes on ice to chelate the zinc ion, before buffer exchanging into 50 mM Tris pH 7.5, 100 mM NaCl, 2 mM DTT to remove the EDTA and zinc. Association experiments were repeated under identical conditions at 25°C using RsrA in the absence of zinc (Figure 65). The data showed a monophasic exponential decay in fluorescence intensity, corresponding to a rapid bimolecular association of SigR-RsrA in the absence of zinc. The fluorescence kinetic traces were fitted from 2 ms to 1.5 seconds. This was repeated four times, using different protein stocks to obtain an average bimolecular association rate k_{on} of 11.49 (±1.67) x10^6 $M^{-1}s^{-1}$ for SigR-RsrA in the absence of zinc at 25°C (Figure 66). This tells us that zinc does not play a large role in the rate of association between SigR-RsrA.

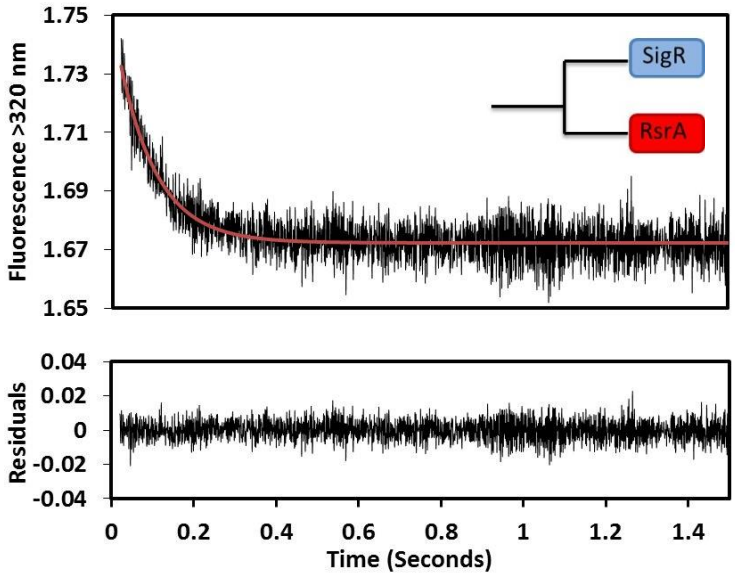


Figure 65- Representative association kinetic trace of SigR-RsrA complex in the absence of zinc at 25°C. RsrA was treated with 1 mM EDTA to chelate zinc before buffer exchanging into 50 mM Tris pH 7.5, 100 mM NaCl, 2 mM DTT to remove the EDTA and zinc. The red line and lower panel show the fit and residuals respectively, of single-exponential fits to produce an average k_{obs}= 23.8 s^{-1} for RsrA-Zn binding.

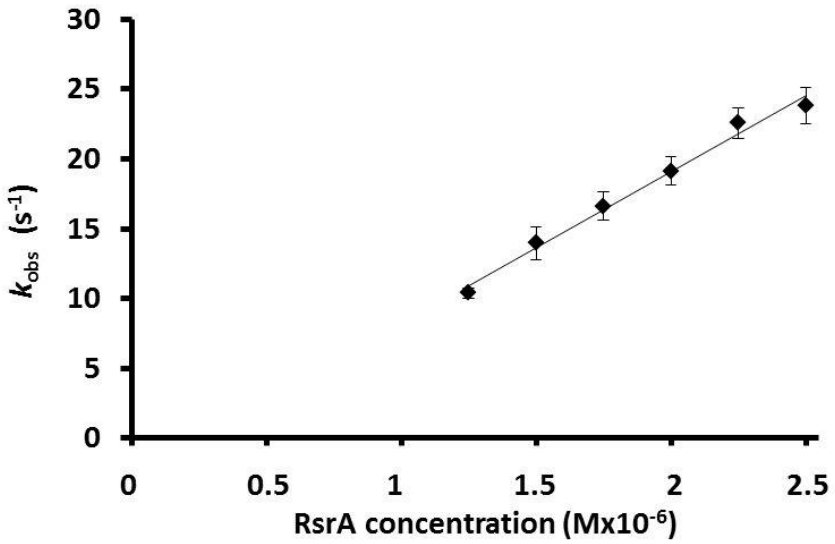


Figure 66- Linear concentration dependence of the observed rates, k_{obs}, between SigR and RsrA under pseudo-first order conditions, at 25°C in the absence of zinc. Data was fitted to equation y=mx+b, (R^2>0.98). Error bars correspond to the averages of 3 measurements per sample with 4 repeats.

Association experiments using RsrA in the presence and absence of zinc were repeated under identical conditions at 35°C (33.7°C actual temperature). This was to determine the K_d ($K_d = k_{off}/ k_{on}$) for SigR-RsrA association by stopped-flow, which could then be compared directly to the K_d obtained by ITC at the same temperature (no significant heats of binding were obtained at 25°C). As expected, association at 35°C was much faster than at 25°C (Figure 67).

A monophasic exponential decay was again observed, an average k_{on} of 8.9 (±1.4) x10^6 $M^{-1}s^{-1}$ (Figure 67 a and b) and 17.3 (±1.3) x10^6 $M^{-1}s^{-1}$ (Figure 67 c and d), in the presence and absence of zinc, respectively (Table 11). Association rates in the presence and absence of zinc at 25°C differs by ~3-fold, the difference at 35°C is ~2-fold. The difference in rate with the 10°C increase in temperature is ~2.5-fold and ~1.5-fold in the presence and absence of zinc respectively.

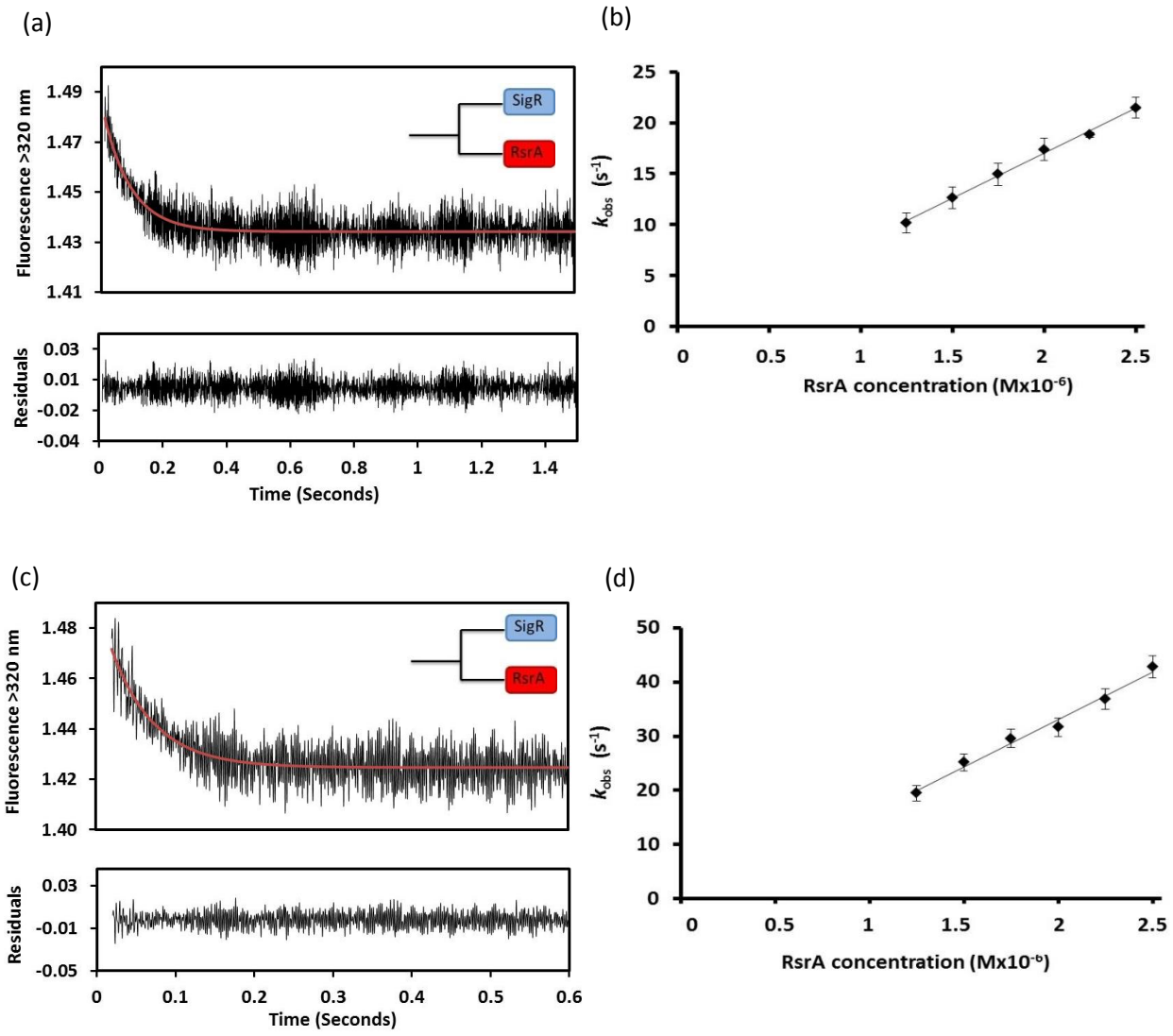


Figure 67- Representative association kinetic traces of SigR-RsrA complex in the presence (a) and absence (c) of zinc at 35°C. SigR was used at a cell concentration of 0.125 µM and measured against 1.25-2.5 µM RsrA (10-20 fold excess). These traces are an example of the association using 0.125 µM SigR and 2.5 µM RsrA (20-fold excess). Excitation at 295 nm, and emission measured using a 320 nm cut-off filter, 5000 points with 24 samples collecting range. The red line and lower panel show the fit and residuals respectively, of single-exponential fits to produce an average k_{obs}= 21.61 s^{-1} for RsrA+Zn binding and 41.45 s^{-1} for RsrA-Zn binding. Linear concentration dependence of the observed rates, k_{obs}, between SigR and RsrA under pseudo-first order conditions, at 35°C in the presence (b) (R^2>0.95) and absence (d) (R^2>0.96) of zinc. Data was fitted to equation y=mx+b. Error bars correspond to the averages of 3 measurements per sample with 4 repeats.

Table 11- Rates of association of SigR-RsrA in the presence and absence of zinc at 25°C and 35°C. Association +Zn/-Zn experiments (N=4) for each association experiment between SigR-RsrA.

	Temp. (°C)	Average Association $M^{-1}s^{-1}$
Holo-RsrA	25	3.55 (±0.4) $x10^6$
	35	8.9 (±1.4) $x10^6$
Apo-RsrA	25	11.49 (±1.67) $x10^6$
	35	17.3 (±1.3) $x10^6$

4.2.2. Dissociation kinetics

The dissociation rate for SigR-RsrA complex (k_{off}) could not be estimated from the intercept of the pseudo-first order plot (where RsrA was in excess), due to the intercept being very close to 0. Therefore the dissociation rate was measured directly through competition stopped-flow experiments. SigR-RsrA complexes were prepared in the presence and absence of zinc, incubating SigR in the presence of a 5-fold molar excess of RsrA and the excess RsrA removed by gel filtration. Complexes were buffer exchanged into 50 mM Tris pH 7.5, 100 mM NaCl and 2 mM DTT, in the presence and absence of zinc. SigR-RsrA was mixed with excess SigR*, which is devoid of tryptophan residues. Measurements were made at both 25°C and 35°C. Dissociation was monitored by the increase in fluorescence intensity as the wild-type complex dissociated and SigR was replaced with SigR*.

The dissociation of SigR-RsrA in the presence of zinc at 25°C (24.2°C actual sample handling unit temperature) was recorded for a total of ~8000 seconds measuring 5000 points (160,000 samples), and resulted in a very slow increase in fluorescence intensity (Figure 68). The data showed a monophasic enhancement in fluorescence intensity, corresponding to the dissociation of the SigR-RsrA complex. The first-order kinetic traces were fitted from 100 to 2000 seconds. This was done using nonlinear least-squares regression analysis to a single-exponential rate equation: $F=\Delta F_1 \exp(+k_{obs1} t)+Fe$

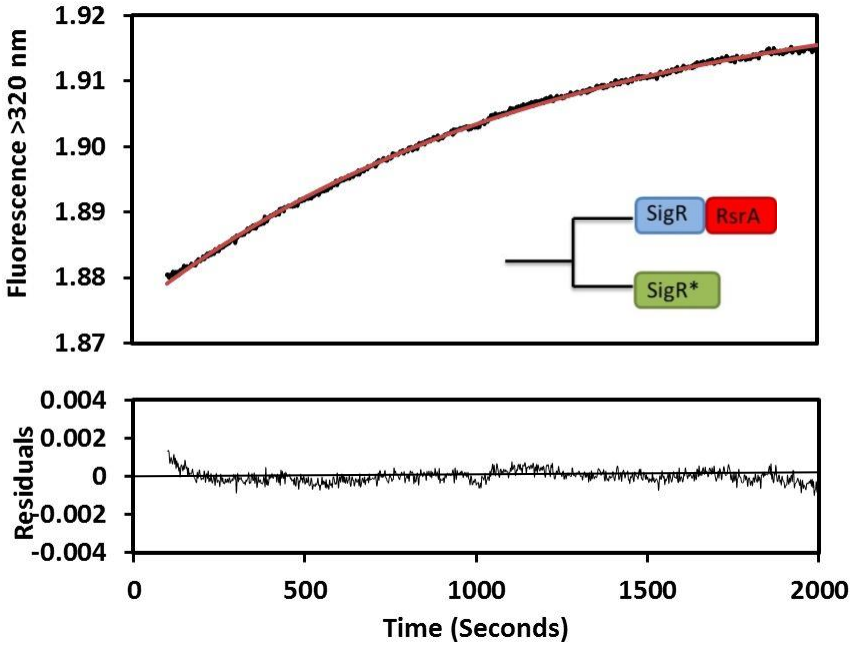


Figure 68- Representative dissociation kinetic trace of SigR-RsrA complex using pre-steady state tryptophan fluorescence stopped-flow at 25°C. Complex in the presence of zinc was used at a constant cell concentration of 0.5 µM and measured against 5 µM SigR* (10-fold excess). This trace is an example of the dissociation in the presence of zinc at 25°C. Excitation at 295 nm, and emission measured using a 320 nm cut-off filter, 5000 points with 160,000 samples collecting range. Data was fitted to a single-exponential rate equation from 100 to 2000 seconds. The red line and lower panel show the fit and residuals respectively, of single-exponential fits to produce an average ΔF= 0.049 (± 0.001) for the fitted data.

k_{obs} from the dissociation trace represents the rate of dissociation k_{off} for SigR-RsrA. The same result was obtained using SigR* 20-fold. An average dissociation rate k_{off} of 8.6 (±0.00) x10^{-4} s^{-1} for SigR-RsrA in the presence of zinc was obtained at 25°C. Dissociation measurements over long time courses showed a very small gradual decline in fluorescence intensity at a rate of ~0.015 intensity per 1000 seconds. This was observed for all dissociation reactions, in the presence and absence of zinc at 25°C and 35°C. This may be explained by the constant excitation of the tryptophan fluorophores over long periods of time, causing them to lose their ability to become excited and therefore appear as a loss of fluorescence. Alternatively they could still be excited but not emit their fluorescence.

Dissociation kinetic experiments were repeated under equivalent conditions at 25°C using SigR-RsrA complex in the absence of zinc. Data were recorded for a total of 1000 seconds measuring 5000 points (16,000 samples), and resulted in a rapid fluorescence enhancement (figure 69). The kinetic traces were fitted from 10 ms to 30 seconds, to a single-exponential rate equation. An average dissociation rate of k_{off} of 0.336 (±0.006) s^{-1} for SigR-RsrA in the absence of zinc was obtained at 25°C.

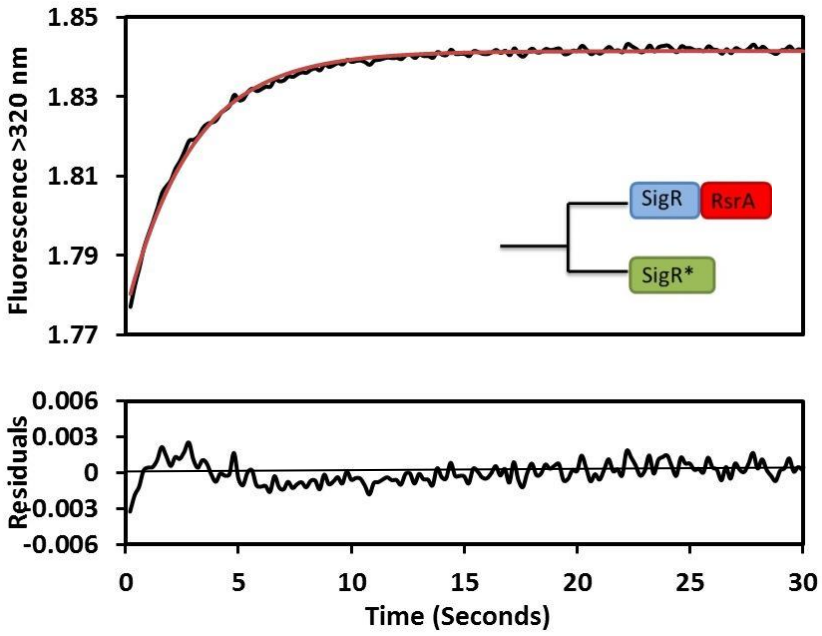


Figure 69- Representative dissociation kinetic trace of SigR-RsrA complex in the absence of zinc at 25°C. Complex in the absence of zinc was used at a constant concentration of 0.5 µM and measured against 5 µM SigR* (10-fold excess). This trace is an example of the dissociation in the absence of zinc at 25°C. Excitation at 295 nm, and emission measured using a 320 nm cut-off filter, 5000 points with 16,000 samples collecting range. Data was measured for a total of 1000 seconds but was fitted to a single-exponential rate equation from 10 ms to 30 seconds. The red line and lower panel show the fit and residuals respectively, of single-exponential fits to produce an average ΔF= 0.063 (± 0.002) for the data fitted.

Dissociation kinetics were repeated under identical conditions at 35°C (33.7°C actual temperature), to determine the K_d ($K_d = k_{off}/ k_{on}$) for SigR-RsrA by stopped-flow. Dissociation is faster at 35°C than at 25°C (Figure 70). An average k_{off} of 2.4 (±0.0004) x10^{-3} s^{-1} (Figure 70 a) and 1.08 (±0.01) s^{-1} (Figure 70 b), in the presence and absence of zinc respectively, was obtained at 35°C. Dissociation rates in the presence and absence of zinc at 25°C differ by ~390-fold, the difference at 35°C is ~450-

fold. The difference in rate with the 10°C increase in temperature are ~2.8 and ~3.2-fold in the presence and absence of zinc respectively (Table 12).

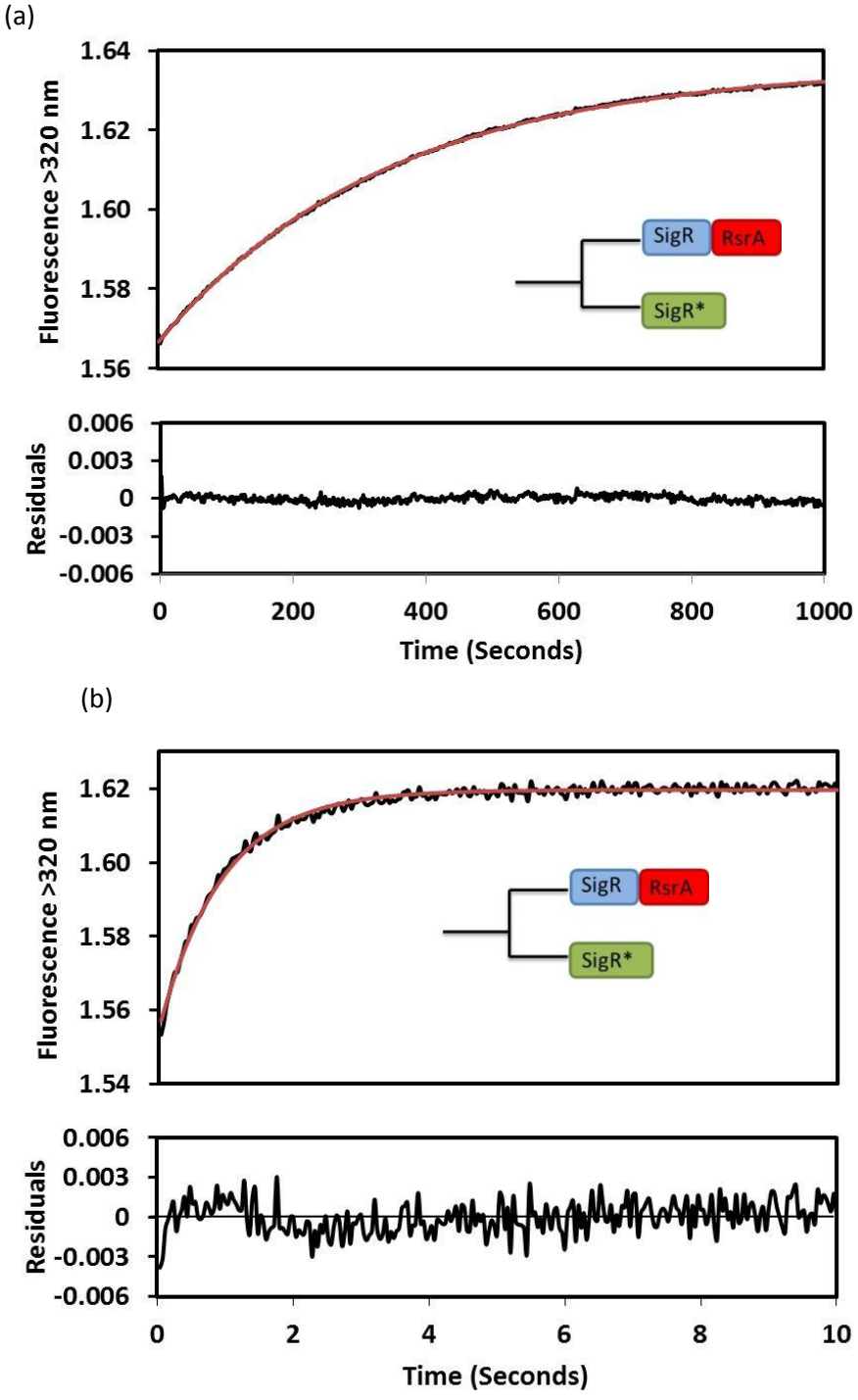


Figure 70- Representative dissociation kinetic traces of SigR-RsrA complex in the presence and absence of zinc at 35°C. Complex in the presence (a) and absence (b) of zinc was used at a constant concentration of 0.5 µM and measured against 5 µM SigR* (10-fold excess). Excitation at 295 nm, and emission measured using a 320 nm cut-off filter. Data was measured for a total of 8000 seconds, 5000 points (128,000 samples) (a) and 200 seconds, 5000 points (3200 samples) (b) in the presence and

absence of zinc respectively. Data was fitted to a single-exponential rate equation from 10 ms-1000 seconds in the presence of zinc (a) and 10 ms to 10 seconds in the absence of zinc (b). The red line and lower panel show the fit and residuals respectively, of single-exponential fits to produce an average ΔF= 0.079 (± 0.009) and 0.066 (± 0.0006) in the presence and absence of zinc for data fitted.

Table 12- Rates of association and dissociation of SigR-RsrA in the presence and absence of zinc at 25°C and 35°C. Average of three repeats for complex +Zn/-Zn competition experiments against SigR*, the k_{obs} and K_d are shown.

Reaction	**Temp.**	k_{on} $M^{-1}s^{-1}$	k_{off} s^{-1}	K_d **(nM)**
Complex+Zn v. SigR*	25°C	3.55 (±0.4) $x10^6$	0.00086 (± 1.5 $x10^{-5}$)	0.24 (±0.004)
Complex+Zn v. SigR*	35°C	8.9 (±1.4) $x10^6$	0.0024 (± 0.0004)	0.27 (±0.05)
Complex-Zn v. SigR*	25°C	11.49 (±1.67) $x10^6$	0.336 (± 0.006)	29.2 (±0.6)
Complex-Zn v. SigR*	35°C	17.3 (±1.3) $x10^6$	1.08 (± 0.01)	62.2 (±0.7)
Complex-Zn (EDTA in buffer)	25°C	N/A	0.34 (± 0.007)	30 (±0.7)
Complex-Zn (EDTA in buffer)	35°C	N/A	1.12 (± 0.015)	64.9 (±0.9)

Dissociation rate constants were also determined in the absence of zinc, where proteins were first treated with 1 mM EDTA for 15 minutes on ice, before buffer exchanging into 50 mM Tris pH 7.5, 100 mM NaCl, 2 mM DTT and 1 mM EDTA, along with SigR* in the same buffer. The rates obtained were identical to those obtained previously, demonstrating that the complex was indeed zinc-free (Table 12).

In order to ensure EDTA was not influencing the rate of dissociation, the experiment was similarly repeated, treating the complex in the absence of zinc with 1 mM EDTA for 1.5 hours on ice, before buffer exchanging into 50 mM Tris pH 7.5, 100 mM NaCl and 10 mM DTT, with no EDTA in the buffer. This was to ensure that RsrA in the complex was fully reduced and that oxidation was not occurring and affecting the dissociation rates of SigR-RsrA. It was also to show that EDTA in the buffer did not affect the rate or fluorescence measurements. These rates for complex in the absence of zinc were very similar to those previously obtained with k_{off} = 0.28 (± 0.012) and 0.79 (± 0.046), at 25°C and 35°C respectively, and a K_d of 24.3 (±0.7) and 45.9 (±2.7) respectively.

Dissociation kinetics were repeated using double the concentration of both complex in the presence and absence of zinc and SigR*. This was to demonstrate that rate of dissociation was not

concentration dependent. These rates were identical to those previously obtained with k_{off} =0.0019 (± 0.00017) and 0.91 (± 0.014), at 35°C in the presence and absence of zinc respectively, and a K_d of 0.21 (±0.02) and 52.3 (±0.8) respectively.

4.2.3. Binding affinity of SigR-RsrA through Pre-steady-state stopped-flow

An important validation of a kinetic model for binding is that the stopped-flow kinetically derived equilibrium constant (K_d), agrees with the equilibrium constant derived by ITC. K_d values for SigR-RsrA complex in the presence and absence of zinc were determined from the individual dissociation (k_{off}) and association (k_{on}) rate constants at both 25°C and 35°C, where K_d=k_{off}/k_{on}. This mechanism suffices to explain the data, as there are no additional phases in the kinetic traces.

Conditions for measuring the change in fluorescence intensity for SigR-RsrA association and dissociation by stopped-flow were at 25°C. This is because it gave a good signal change and was not too fast or too near the stopped-flow dead time. This allowed a good fit of the data to a single-exponential equation, as represented by the residuals for each data set collected. However, measuring binding affinity by ITC at 25°C was unfavourable (as performed by Dr Karthik Rajasekar) due to a high signal-to-noise ratio and low heats, preventing the accurate determination of thermodynamic binding affinity. ITC was therefore performed at 35°C to obtain an accurate binding affinity. Hence association and dissociation experiments in the presence and absence of zinc were repeated at 35°C, to determine the binding affinity at similar temperatures to allow comparison with the values obtained through ITC.

The equilibrium constant by stopped-flow yielded a K_d of 0.24 (±0.004) nM and 29.2 (±0.55) nM in the presence and absence of zinc respectively at 25°C, which represents very strong binding for both (Table 13). At 35°C, a K_d of 0.27 (±0.047) nM and 62.4 (±0.69) nM were obtained in the presence and absence of zinc respectively. These affinities were independently validated by determining the equilibrium K_d values between SigR-RsrA with and without zinc by ITC, obtaining values of 0.78 (±0.033) nM (performed by Dr Karthik Rajasekar) and 101.7 (±27.4) nM respectively. These values are

in good agreement and suggest that binding between SigR-RsrA can be described simply by a one-step binding mechanism.

Table 13- Summary of rate constants and binding constants for the association (k_{on}) and dissociation (k_{off}) of SigR-RsrA in the presence and absence of zinc at 25°C and 35°C. Binding constants shown are determined indirectly through stopped-flow and directly through ITC. The K_d estimated from kinetics equals k_{off}/ k_{on}. Standard errors from the linear least-squares regression analysis are shown for association data, and the standard deviation between repeats for the dissociation data and kinetic K_d are shown.

			Rate constants		**Binding constants (nM)**	
Protein complex	Temp.	Zn^{2+}	**k_{on} (M^{-1} s^{-1})**	**k_{off} (s^{-1})**	**Kinetics K_d**	**ITC K_d**
SigR-RsrA	25°C	+	3.55 (±0.4) x10^{6}	8.6 (±0.000015) x10^{-4}	0.24 (±0.004)	N/A
	25°C	-	11.49 (±1.67) x10^{6}	0.336 (±0.006)	29.2 (±0.55)	
SigR-RsrA	35°C	+	8.9 (±1.4) x10^{6}	2.4 (±0.0004) x10^{-3}	0.27 (±0.047)	0.78 (±0.033)
	35°C	-	17.3 (±1.3) x10^{6}	1.08 (±0.01)	62.4 (±0.69)	101.7 (±27.4)

Binding affinities determined through ITC and stopped-flow have highlighted the importance of zinc in the SigR-RsrA complex. Zinc increases significantly the affinity of the complex compared to the metal-free state (Table 13). This is manifested through a minor effect on k_{on}, a 2-3-fold difference. In contrast, zinc has a large effect on the rate of dissociation for the SigR-RsrA complex, with values for k_{off} of 8.6 (±0.00) x10^{-4} s^{-1} and 0.336 (±0.006) s^{-1} at 25°C and 2.4 (±0.0004) x10^{-3} s^{-1} and 1.08 (±0.01) s^{-1} at 35°C, in the presence and absence of zinc respectively. This corresponds to a ~390-fold difference at 25°C and ~450-fold difference at 35°C between zinc-bound and zinc-free complex.

Hence, zinc impacts the binding affinity of this complex by slowing down the rate of dissociation. This could contribute to our understanding of the mechanism by which the complex responds to oxidative stress to dissociate and initiate gene transcription.

4.3. Developing an oxidation assay for the dissociation of SigR-RsrA complex

SigR-RsrA complex senses oxidative stress and responds to a change in the redox environment of the cytoplasm. The cysteine residues in RsrA anti-sigma become oxidised forming disulphide bonds,

causing the dissociation of zinc, a conformational re-arrangement, and a loss of its structural and functional ability to bind and inhibit the activity of SigR.

Dissociation kinetics have been determined under reducing conditions in the presence and absence of zinc. However, the rate at which the complex dissociates in response to oxidative stress has not been determined. This will allow a better understanding of the mechanism of the complex for the sensing and response to oxidative stress as a survival mechanism. The rates obtained under reducing conditions are important as they have provided an idea of the range for kinetics of the complex, which can be used to compare to rates of dissociation on oxidation. It has also provided information about the role and importance of zinc in the kinetics of the complex.

I aimed to develop an oxidation assay and determine the conditions under which to perform the dissociation kinetics. The three oxidants selected where hydrogen peroxide (H_2O_2), diamide and oxidised DTT. H_2O_2 (Bae et al. 2004) and diamide have previously been reported in the literature for the use in dissociating SigR-RsrA (Li et al. 2003), oxidised DTT complements the use of DTT as a reducing agent.

4.3.1. Oxidation of complex by Native PAGE

Fully reduced SigR-RsrA complex in the presence and absence of zinc were buffer exchanged into 50 mM Tris pH 7.5 and 100 mM NaCl. Three oxidants were chosen; diamide, oxidised DTT and hydrogen peroxide (H_2O_2). Complex in the presence and absence of zinc was incubated with 250 µM, 2 mM and 10 mM of each oxidant for 15 minutes, 1, 2 and 4 hours. Samples were loaded onto 12% Native PAGE and run using Tris glycine buffer to monitor migration. No difference was observed between oxidant concentrations or length of incubation. Oxidation has appeared to occur but clear separation via native PAGE is difficult due to the small difference in migration of the complex and free SigR due to the more compact structure of the complex.

Absorbance and emission properties of each oxidant showed diamide absorbs in the excitation and emission wavelengths of tryptophan, preventing its use in monitoring complex dissociation by tryptophan fluorescence.

Optimal conditions as identified by native PAGE were found to be using 30 µM Complex in the presence and absence of zinc with 2 mM H_2O_2 for 1 hour on ice (Figure 71).

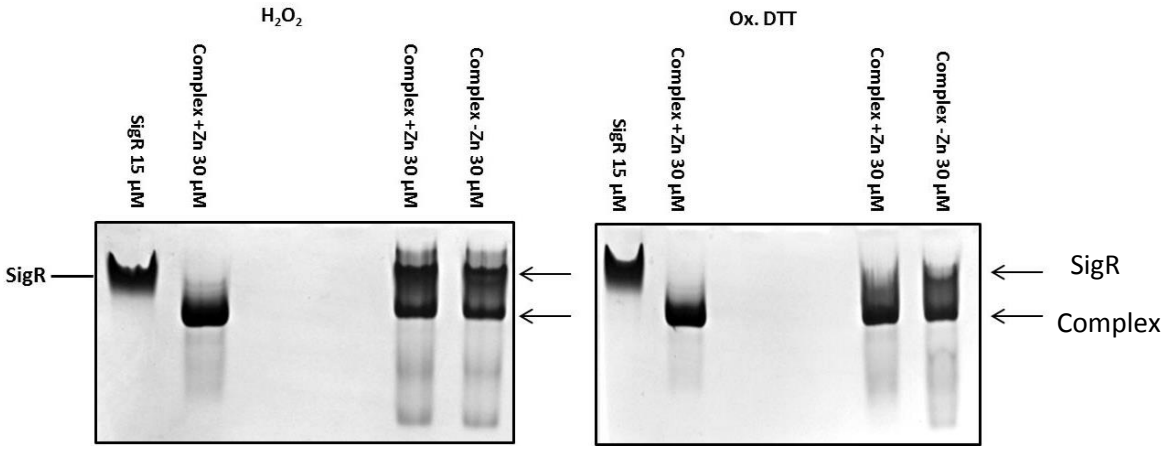


Figure 71- 12% Native PAGE of complex in the presence and absence of zinc under oxidising conditions. 15 µM SigR and 30 µM complex in the presence of zinc were fully reduced in the presence of 2 mM DTT. 30 µM complex in the presence and absence of zinc were treated with 2 mM H_2O_2 and oxidised DTT for 1 hour on ice. Both 12% native page gels were pre-run in tris-glycine buffer containing 2 mM H_2O_2 and 2 mM oxidised DTT respectively, for 2.5 hours. Both gels had oxidised samples loaded and run in tris-glycine buffer containing their respective oxidants, migrating for 30 minutes at room temperature. Arrows indicate two overlapping bands, the higher molecular weight representing SigR, the lower corresponding to remaining reduced complex.

There was difficulty in obtaining clear gels showing complex dissociation with the oxidants and with time constraints of the project, therefore further investigation was not possible. Future work would involve repeating fluorescence stopped-flow using the fluorescence-based assay previously developed, looking at pre-formed complex against different oxidants to determine the rates of dissociation.

5- Discussion

5.1. Where does RsrA bind on SigR during complex formation and how does it suppress transcriptional activity of SigR?

The structure of SigR-RsrA and mechanism of transcriptional repression of SigR have yet to be determined. In this study, I created a series of SigR region 2, linker region and region 4 tryptophan mutants. I used *in vitro* tryptophan fluorescence-based quenching experiments, which enabled me to confirm that SigR-RsrA forms a 1:1 complex, to develop an assay to monitor complex formation and to indirectly characterise the binding sites for RsrA on SigR as region 2 and region 4.

Previous studies by Li et al. (2002) used proteolysis of SigR to identify fragments protected from protease cleavage and that bound RsrA. Fragments obtained were identified by N-terminal sequencing and SELDI-MS, as the majority of SigR region 2 (subregions 2.1, 2.3, 2.4) and a fragment of region 4 (subregions 3.2, 4.1 and some of 4.2). They performed a pull-down assay using SELDI-IMAC chip, attaching RsrA and identifying if the two fragments of SigR bound RsrA. They identified that SigR region 2 was capable of binding RsrA but region 4 was not. This conflicts with the findings of this study.

The fragment of region 4 which Li et al. (2002) were able to isolate did not encompass subregion 4.2, which the literature describes as containing residues involved in the interaction with the -35 DNA promoter region (Campbell et al. 2002). Therefore it is premature to conclude that region 4 is not involved in the interaction with RsrA until a complete fragment is isolated.

Further evidence from this study is the thermodynamic data derived through ITC, which showed binding of RsrA to SigR* F171W region 4 mutant with a K_d of ~265.8 ± 62.7 nM, ~340-fold weaker than SigR wild-type. This large decrease in binding affinity, suggested that either the phenylalanine residue mutated from this position or the environment surrounding it in region 4 was involved in the interaction with RsrA. It was verified using CD far and near UV that no structural change to SigR had occurred in this protein as a result of the mutation affecting its stability, to explain the decrease in affinity.

Further evidence to support interaction of RsrA with SigR region 4, is found in homologous sigma anti-sigma complexes. ChrR-SigE from *Rhodobacter sphaeroides* is a similar ZAS-ECF complex. ChrR is composed on an N-terminal anti-sigma domain (ASD) and a C-terminal Cupin-like domain (CLD). It is the ASD that occludes the RNA polymerase binding sites of SigE by binding to and altering the structure of region 4 in an unfavourable conformation (Campbell et al. 2008). This domain organisation and mechanism of inhibition is also observed with SigL-RslA ZAS-ECF from *Mycobacterium tuberculosis*, FlgM-σ^{28} from *Aquifex aeolicus* and in SigE-RseA ECF-anti-sigma from *Escherichia coli*, where an α-helix is almost completely buried between region 2 and 4 of SigE. In *Cupriavidus metallidurans* CnrH-CnrY ECF-anti-sigma, certain helices of both region 2 and region 4 provide a 40 Å-long hydrophobic groove that fits the cytosolic domain of CnrY (Maillard et al. 2014).

It appears a common mechanism across Gram-positive and negative species, that complex formation and inhibition of transcription by the anti-sigma involves sterically occluding the DNA promoter and RNA polymerase binding domains region 2 and region 4.

Mechanism of transcriptional repression

Evidence to help understand the mechanism for how RsrA suppresses the transcriptional activity of SigR was also identified by the fluorescence-based quenching experiments. On titration of RsrA with region 4 mutant SigR* F159W, a concentration-dependent increase in fluorescence intensity was observed until a 1:1 complex formed. This is suggestive of a conformational change in region 4 on binding RsrA.

Free ECF sigma factors have a distance of ~40 Å between the DNA binding domain regions 2.2 and 4.2 in their unbound states (Borukhov and Severinov 2002). Free sigma factors are unable to bind the -10 and -35 DNA promoter regions due to this distance constraint. When RNA polymerase binds and forms the holoenzyme with the sigma factor, the β subunit causes a conformational change separating region 2

and region 4 to a distance capable of binding the -10 and -35 DNA promoter regions (Borukhov and Severinov 2002).

Evidence of a conformational change of region 4 is seen in many other sigma factors across bacterial species. ChrR forms a complex with SigE via its ASD by altering the structure of region 4 in an unfavourable conformation (Campbell et al. 2008). CnrH regions 2 and 4 are brought together to provide a site for CnrY anti-sigma to bind, which forces a sigma factor orientation that causes the CnrH sigma region 4 to conceal sigma region 2 DNA binding region (Maillard et al. 2014). FlgM causes a conformational change of both σ^{28} region 2 and 4 to prevent their association with DNA promoters. RseA binds SigE inserting an α-helix between region 2 and region 4 causing their seperation (Campbell et al. 2003).

This would suggest SigR-RsrA uses a similar mechanism of binding to SigR, causing a conformational change in the DNA binding domains to prevent association with RNA polymerase and DNA promoter regions thereby inhibiting gene transcription.

5.2. What is the importance and role of zinc in RsrA?

RsrA has been shown to bind zinc stoichiometrically, it is coordinated via a conserved HCC motif (Bae et al. 2004) and has been shown to play a role in the activity and structure of RsrA and protection against oxidation (Li et al. 2003).

In this study, I performed ITC between SigR-RsrA in the presence and absence of zinc, to see what effect zinc had on the thermodynamics. My data revealed equilibrium dissociation constants K_d of <10.5 (± 0.99) nM and 101.7 (± 27.5) nM, in the presence and absence of zinc respectively. This represented a ~9.7-fold difference and higher affinity in the presence of zinc. These values agree with the K_d obtained in the study of Kang et al. (1999), who performed surface plasmon resonance (SPR) experiments, immobilising RsrA onto the chip and monitoring binding of SigR in the presence of zinc. A K_d of 11 nM was

obtained by this method. Bae et al. (2004) repeated SPR of SigR-RsrA in the presence and absence of zinc and found an ~8.7-fold higher affinity in the presence of zinc. Wei et al. (2014) obtained kinetic parameters using FRET, to obtain a K_d of 81 (± 29) nM for SigR-RsrA in the absence of zinc under fully reduced conditions.

The ZAS-ECF SigL-RslA complex from *Mycobacterium tuberculosis* has a similar structure, function and mechanism of activation by oxidative stress to SigR-RsrA. SPR was used to examine the interaction between SigL-RslA, a dissociation constant K_d of 20 nM and 150 nM were obtained in the presence and absence of zinc respectively. This corresponds to a ~7.5 fold difference (Thakur et al. 2010). SigH-RshA, the closest homologue to SigR-RsrA was shown by SPR to have a dissociation constant K_d of 15 nM in the presence of zinc (Jeong et al. 2006).

The values obtained by SPR and FRET for SigR-RsrA closely agree with the values obtained in this study by ITC. The values also correspond to those obtained for other homologous ZAS-ECF sigma anti-sigma complexes. This highlights that zinc plays an important role in the thermodynamics and increases the binding affinity between sigma factors and their anti-sigma factor proteins.

Unexpectedly, however, the K_ds obtained for SigR-RsrA by ITC in this study were found to conflict with the values obtained indirectly through pre-steady state kinetics ($K_d = k_{off}/k_{on}$). I obtained an average K_d of 0.27 (±0.047) nM and 62.4 (±0.69) nM by kinetics, in the presence and absence of zinc respectively. This led us to investigate in more detail the binding affinities by ITC. Dr Karthik Rajasekar has since performed competition ITC experiments from which the binding affinity between SigR-RsrA in the presence of zinc was 0.78 (±0.033) nM. In other words, within 3-fold of the value I determined kinetically. Hence, our data demonstrate that binding affinity between SigR and RsrA in the presence of zinc is ~13-fold stronger than previously determined by ITC and SPR. Moreover, these combined data show that zinc improves the binding of RsrA for SigR by >130-fold between SigR-RsrA in the presence and absence of zinc.

The zinc ions in ZAS proteins in complex with their sigma factors, do not appear to make contact with the sigma factor, an example of this is seen with ChrR-SigE from *Rhodobacter sphaeroides*. Zinc has been shown to play a role in increasing the affinity and improving binding for the sigma-anti-sigma complexes. This might be explained by zinc holding the ZAS HCC motif and surrounding residues in a conformation that is more favourable for the binding of the sigma factor.

Zinc has been shown to play a role in the kinetics and structure of RsrA with oxidation. Bae et al. (2004) used the colorimetric PAR assay to determine the kinetics of zinc release from RsrA following oxidation with H_2O_2. They showed that zinc was released with a $t_{1/2}$ of 1.8 minutes and that zinc had an affinity of K_d $0.5x10^{-12}$ pM for RsrA, not affected by the binding of SigR. This is similar to the affinity of Hsp33 for zinc, K_d= $4x10^{-18}$ aM. Thakur et al. (2010) performed similar kinetics on SigL-RslA, they observed a $t_{1/2}$ of 3.5 minutes, this rate was affected by SigL in complex with a $t_{1/2}$ of 7 minutes. Both of which are much slower than the dissociation of zinc from oxidised RsrA reported by Bae et al. (2004).

Thakur et al. (2010) looked at the conformational change that occurred with the association and dissociation of zinc in RslA. They showed an increase in the α-helical content of the secondary structure of RslA upon binding zinc. The rate of this conformational change after zinc release was found to be $t_{1/2}$ of 7 minutes from RslA and $t_{1/2}$ of 12 minutes from the SigL-RslA complex, suggesting zinc release is a rapid process followed by a much slower conformational change. The changes in structure of RsrA are associated with the formation of the disulphide bond between the trigger disulphides Cys11 and Cys41 or Cys44 on oxidation (Li et al. 2003).

This appears to suggest a difference in the mechanism for anti-sigma dissociation from the sigma factor between these two complexes. RsrA dissociates from SigR after oxidation, formation of a disulphide bond and a large conformational change resulting in the expulsion of zinc. However RslA appears to dissociate from SigL after oxidation and expulsion of zinc causing a conformational change in RslA.

This therefore confers several differences in the importance of zinc between members of the ZAS family, in terms of the thermodynamics, kinetics of oxidation, protection of the cysteine thiols to oxidation, conformational changes that occur to cause sigma anti-sigma dissociation and the sensitivity to proteolysis. These are all differences that require further study.

5.3. The kinetics of SigR-RsrA complex formation

Little is known of the mechanism of RsrA binding to SigR or how the kinetics are affected by oxidation. In this study, I used pre-steady state fluorescence stopped-flow to monitor complex formation in the presence and absence of zinc. This allowed determination of the association and dissociation rate constants for SigR-RsrA for comparison to previous SPR studies.

I obtained an average association rate (k_{on}) for SigR-RsrA of 3.55 (±0.4) x10^6 M^{-1} s^{-1} and 11.49 (±1.67) x10^6 M^{-1} s^{-1}, at 25°C in the presence and absence of zinc, respectively. This represents a difference in association of 3.2-fold faster in the absence of zinc. This might be explained by the understanding that in the absence of zinc, binding between SigR-RsrA is weaker. This may be due to non-specific interactions or a slight flexibility in RsrA that aids in the interaction of the complex, which is not observed in zinc bound RsrA due to a steric hindrance and lack of flexibility. Alternatively, this could be explained by the exposure of the residues found to be essential for complex formation; Cys11, Cys41 and Cys44 (Paget et al. 2001).

Clearly, therefore zinc has little role to play in the rate of association of the two proteins. Hence zinc is not required for long-range, electrostatically driven interactions of the two proteins. Finally, it is worth noting that a monophasic exponential decay in fluorescence intensity was observed in all stopped-flow association experiments, suggesting that binding can be described by a single bimolecular association with no detectable intermediates.

The dissociation rate (k_{off}) for SigR-RsrA complex could not be estimated from the intercept of the pseudo-first order k_{obs} plot when RsrA was in excess, due to the intercept crossing very close to 0 and giving very large errors. Therefore, the dissociation rate was measured by competition stopped-flow using SigR-RsrA complex and a competitor SigR lacking tryptophan residues. I obtained an average dissociation rate (k_{off}) for SigR-RsrA of 8.6 (±0.00) x10^{-4} s^{-1} and 0.336 (±0.01) s^{-1}, at 25°C in the presence and absence of zinc, respectively.

This represents a 390-fold faster dissociation in the absence of zinc. This correlates with the effect of zinc on the binding affinity. SigR-RsrA in the presence of zinc has a very strong binding affinity and very long dissociation rate ($t_{1/2}$ of 13.4 minutes), when the affinity between SigR-RsrA is dramatically reduced in the absence of zinc, the dissociation rate is much faster. As with association, dissociation was characterised by a monophasic enhancement in fluorescence intensity in all my stopped-flow experiments, suggesting the absence of any detectable intermediate states.

Stopped-flow also allowed the determination of kinetically derived binding affinities, for comparison to that obtained thermodynamically by ITC. This allowed a validation of the kinetic model for binding.

Jeong et al. (2006) used SPR to determine the kinetics of association and dissociation of SigH-RshA from *Mycobacterium tuberculosis*. They captured SigH onto the sensor chip and injected RshA over its surface using different concentrations. They determined an association rate constant of k_{on} = 1.15 x 10^5 $M^{-1}s^{-1}$ and a dissociation rate constant of k_{off} = 1.7 x10^{-3} s^{-1} by injection of buffer over the chip. This corresponds to a ~31-fold faster association rate with SigR-RsrA, and a ~50.6-fold slower dissociation rate than SigH-RshA.

The development of this fluorescence-based assay to monitor complex formation has allowed determination of the kinetics of this complex under reducing conditions by stopped-flow. This fluorescence-based assay can be used to allow a more detailed investigation of the kinetics of oxidation, comparing the rate of zinc release by colorimetric PAR assay. Initial studies were performed to determine

the optimal conditions by which to perform stopped-flow to determine the rate of dissociation under oxidising conditions. These experiments were however limited in scope due to time constraints of the project.

5.4. Major conclusions from this study

One finding from this study provides additional evidence of RsrA binding SigR region 2 and new insight into the binding of region 4 to form a complex. In addition I have highlighted data demonstrating a conformational rearrangement of region 4 on complex formation, to contribute to the understanding of the mechanism for how RsrA binds and suppresses the transcriptional activity of SigR.

This study has identified the importance and role of zinc in SigR-RsrA for the thermodynamics of the complex. I have provided additional insight into the binding affinity between SigR-RsrA in the presence of zinc, ~13-fold stronger than previously reported by SPR and ITC.

I have developed a fluorescence-based assay to monitor complex formation in SigR-RsrA for use in determining the kinetics of the complex. My main finding in this study is determining the kinetic association and dissociation rate constants for SigR-RsrA and highlighting the importance of zinc in the kinetics. These rates have not been described prior to this study. The association rate and fluorescence changes suggest a single-step binding model for complex-formation. The dissociation rates highlight a link between binding affinity and rates of dissociation based on the presence and absence of zinc. Further studies involving dissociation in response to different oxidants will provide an understanding of how quickly the complex responds to a change in the redox status. In combination with future *in vivo* studies, the rate at which the complex recovers from oxidative stress will prove interesting.

This knowledge of SigR-RsrA can be transferred to poorer understood complexes with similar features, involving other ZAS-ECF complexes and complexes that respond to oxidative or disulphide

stress. It can also lead to the eventual development of therapeutic drug design for use in disabling this bacterial survival mechanism in pathogenic bacterial strains like *Mycobacterium tuberculosis*.

5.5. Implications of study for future research

Development of the fluorescence-based assay showing complex formation and identifying regions of interaction can be applied to other ZAS-ECF complexes to identify if there is a trend in the mechanism of complex formation and therefore gene transcription regulation, as well as kinetic rates of association and dissociation.

Although these data highlight dissociation constants for the complex in the presence and absence of zinc, it is the response of the complex to oxidation that is of more interest and would contribute to the understanding of the system. Future work involving pre-steady state fluorescence stopped-flow against various oxidation agents would prove interesting and answer some crucial questions of how this complex responds to oxidative stress. Future *in vivo* work to confirm findings found *in vitro*, would allow confirmation of our understanding of this system.

The structure of SigR region 2 has been solved, the structure of RsrA in both the oxidised and reduced form have also been solved (Zdanowski, Potts & Kleanthous, unpublished results). The structure of SigR-RsrA in both the presence and absence of zinc, which has not been determined, would contribute to understanding the mechanism, providing the evidence to support the conformational changes that indirect evidence through the present study has shown, the location and importance of zinc in these interactions and response to oxidative stress.

An important question to address in future research is to identify if results found *in vitro* also occur *in vivo*, and if results found under laboratory conditions reflect what occurs in the natural environment of the bacteria.

Word count = 24,787 words

Appendix

A second objective was to develop expression strategies for other novel sigma anti-sigma proteins for future structural studies. SigH RshA from *Mycobacterium tuberculosis* and several ZAS-ECF complexes from *Streptomyces coelicolor* were cloned and expressed as described below.

1.1. Developing expression systems for other sigma factors and anti-sigma proteins

A previous member of the lab (Colin Seepersad) cloned SigH and RshA into pET-21a expression vectors.

RshA in pET-21a (pCES003) was transformed into Rosetta 2 pLysS, BL21 (DE3) and BL21 (DE3) pLysS cells. Test expressions were performed using the same conditions as SigR and RsrA (Materials and methods section 2.3.5.), in the presence of 10 µM Zinc, and reported here.

1.1.1. RshA

RshA is 12.6 kDa protein. RshA pET-21a (pCES003) was expressed in all cell types at 20°C in the presence of zinc and at much higher concentrations to that seen at 37°C. There is a linear increase in protein expressed in all the cells from 3 hours to overnight expression. Optimum expression was in BL21 (DE3) cells at 20°C overnight (Figure 72).

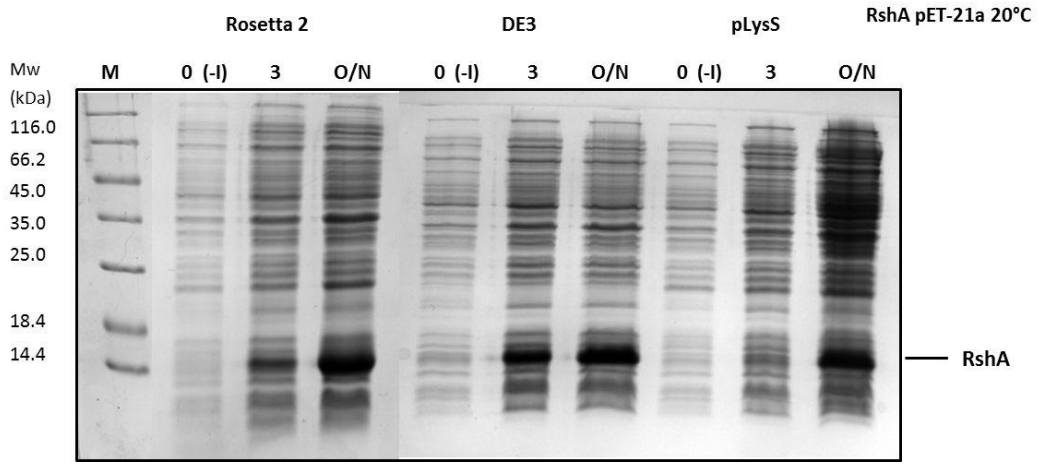


Figure 72- RshA pET-21a test expression in Rosetta 2 pLysS, BL21 (DE3) and BL21 (DE3) pLysS at 20°C. 16% SDS-PAGE coomassie gel showing the marker (M), RshA prior to expression with 1 mM IPTG (0(-I)), and after 3 hours and overnight (O/N) expression.

1.1.2. SigH

SigH is a 24.3 kDa protein. SigH pET-21a (pCES004) was only expressed in BL21 (DE3) cells as previous experiments had already identified that there was no expression in other cells. SigH expressed well at both 37°C and 20°C and at high concentrations, with an obvious increase in protein from 1 to 3 hours at 37°C, and 3 hours to overnight at 20°C. Optimum expression was overnight at 20°C (Figure 73).

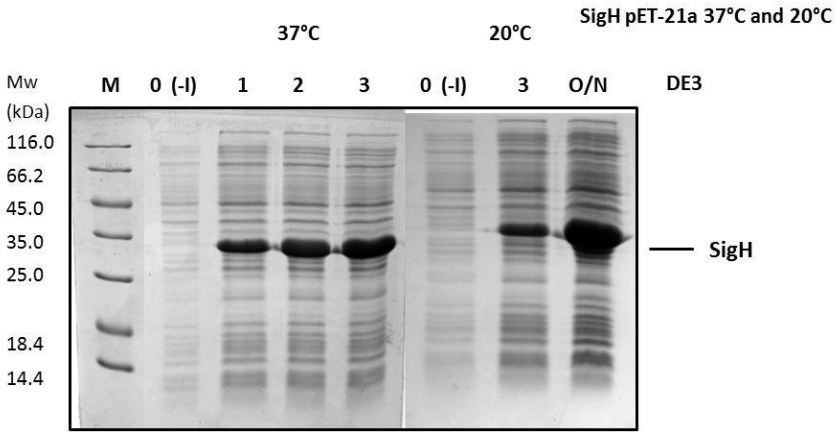


Figure 73- SigH pET-21a test expression in BL21 (DE3) at 37°C and 20°C. 16% SDS-PAGE coomassie gel showing the marker (M), SigH prior to expression with 1 mM IPTG (0(-I)), after 1-3 hours and overnight (O/N) expression.

SigH was cloned into pCDFDuet-1 (pMLF06) and transformed into all three cell types. SigH expressed well in BL21 (DE3) cells at 20°C at high concentrations, with an obvious increase in protein from 1 hour to overnight. Optimum expression was overnight at 20°C (Figure 74).

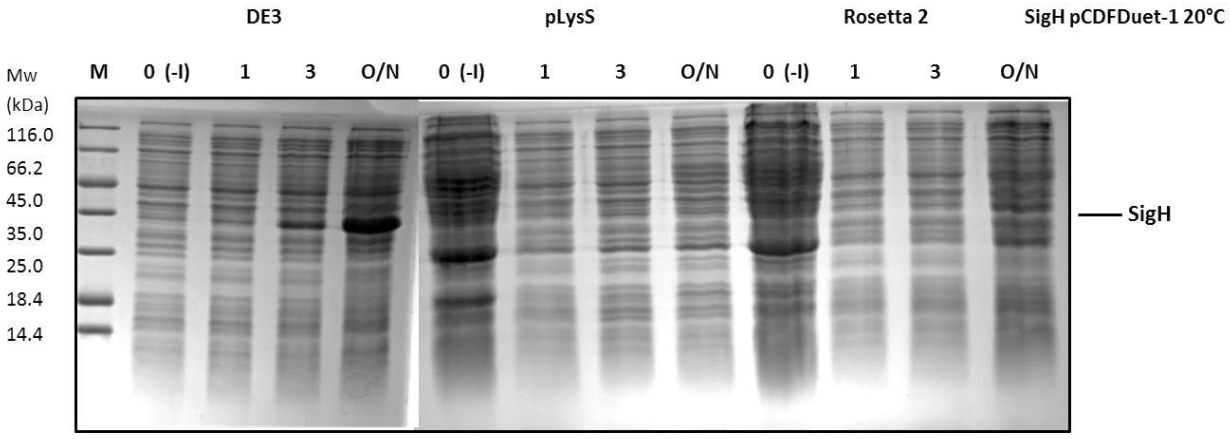


Figure 74- SigH pCDFDuet-1 test expression in Rosetta 2 pLysS, BL21 (DE3) and BL21 (DE3) pLysS at 20°C. 16% SDS-PAGE coomassie gel showing the marker (M), SigH prior to expression with 1 mM IPTG (0(-I)), and after 1, 3 hours and overnight expression.

The optimum conditions for expression were SigH pCDFDuet-1 and RshA pET-21a in BL21 (DE3) cells, expressed at 20°C overnight. These plasmids were then co-transformed into BL21 (DE3) cells. A single colony was used to grow a 50 ml starter culture at 37°C in the presence of 10 µM Zinc and AmpStrep, until an OD_{600} reached 0.6. 22 ml was diluted into an 800 ml flask (x2) and grown at 37°C to OD_{600} 0.6 before adding 1 mM IPTG and inducing expression at 20°C overnight.

RshA pET-21a expressed well in BL21 (DE3) cells at 20°C overnight, however SigH pCDFDuet-1 did not express well and SDS-PAGE showed two bands at the molecular weight of SigH (Figure 75). This is much less expression than seen previously when expressed by itself in a small 10 ml test expression.

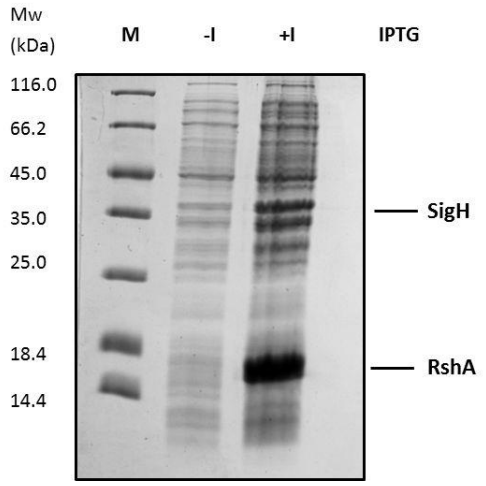


Figure 75- SigH pCDFDuet-1 and RshA pET-21a large scale expression in BL21 (DE3) cells at 20°C overnight. 16% SDS-PAGE coomassie gel showing the marker (M), SigH and RshA prior to expression with 1 mM IPTG (-I), and after expression (+I) overnight expression.

The pellet of cells containing the expressed proteins was lysed to check solubility of the proteins. The cells were re-suspended in 25 ml 50 mM Tris pH 7.5, 100 mM NaCl, 0.1 mM $ZnCl_2$ and 1 mM PMSF, and centrifuged for 20 minutes at 17,000 rpm. Samples of the pellet and supernatant were then run on SDS-PAGE to locate the proteins and determine their solubility (Figure 76).

SDS-PAGE gel confirmed SigH is being expressed to a lesser extent than RshA and lower to previous test expressions. RshA appears to remain largely in the pellet fraction with possible low concentrations in the supernatant (Figure 76). SigH appears to be present as two bands at the molecular weight of SigH, with the lower molecular weight present to a higher level in the supernatant and the higher molecular weight present to a higher level in the pellet fraction. It would suggest that both SigH and RshA are insoluble when co-expressed at 20°C.

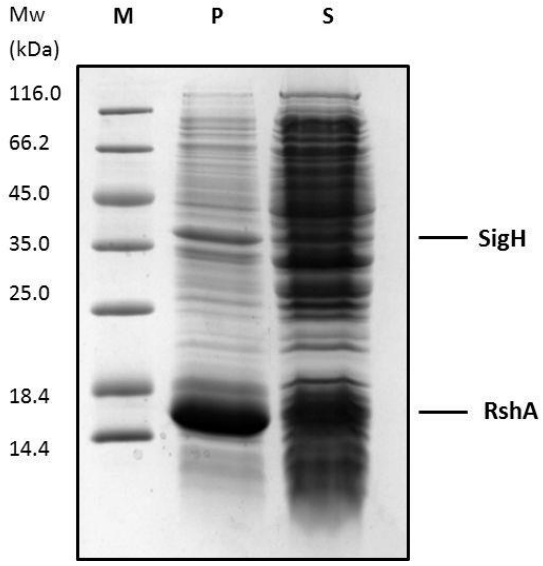


Figure 76- SigH pCDFDuet-1 and RshA pET-21a DE3 expression after lysis of cells. Cells from a 2L expression of SigH pCDFDuet-1 and RshA pET-21a in BL21 (DE3) cells using 1 mM ITPG overnight at 20°C. Cells were lysed using 50 mM Tris pH 7.5, 100 mM NaCl, 0.1 mM $ZnCl_2$ and 1 mM PMSF. 16% SDS-PAGE coomassie gel showing the marker (M), pellet of cellular debris (P) and supernatant (S).

A test expression was performed at 20°C with a fresh transformation of SigH pET-21a and pCDFDuet-1 in BL21 (DE3) cells. Different conditions were tried; IPTG induction no zinc and with IPTG induction and zinc, to see the effect zinc has on expression of SigH (Figure 77). RshA expressed in the presence and absence of zinc, with a higher level of expression with zinc. Zinc had no effect on the expression of SigH. Poor expression of SigH therefore comes from the co-expression with RshA.

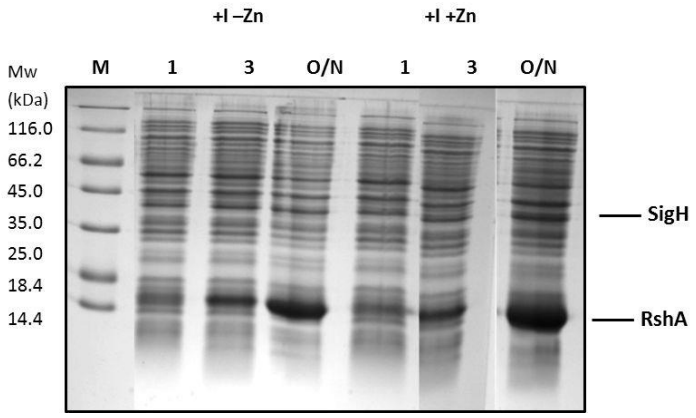


Figure 77- SigH pCDFDuet-1 and RshA pET-21a test expression in BL21 (DE3) cells at 20°C in the presence and absence of 10 µM zinc. SDS-PAGE coomassie gel showing the marker (M), SigH and RshA after expression with 1 mM IPTG (+I) in the presence and absence of zinc for 1, 3 hours and overnight expression.

Further work would involve the expression of SigH in pCDFDuet-1 or pET-21a and RshA pET-21a separately. The two pellets of expressed protein can then be mixed on lysis allowing for their co-purification.

1.2. New ZAS-ECF complexes

ZAS stands for Zinc-binding anti-sigma and ECF stands for extracytoplasmic function, the equivalents of RsrA and SigR respectively. They do not have a name assigned to them, as no information has been determined for them, however their location within the *Streptomyces coelicolor* genome is listed in Appendix table 1. The four sets are therefore referred to as ZAS1-ECF1 (pCES024), ZAS2A-ECF2 (pCES025), ZAS2B-ECF2 (pCES026) and ZAS3-ECF3 (pCES027) in their cognate sigma-anti-sigma groups. A previous member of the lab (Colin Seepersad) cloned each ZAS and ECF into pCDFDuet-1 expression vector. Molecular weights of each ZAS ECF are shown in Appendix table 1.

Appendix table 1- Molecular weight and genome location of the ZAS and ECF proteins used in this study.

Protein	Location in *Streptomyces coelicolor* genome	Molecular weight kDa
ZAS1	SCO196	15.7
ZAS2A	SCO3449	11.6
ZAS2B	SCO3451	11.3
ZAS3	SCO4408	44.6
ECF1	SCO0194	22.1
ECF2	SCO3450	22.1
ECF3	SCO4409	21.5

Each cognate ZAS-ECF in pCDFDuet-1 vector was transformed into Rosetta 2 pLysS, BL21 (DE3) and BL21 (DE3) pLysS cells. Test expressions were performed using the same conditions as SigR and RsrA (See materials and methods section 2.3.5.), in the presence and absence of 10 µM zinc.

1.2.1. ZAS1-ECF1

ECF1 expressed well in the presence of zinc at 37°C and 20°C in BL21 (DE3) cells, but poorly in BL21 (DE3) pLysS and Rosetta 2 pLysS cells. ZAS1 did not appear to express in any of the cells. Optimum expression occurred overnight at 20°C in the presence of zinc (Figure 78).

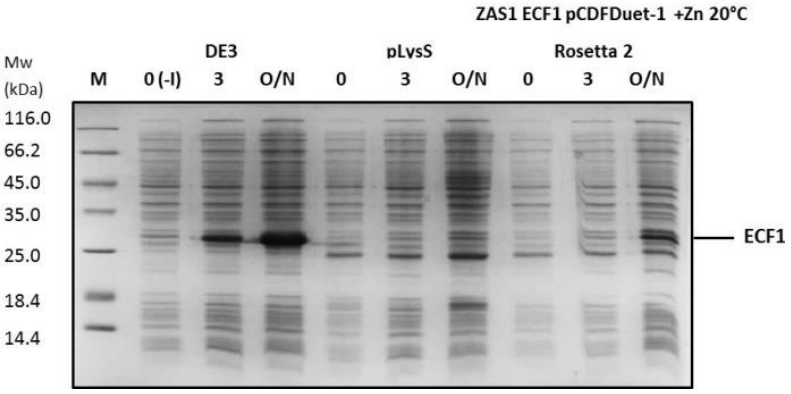


Figure 78- ZAS1-ECF1 pCDFDuet-1 test expression in BL21 Rosetta 2, DE3 and pLysS at 20°C in the presence of zinc. 16% SDS-PAGE coomassie gel showing the marker (M), ZAS1-ECF1 prior to expression with 1 mM IPTG (0(-I)), and after 3 hours and overnight (O/N) expression.

1.2.2. ZAS2A-ECF2

ECF2 expressed well in the presence of zinc at 20°C in BL21 (DE3) cells, but poorly in BL21 (DE3) pLysS and Rosetta 2 pLysS cells. ZAS2A did not appear to express in any of the cells. Optimum expression occurred overnight at 20°C in the presence of zinc (Figure 79).

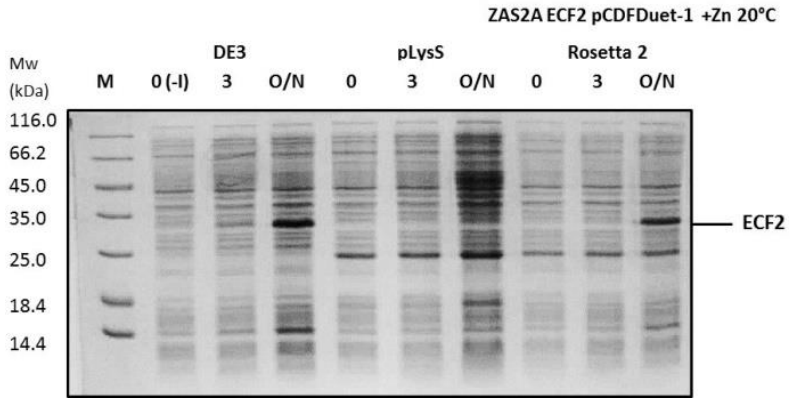


Figure 79- ZAS2A-ECF2 pCDFDuet-1 test expression in BL21 Rosetta 2, DE3 and pLysS at 20°C in the presence of zinc. 16% SDS-PAGE coomassie gel showing the marker (M), ZAS2A-ECF2 prior to expression with 1 mM IPTG (0(-I)), and after 3 hours and overnight (O/N) expression.

1.2.3. ZAS2B-ECF2

ECF2 expressed well in the presence of zinc at 37°C and 20°C in BL21 (DE3) cells, but poorly in BL21 (DE3) pLysS and Rosetta 2 pLysS cells. ZAS2B appeared to express in BL21 (DE3) cells in the presence of zinc at 20°C. Optimum expression occurred overnight at 20°C in the presence of zinc (Figure 80).

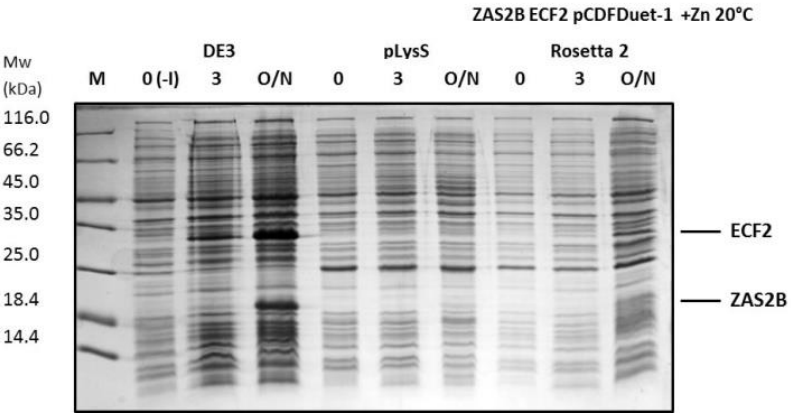


Figure 80- ZAS2B-ECF2 pCDFDuet-1 test expression in BL21 Rosetta 2, DE3 and pLysS at 20°C in the presence of zinc. 16% SDS-PAGE coomassie gel showing the marker (M), ZAS2B-ECF2 prior to expression with 1 mM IPTG (0(-I)), and after 3 hours and overnight (O/N) expression.

1.2.4. ZAS- ECF3

ECF3 expressed poorly in BL21 (DE3) cells after overnight expression at 20°C in the absence of zinc and not in the presence of zinc. ZAS3 appeared not to express under any conditions (Figure 81).

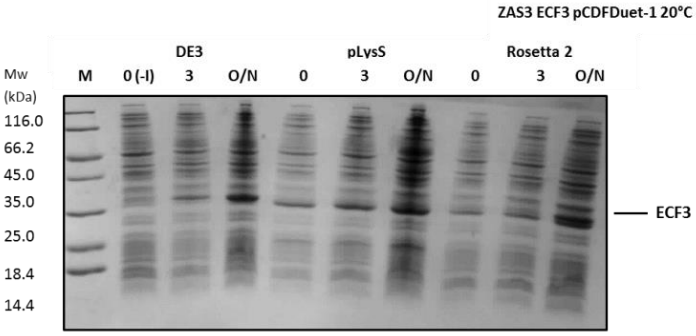


Figure 81- ZAS3-ECF3 pCDFDuet-1 test expression in BL21 Rosetta 2, DE3 and pLysS at 20°C in the absence of zinc. 16% SDS-PAGE coomassie gel showing the marker (M), ZAS3-ECF3 prior to expression with 1 mM IPTG (0(-I)), and after 3 hours and overnight (O/N) expression.

ZAS2B-ECF2 appeared to be the only construct able to express both the ZAS and ECF, under the conditions of BL21 (DE3) cells in the presence of zinc at 20°C after overnight expression. A large scale 1L expression under these conditions was performed to develop a purification strategy. The ECF has an N-terminal His-tag, allowing the co-purification of the complex. The pellet was lysed in 25 ml 50 mM Tris pH 7.5, 100 mM NaCl, 1 mM PMSF and 0.1 mM zinc, before loading the lysate onto an IMAC nickel column for purification via its His-tag (Figure 82). SDS-PAGE gel identified eluted fractions containing ZAS2B-ECF2 and demonstrating its purity (Figure 83).

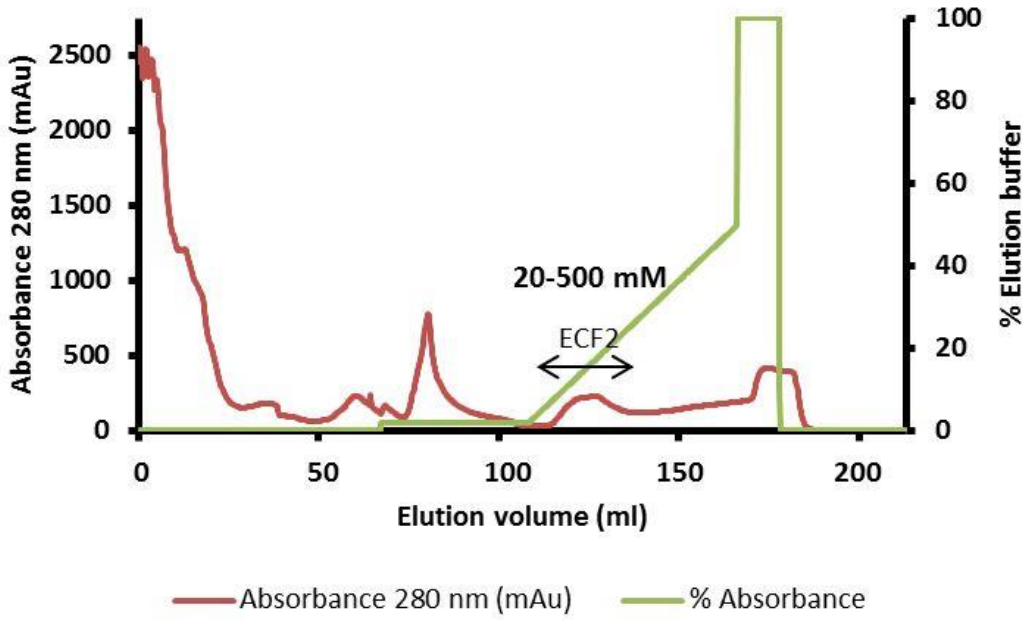


Figure 82- ZAS2B-ECF2 IMAC Nickel affinity purification. Fractions were run on SDS-PAGE gel to locate ZAS2B and ECF2 and demonstrate its purity.

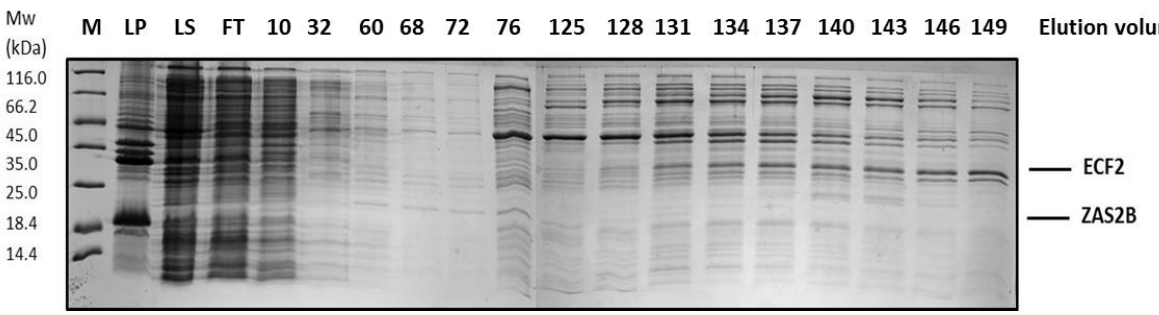


Figure 83- ZAS2B-ECF2 Immobilised metal affinity chromatography (IMAC) Nickel column purification. 16% SDS-PAGE coomassie gel showing the marker (M), ZAS2B-ECF2 pellet after lysis (LP) and supernatant after lysis (LS), flow-through (FT) and fractions from Nickel column elution profile.

SDS-PAGE gels show that the pellet (LP) still contains a large concentration of ECF2 and all of the ZAS2B, which has expressed at a much higher concentration in a larger volume of media. Some ECF2 was present in the supernatant and appears in elution volume 131-149 ml corresponding to the 20-500 mM imidazole elution. This suggests that both ZAS2B and ECF2 appear insoluble.

Further work could involve the expression of ZAS2B and ECF2 in separate plasmids rather than in pCDFDuet-1 as they may express better separately with more resources available in the media for their expression. To improve the solubility, the concentration of ITPG could be decreased from 1 mM, the growth media could also be changed to find one for more optimal expression. Alternatively, the two proteins could be solubilised and denatured using guanidine or urea under reducing conditions and then re-folded to isolate both proteins.

<u>Appendix components</u>

Agar: 1.5% Agar No.3 in LB

SDS-PAGE coomassie blue stain (1L): 10% v/v Acetic acid, 50% v/v ethanol, 2g coomassie brilliant blue R250 0.2% (w/v) Coomassie brilliant blue R250

References

Ades S.E., (2004), Control of the alternative sigma factor σ^E in *Escherichia coli*, *Current Opinion in Microbiology*, Vol. 7, pp. 157-162

Aldridge, P., Karlinsey, J.E., Becker, E., Chevance, F.V., and Hughes, K.T., (2006), Flk prevents premature secretion of the anti-σ factor FlgM into the periplasm, *Mol. Microbiol*, Vol. 60, No. 3, pp. 630-643

Antelmann, H., and Zuber, P., (2010) Thiol-based sensory factors. In: Spiro, S., and Doxin, R., Sensory *Mechanisms in Bacteria; Molecular Aspects of Signal Recognition*, Caister Academic Press, UK

Bae, J.B., Park, J.H., Hahn, M.Y., Kim, M.S., and Roe, J.H., (2004), Redox-dependent Changes in RsrA, an Anti-sigma Factor in *Streptomyces coelicolor*: Zinc Release and Disulfide Bond Formation, *J. Mol. Biol*., Vol 335, pp. 425-435

Barik, S., Sureka, K., Mukherjee, P., Basu, J., and Kundu, M., (2010), RseA, the SigE specific anti-sigma factor of *Mycobacterium tuberculosis*, is inactivated by phosphorylation-dependent ClpC1P2 proteolysis, *Molecular Microbiology*, Vol. 75, No.3, pp.592–606

Bentley, S.D., Chater, K.F., Cerdeno-Tarraga, A.M., Challis, G.L., Thomson, N.R., James, K.D., Harris, D.E., Quail, M.A., Kieser, H., Harper, D., Bateman, A., Brown, S., Chandra, G., Chen, C.W., Collins, M., Cronin, A., Fraser, A., Goble, A., Hidalgo, J., Hornsby, T., Howarth, S., Huang, C.H., Kieser, T., Larke, L., Murphy, L., Oliver, K., O'Neil, S., Rabbinowitsch, E., Rajandream, M.A., Rutherford, K., Rutter, S., Seeger, K., Saunders, D., Sharp, S., Squares, R., Squares, S., Taylor, K., Warren, T., Wietzorrek, A., Woodward, J., Barrell, B.G., Parkhill, J., and Hopwood, D.A., (2002), Complete genome sequence of the model actinomycete Streptomyces coelicolor A3(2), *Nature*, Vol. 417, pp. 141-147

Borukhov, S., and Severinov, K., (2002), Role of the RNA polymerase sigma subunit in transcription initiation, *Research in Microbiology*, Vol. 153, pp. 557-562

Brooks, B.E., and Buchanan, S.K., (2008) Signalling mechanisms for activation of extracytoplasmic function (ECF) sigma factors, *Biochimica et Biophysica Acta 1778*, pp. 1930-1945

Browning, D.F., and Busby, S.J.W., (2004) The regulation of Bacterial Transcription on Initiation, *Nature Reviews, Microbiology*, Vol. 2, pp. 1-9

Cabiscol, E., Tamarit, J., and Ros, J., (2000), Oxidative stress in bacteria ad protein damage by reactive oxygen species, *Internatl. Microbiol*. Vol. 3, pp. 3-8

Campbell, I.D., (2012) *Biophysical Techniques*, Oxford University Press, Oxford

Campbell, E.A., Muzzin, O., Chlenov, M., Sun, J.L., Olson, C.A., Weinman, O., Trester-Zedlitz, M.L., and Darst, S.A., (2002), Structure of the Bacterial RNA Polymerase Promoter Specificity σ Subunit, *Molecular Cell,* Vol. 9, pp. 527-539

Campbell, E.A., Tupy, J.L., Gruber, T.M., Wang, S., Sharp, M.M., Gross, C.A., Darst, S.A., (2003) Crystal Structure of Escherichia coli σ^E with the Cytoplasmic Domain of Its Anti-σ RseA, *Molecular Cell*, Vol. 11, pp. 1067-1078

Campbell, E.A., Greenwell, R., Anthony, J.R., Wang, S., Lim, L., Das, K., Sofia, H.J., Donohue, T.J., and Darst, S.A., (2007), A Conserved Structural Module Regulates Transcriptional Responses to Diverse Stress Signals in Bacteria, *Molecular Cell*, Vol. 27, pp. 793-805

Campbell, E.A., Westblade, L.F., and Darst, S.A., (2008), Regulation of bacterial RNA polymerase σ factor activity: a structural perspective, *Current Opinion in Microbiology*, Vol. 11, No. 2, pp. 121-127

Chater, K.F. (2000) Developmental decisions during sporulation in the aerial mycelium in Streptomyces. In Prokaryotic Development. Brun, Y.V., and Shimkets, L.J. (eds). Washington, DC: *American Society for Microbiology Press,* pp. 33-48

Cho, B.K., Kim, D., Knight, E.M., Zengler, K., and Palsson, B.O, (2014), Genome-scale reconstruction of the sigma factor network in *Escherichia coli*: topology and functional states, *BMC Biology*, Vol. 12, No. 4, pp. 1-11

Cole, S.T., Brosch, R., Parkhill, J., Garnier, T., Churcher, C., Harris, D., Gordon, S.V., Eiglmeier, K., Gas, S., Barry III, C.E., Tekaia, F., Badcock, K., Basham, D., Brown, D., Chillingworth, T., Connor, R., Davies, R., Devlin, K., Feltwell, T., Gentles, S., Hamlin, N., Holroyd, S., Hornsby, T., Jagels, K., Krogh, A., McLean, J., Moule, S., Murphy, L., Oliver, Osborne, J., Quail, M.A., Rajandream, M.A., Rogers, J., Rutter, S., Seeger, K., Skelton, J., Squares, R., Squares, S., Sulston, J.E., Taylor, K., Whitehead, S., and Barrel, B.G., (1998) Deciphering the biology of Mycobacterium tuberculosis from the complete genome sequence, *Nature*, Vol. 396, pp. 537-544

Darst, S., (2001) Bacterial RNA polymerase, *Current Opinion in Structural Biology*, Vol. 11, pp. 155-162

D'Autreaux, B., and Toledano, M.B., (2007) ROS as signalling molecules: mechanisms that generate specificity in ROS homeostasis, *Nature Reviews; Molecular Cell Biology*, Vol. 8, pp. 813-824

Georg, J., and Hess, W.R., (2011), *cis*-Antisense RNA, Another Level of Gene Regulation in Bacteria, *Microbiology and Molecular Biology Reviews*, Vol. 75, No. 2, pp. 286-300

Gil, R., Silva, F.J., Pereto, J., and Moya, A., (2004), Determination of the Core of a Minimal Bacterial Gene Set, *Microbiol Mol Biol Rev*., Vol. 68, no. 3, pp. 518-537

Gill, S.C., and Von Hippel, P.H., (1989), Calculation of Protein Extinction Coefficients from Amino Acid Sequence Data, *Analytical Biochemistry*, Vol. 182, pp. 319-326

Greenstein, A.E., MacGurn, J.A., Baer, C.E., Falick, A.M., Cox, J.S. and Alber, T., (2007), *M. tuberculosis* Ser/Thr Protein Kinase D Phosphorlyates an Anti-Anti-Sigma Factor Homolog, *PLoS Pathogens*, Vol. 3., No. 4, pp. 475-483

Green, J., and Paget, M.S., (2004), Bacterial Redox Sensors, Nature Reviews; *Microbiology*, Vol. 2, pp. 954-967

Groitl, B., and Jakob, U., (2014), Review; Thiol-based redox switches, *Biochimica et Biophysica Acta 1844*, pp. 1335-1343

Gu, M., and Imlay, J.A., (2011) The SoxRS response of *Escherichia coli* is directly activated by redox-cycling drugs rather than by superoxide, *Molecular Microbiology*, Vol. 79, No. 5, p. 1136-1150

Helmann, J.D., (1999), Anti-sigma factors, *Current Opinion in Microbiology*, Vol. 2, pp. 135-141

Helmann, J.D., (2002), The extracytoplasmic function (ECF) sigma factors, *Adv. Microb., Physiol*., Vol. 46, pp. 47-110

Heras, B., Kurz, M., Shouldice, S.R., and Martin, J.L., (2007) The name's bond……disulfide bond, Current *Opinion in Structural Biology*, Vol. 17, pp. 691-698

Hughes, K.T., and Mathee, K., (1998), The Anti-Sigma Factors, *Annual Review of Microbiology*, Vol. 52, pp. 231-286

Janaszak, A., Majczak, W., Nadratowska, B., Szalewska-Palasz, A., Konopa, G., and Taylor, A., (2007), A σ^{54}-dependent promoter in the regulatory region of the *Escherichia coli rpoH* gene, *Microbiology*, Vol. 153, pp. 111-123

Jeong, E.H., Son, Y.M., Hah, Y.S., Choi, Y.J., Lee, K.H., Song, T., and Kim, D.R., (2006), RshA mimetic peptides inhibiting the transcription driven by a *Mycobacterium tuberculosis* sigma factor SigH, *Biochemical and Biophysical Research Communications*, Vol. 339, pp. 392-398

Jung, Y.G., Cho, Y.B., Kim, M.S., Yoo, J.S., Hong, S.H., and Roe, J.H., (2011), Determinants of redox sensitivity in RsrA, a zinc-containing anti-sigma factor for regulating thiol oxidative stress response, *Nucleic Acids Research*, Vol. 39, No. 17, pp. 7586-7597

Kallifidas, D., Thomas, D., Doughty, P., and Paget, M.S.B., (2010), The σ^{R} regulon of Streptomyces coelicolor A3(2) reveals a key role in protein quality control during disulphide stress, *Microbiology,* Vol. 156, pp. 1661-1672

Kang, J-G., Paget, M.S.B., Seok, Y-J., Hahn, M-Y., Bae, J-B., Hahn, J-S., Kleanthous, C., Buttner, M.J., and Roe, J-H., (1999) RsrA, an anti-sigma factor regulated by redox change, *The EMBO Journal*, Vol. 18, No. 15, pp. 4292-4298

Kazmierczak, M.J., Wiedmann, M., and Boor, K.J., (2005) Alternative Sigma Factors, and Their Roles in Bacterial Virulence, *Microbiology and Molecular Biology Reviews*, Vol. 69, No. 4, pp. 527-543

Kelly, S.M., Jess, T.J., and Price, N.C. (2005), How to study proteins by circular dichroism, *Biochimica et Biophysica Acta*, Vol. 1751, pp. 119-139.

Kim M.S., Dufour, Y.S., Yoo, J.S., Cho, Y.B., Park, J.H., Nam, G.B., Kim, H.M., Lee, K.L., Donohue, T.J., and Roe, J.H., (2012), Conservation of thiol-oxidative stress responses regulated by SigR orthologues in Actinomycetes, *Molecular Microbiology*, Vol. 85, No. 2, pp. 326-344

Kim, K.Y., Kim, S., Park, J.K., Song, H., and Park, S.Y., (2014), Crystallization and preliminary X-ray crystallographic analysis of carboxyl-terminal region 4 of SigR from *Streptomyces coelicolor A3(2)*, *Acta Cryst*. Vol. F70, pp. 747-749

Li, W., Stevenson, C.E.M., Burton, N., Jakimowicz, P., Paget, M.S.B., Buttner, M.J., Lawson, D.M., and Kleanthous, C., (2002), Identification and Structure of the Anti-sigma Factor-binding Domain of the Disulphide-stress Regulated Sigma Factor σ^{R} from *Streptomyces coelicolor*, *J. Mol. Biol*, Vol. 323, pp. 225-236

Li, W., Bottrill, A.R., Bibb, M.J., Buttner, M.J., Paget, M.S.B., and Kleanthous, C., (2003), The Role of Zinc in the Disulphide Stress-regulated Anti-sigma Factor RsrA from *Streptomyces coelicolor*, *J. Mol. Biol*., Vol. 333, pp. 461-472

Linke, K., and Jakob, U., (2003) Not Every Disulfide Lasts Forever: Disulfide Bond Formation as a Redox Switch, *Antioxidants & Redox Signalling*, Vol. 5, No. 4, pp. 425-434

Madigan, M.T., Martinko, J. M., and Parker, J., (2000), *Brock: Biology of Microorganisms 9th Edition* New Jersey, Prentice Hall

Maillard, A.P., Girard, E., Ziani, W., Petit-Hartlein, I., Kahn, R., Coves, J., (2014), The Crystal Structure of the Anti-σ Factor CnrY in Complex with the σ Factor CnrH Shows a New Structural Class of Anti-σ Factors Targeting Extracytoplasmic Function σ Factors*, J. Mol. Biol*., Vol. 426, pp. 2313-2327

Mayer, G., (2010), *Bacteriology-Chapter Nine Genetic Regulatory Mechanisms*, The Board of Trustees of the University of South Carolina, Seen: 02/06/2014 http://pathmicro.med.sc.edu/mayer/geneticreg.htm

Miller, J. H., (1972), *Experiments in molecular genetics*, Cold Spring Harbor Laboratory, Cold Spring Harbor, New York

Mooney, R.A., Darst, S.A., and Landick, R., (2005), Sigma and RNA Polymerase: An On-Again, Off-Again Relationship? *Molecular Cell*., Vol. 20, pp. 335-345

Murakami, K.S., Masuda, S., Campbell, E.A., Muzzin, O., and Darst, S.A., (2002) Structural Basis of Transcription Initiation: An RNA Polymerase Holoenzyme-DNA Complex, *Science*, Vol. 296, 1285-1290

Murakami, K.S., (2013), X-ray Crystal Structure of Escherichia coli RNA Polymerase σ^{70} Holoenzyme, *The Journal of Biological Chemistry*, Vol. 288, No 13, pp. 9126-9134

Newman, J.D., Anthony, J.R., and Donohue, T.J., (2001), The Importance of Zinc-binding to the Function of Rhodobacter sphaeroides ChrR as an Anti-sigma Factor, J*. Mol. Biol.* Vol. 313, pp. 485-499

Newton, G.L., and Fahey, R.C., (2002), Mycothiol Biochemistry, *Arch Microbiol*, Vol. 178, pp. 388-394

Newton, G.L., Rawat, M., La Clair, J.J., Jothivasan, V.K., Budiarto, T., Hamilton, C.J., Claiborne, A., Helmann, J.D, and Fahey, R.C., (2009), Bacillithiol is an antioxidant thiol produced in Bacilli, Brief Communications; *Nature Chemical Biology*, Vol. 5, No. 9, pp. 625-627

Nishizawa, M., Okumura, T., Ikeya, Y., and Kimura, T., (2012) Regulation of inducible gene expression by natural antisense transcripts, *Front Biosci* (Landmark Ed.), Vol. 1, No. 17, pp. 938-958

Paget, M.S.B., Bae, J.B., Hahn, M.Y., Li, W., Kleanthous, C., Roe, J.H., and Buttner, M.J., (2001), Mutational analysis of RsrA, a zinc-binding anti-sigma factor with a thiol-disulfide redox switch, *Molecular Microbiology*, Vol. 39, No. 4, pp. 1036-1047

Paget, M.S.B., Hong, H.J., Bibb, M., and Buttner, M., (2002), The ECF sigma factors of Streptomyces coelicolor A3(2), *SGM symposium 61: Signals, switches, regulons and cascades: control of bacterial gene expression* pp. 105-125

Paget, M.S.B., and Buttner, M.J., (2003), Thiol-Based Regulatory Switches, *Annu. Rev. Genet*. Vol. 37, pp. 91-121

Paget, M.S.B., and Helmann, J.D., (2003), Protein family review; The σ^{70} family of sigma factors, *Genome Biology*, Vol. 4, pp. 203.1-203.6

Paget, M.S.B., Kang, J.G., Roe, J.H., and Buttner, M.J., (1998), σ^{R}, and RNA polymerase sigma factor that modulates expression of the thioredoxin system in response to oxidative stress in Streptomyces coelicolor A3(2), *The EMBO Journal*, Vol. 17, No. 19, pp. 5776-5782

Park, S.T., Kang, C.M., and Husson, R.N., (2008), Regulation of the SigH stress response regulon by an essential protein kinase in *Mycobacterium tuberculosis*, *PNAS*, Vol. 105, No. 35, pp. 13105-13110

PDB,Thakur, K.G., Praveena, T., and Gopal, B., (2010) Structural and Biochemical Bases for the Redox Sensitivity of *Mycobacterium tuberculosis* RslA, *J. Mol Biol*. Vol. 397, pp. 1199-1208 http://www.rcsb.org/pdb/explore/jmol.do?structureId=3HUG&opt=3&bionumber=1 Seen: 24/12/2013

PDB, Campbell, E.A., Tupy, J.L., Gruber, T.M., Wang, S., Sharp, M.M., Gross, C.A., Darst, S.A., (2003) Crystal Structure of Escherichia coli σ^{E} with the Cytoplasmic Domain of Its Anti-σ RseA, *Molecular Cell*, Vol. 11, pp. 1067-1078 http://www.rcsb.org/pdb/explore/jmol.do?structureId=1OR7&bionumber=1 Seen: 24/12/2013

Phillips, T., (2008) Regulation of Transcription and Gene Expression in Eukaryotes, *Nature Education 1* (1):199

Pierce, M.M., Raman, C.S., and Nall, B.T., (1999), Isothermal Titration Calorimetry of Protein-Protein Interactions, *Methods*, Vol. 19, pp. 213-221

Procopio, R.E., da Silva, I.R., Martins, M.K., de Azevedo, J.L., de Araujo, J.M., (2012) Antibiotics produced by Streptomyces, *The Brazilian Journal of Infectious Diseases*, Vol. 16, No. 5, pp. 466-471

Qui, J., and Helmann, J.D., (2001), The -10 region is a key promoter specificity determinant for the Bacillus subtilis extracytoplasmic-function sigma factors σ^{X} and σ^{W}, *Journal of Bacteriology*, Vol. 183, pp. 1921-1927

Raivio, T.L., and Silhavy, T.J., (2001), Periplasmic Stress and ECF Sigma Factors, *Annu. Rev. Microbiol*. Vol. 55, pp. 591-624

Rodrigue, S., Provvedi, R., Jacques, P.E., Gaudreau, L. and Manganelli, R., (2006), The sigma factors of Mycobacterium tuberculosis, *FEMS Microbiol* Vol. 30, pp. 926- 941

Ross, W., Ernst, A., and Gourse, R.L., (2001) Fine structure of *E. coli* RNA polymerase-promoter interactions: α-subunit binding to the UP element minor groove, *Genes & Development*, Vol. 15, pp. 491-506

Shaw, K., (2008), Negative Transcription Regulation in Prokaryotes, *Nature Education*, Vol. 1, No. 1, pp. 122

Schobel, S., Zellmeir, S., Schumann, W., and Wiegert, T., (2004), The *Bacillus subtilis* σ^W anti-sigma factor RsiW is degraded by intramembrane proteolysis through YluC, *Molecular Microbiology*, Vol. 52, No. 4, pp. 1091-1105

Song, T., Dove, S.L., Lee, K.H., and Husson, R.N., (2003), RshA, an anti-sigma factor that regulates the activity of the mycobacterial stress response sigma factor SigH, *Molecular Microbiology*, Vol. 50, No. 3, 949-959

Sterberg, S.O., Peso-Santos, T.D., Shingler, V., (2011), Regulation on Alternative Sigma Factor Use, *Annu. Rev. Microbiol.* Vol. 65, p. 37-55

Thakur, K.G., Praveena, T., and Gopal, B., (2010), Structural and Biochemical Bases for the Redox Sensitivity of *Mycobacterium tuberculosis* RslA, *J. Mol Biol*. Vol. 397, pp. 1199-1208

Ung, K.S.E., and Av-Gay, Y., (2006), Mycothiol-dependent mycobacterial response to oxidative stress, *FEBS Letters*, vol. 580, pp. 2712-2716

Ventura, M., Canchaya, C., Tauch, A., Chandra, G., Fitzgerald, G.F. Chater, K.F., and Sinderen, D.V., (2007) Genomics of *Actinobacteria*: Tracing the Evolutionary History of an Ancient Phylum, *Microbiol. Mol. Biol. Rev.*, Vol 71, No. 3, pp. 495-548

Wei, Z.H., Chen, H., Zhang, C., and Ye, B.C., (2014), FRET-Based System for Probing Protein-Protein Interactions between σ^R and RsrA from *Streptomyces Coelicolor* in Response to the Redox Environment, *PLOS ONE*, Vol. 9, Issue 3, pp. 1-11

Winkler, W.C., and Breaker, R.R., (2005), Regulation of Bacterial Gene Expression by Riboswitches, *Annu. Rev. Microbiol*, Vo. 59, pp. 487-517

Wösten, M.M.S.M., (1998), Eubacterial sigma-factors, *FEMS Microbiology Reviews*, Vol. 22, pp. 127-150

Zdanowski, K., Doughty, P., Jakimowicz, P., O'Hara, L., Buttner, M.J., Paget, M.S.B., and Kleanthous, C., (2006), Assignment of the Zinc Ligands in RsrA, a Redox-Sensing ZAS Protein from Streptomyces coelicolor, *Biochemistry*, Vol. 45, pp. 8294-8300